

Quark mass effects in double parton distributions

Markus Diehl¹, Riccardo Nagar² and Peter Plößl¹

¹ Deutsches Elektronen-Synchrotron DESY, Notkestr. 85, 22607 Hamburg, Germany

² Università degli Studi di Milano-Bicocca & INFN Sezione di Milano-Bicocca,
Piazza della Scienza 3, Milano 20126, Italy

Double parton distributions can be computed from the perturbative splitting of one parton into two if the distance between the two observed partons is small. We develop schemes to take into account quark mass effects in this computation, and we study these schemes numerically at leading order in the strong coupling. Furthermore, we investigate in detail the structure of the next-to-leading order corrections to the splitting kernels that include quark mass effects.

Contents

1	Introduction	3
2	Theory background	4
2.1	Scale dependence	5
2.2	Flavour matching	6
2.3	DPDs at short distance	8
3	Schemes for treating heavy quarks in splitting DPDs	9
3.1	Splitting kernels including mass effects	10
3.2	Schemes for one massive flavour	11
3.2.1	Scheme with massless splitting kernels	12
3.2.2	Scheme with massive splitting kernels	13
3.3	Two heavy flavours (charm and bottom)	15
4	Numerical studies with LO splitting kernels	16
4.1	Splitting DPDs	17
4.1.1	Massless scheme	17
4.1.2	Massive scheme	19
4.2	Double parton luminosities	23
4.2.1	Dependence on the scheme parameters	26
4.2.2	Splitting scale variation	29
4.2.3	Variation of the flavour matching scale	29
5	Massive splitting kernels at NLO	32
5.1	Two-loop splitting graphs with massive quarks	33
5.2	Reminders about massless kernels	35
5.3	Limiting behaviour for small or large distances	35
5.4	Scale dependence	36
5.5	An explicit parametrisation	37
5.6	Large logarithms	39
6	NLO splitting kernels with two heavy flavours	41
6.1	Expressions in terms of kernels with one heavy flavour	41
6.2	Limiting behaviour for small or large distances	42
6.3	Scale dependence	45
6.4	Explicit parametrisation	46
7	DPD sum rules and massive splitting kernels	47
7.1	Sum rules for the massive splitting kernels	49
7.1.1	Momentum sum rule	50
7.1.2	Number sum rule	51
7.2	Sum rules for the interpolating function V^I	53
7.3	Explicit determination of the NLO kernel for $g \rightarrow q\bar{q}$	54
8	A model for the unpolarised massive splitting kernels at NLO	55
8.1	Constraints on the interpolating functions	56
8.2	A particular solution for the kernels	60
9	Conclusions	62

A Numerical studies for W pair production	62
B Basis functions for the model in section 8	67
References	70

1 Introduction

To make the best physics use of measurements at the Large Hadron Collider, it is important to understand the strong-interaction dynamics of hadron collisions to the best degree possible. Among many other things, this motivates the study of double parton scattering (DPS), where in a single proton-proton collision two partons in each proton undergo a hard scattering. Generically, the importance of this mechanism increases with collision energy, so that it is relevant for future hadron colliders at least as much as for the LHC.

Significant progress in the theory description of DPS has been made in the last decade [1–16], and there is an increasing set of DPS measurements from the Tevatron and the LHC, see [17–21] and references therein. As an example for the huge body of phenomenological work, let us mention the recent study [22] of four-jet production. A detailed account of theoretical and experimental aspects of DPS is given in the monograph [23].

Double parton distributions (DPDs) are the nonperturbative ingredients in the calculation of DPS cross sections. A corresponding factorisation formalism has been developed in [13] and underlies the present work. In this formalism, a DPD depends on the momentum fractions x_1 and x_2 of the two partons extracted from a proton, and on the transverse distance y between these two partons. It also depends on the renormalisation scales μ_1 and μ_2 associated with each parton. We assume them to be equal throughout this work, since taking $\mu_1 \neq \mu_2$ would not add much to our discussion. We will limit ourselves to DPDs without colour correlations between the two partons; an extension of our results to the colour correlated case should be possible but would require additional work.

Consider a DPS process with the two hard scatterings taking place at a scale μ . The DPDs of the two colliding protons enter the factorisation formula in the form of a double parton luminosity

$$\int d^2y \theta(y - y_{\min}) F_{a_1 a_2}(x_{1a}, x_{2a}, y; \mu) F_{b_1 b_2}(x_{1b}, x_{2b}, y; \mu), \quad (1.1)$$

where a_i and b_i label the species and polarisation of the scattering partons. The lower cutoff y_{\min} in the integration over y is to be taken of order $1/\mu$. In the formalism of [13], a subtraction term depending on the same cutoff appears in the overall cross section and removes double counting between the cross sections for single and for double parton scattering. The dependence on y_{\min} cancels in the sum of terms, up to higher-order corrections beyond the accuracy of the calculation.

It is important to understand which distances y are most relevant in the integral (1.1). In the limit of perturbatively small y , one may decompose the DPD as $F = F^{\text{spl}} + F^{\text{intr}}$. The first term represents the case where the two extracted partons originate from a single parton, which can be computed in terms of a perturbative splitting kernel and an ordinary parton distribution (PDF). The second term represents the “intrinsic” two-parton content of the proton and can be expressed in terms of a twist-four distribution. In fixed-order perturbation theory, one obtains a power behaviour $F^{\text{spl}} \sim y^{-2}$ and $F^{\text{intr}} \sim y^0$ at small y . This suggests that the double parton luminosity (1.1) should be strongly dominated by the region where

y is close to y_{\min} . In the overall cross section, however, the contribution from this region is largely cancelled by the subtraction term just mentioned. Moreover, it was found in [13] that the stated power behaviour can be substantially flattened by evolution from the scale $\sim 1/y$ at which a fixed-order calculation of F^{spl} is reliable to the scale μ of the hard scatterings. Finally, for some parton combinations, F^{spl} is suppressed compared with F^{intr} by α_s^2 rather than by α_s . In summary, the relevant y region in a cross section with hard scale μ extends to values substantially larger than $1/\mu$, with details depending on kinematics and the parton channels. This region may include both perturbative distances, where one has a natural decomposition $F = F^{\text{spl}} + F^{\text{intr}}$, and nonperturbatively large y , where one must resort to modelling F . Guidance for such modelling may for instance be obtained from quark model studies [24–34], from calculations in lattice QCD [35, 36], or from the sum rules that DPDs must obey [1, 37–40].

In the present work, we focus on the perturbative splitting contribution F^{spl} . Its relevance for DPS phenomenology has been highlighted in different theory formalisms [9, 11, 41–45], including the one we are using here [13].

Heavy-quark masses play a quite nontrivial role in the computation of DPS. The number n_F of active quark flavours in a double parton luminosity depends on μ and on the particular scheme used to compute the hard-scattering cross sections. If one has for instance $m_b \ll \mu \ll m_t$, then it is appropriate to use DPDs with $n_F = 5$ active flavours, and m_b and m_c can be neglected in the hard scattering. However, as explained above, the relevant y range in the double parton luminosity may include regions where y is comparable to $1/m_b$ or $1/m_c$. In these regions, computing F^{spl} with massless charm and bottom quarks is a poor approximation. This calls for a more realistic scheme for evaluating F^{spl} across the relevant range of y in the perturbative region. To develop and assess such schemes is the purpose of the present work.

There is a certain similarity between the problem just stated and the role of n_F in the computation of transverse-momentum dependent single-parton distributions (TMDs). Taken in impact parameter space, a TMD $f(x, b; \mu)$ depends on a transverse distance just like $F(x_1, x_2, y; \mu)$, and at small impact parameter b the TMD can be computed in terms of a perturbative matching kernel and a PDF. The treatment of heavy-quark masses in this case was investigated in detail in [46]. An important difference with the present case is that the relevant distances of b in a TMD cross section are of order $1/q_T$, where q_T is a measured transverse momentum, whereas there is no such simple relation between the process kinematics and the relevant distances y in DPS.

This paper is structured as follows. In section 2, we recall some theory results that will be needed in our work. In section 3, we present general schemes for treating heavy flavours in splitting DPDs. In section 4 these schemes are studied numerically at leading order (LO) in α_s . In sections 5 and 6 we analyse the structure of massive splitting kernels at next-to-leading order (NLO) in α_s , first for the case of a single heavy quark and then for the case of charm and bottom. In section 7, we show how the number and momentum sum rules for DPDs imply corresponding sum rules for the massive splitting kernels. This is used in section 8 to construct a model ansatz for these kernels at NLO. Our main results are summarised in section 9. Additional numerical examples are given in appendix A, and technical material relevant to the model in section 8 can be found in appendix B.

2 Theory background

In this section, we set up our notation and recall basic results about scale dependence, flavour matching, and the splitting mechanism for DPDs.

To denote PDFs and DPDs for n_F active flavours, we respectively write $f_{a_1}^{n_F}(x; \mu)$ and

$F_{a_1 a_2}^{n_F}(x_1, x_2, y; \mu)$, where a_1 and a_2 specify the flavour and polarisation of a parton. A generic massive quark flavour is denoted by Q , and light quark flavours by q or q' .

We consider only colour-singlet DPDs in this work. Unless stated otherwise, our arguments apply to both unpolarised and polarised partons. For ease of notation, we will in general give explicit relations for the unpolarised case and note how they generalise to the polarised one. Notice that for transverse quark or linear gluon polarisation, DPDs carry one or more Lorentz indices and depend on the transverse vector \mathbf{y} rather than its length y . For ease of writing, we will not indicate this explicitly.

We will explicitly indicate sums over flavour labels, where it is understood that the flavour sums run over the active flavours of the quantities being summed. We use the convention that

$$f_{a_1}^{n_F} = 0, \quad F_{a_1 a_2}^{n_F} = 0, \quad P_{a_1 a_0}^{n_F} = 0, \quad V_{a_1 a_2, a_0}^{n_F} = 0, \quad U_{a_1 a_2, a_0}^{n_F} = 0$$

if a_0 , a_1 , or a_2 is heavier than the n_F active flavours, (2.1)

where P denotes the DGLAP evolution kernels and the kernels V and U are introduced in sections 2.3 and 7, respectively. For kernels involving n_F light flavours and a heavy flavour Q , we set

$$A_{a_1 Q}^{Q, n_F} = 0, \quad V_{a_1 a_2, Q}^{Q, n_F} = 0, \quad (2.2)$$

where A^Q is the flavour matching kernel for parton distributions (section 2.2) and V^Q the massive DPD splitting kernel defined in section 3.1.

In general, kernels like P^{n_F} or A^{Q, n_F} have an explicit n_F dependence beyond the conditions (2.1) and (2.2) on their flavour indices. This dependence is absent in some channels at low perturbative orders. When this is the case, the superscript n_F is omitted, i.e. its absence signals that the corresponding quantity is n_F independent.

Due to charge conjugation invariance, all kernels in (2.1) and (2.2) remain the same if one changes quarks to antiquarks and vice versa. Furthermore, permutation symmetry implies $F_{a_1 a_2}(x_1, x_2, y) = F_{a_2 a_1}(x_2, x_1, y)$ and corresponding relations for the kernels V and U . We will give explicit results only for channels that are independent w.r.t. these symmetry operations.

2.1 Scale dependence

Throughout this work, we assume that PDFs and DPDs are renormalised by the $\overline{\text{MS}}$ prescription for all of the n_F active flavours, regardless of whether a flavour is considered as massive or massless. The corresponding DGLAP evolution kernels are denoted by $P_{a_1 a_0}^{n_F}$. For PDFs, we then have

$$\frac{d}{d \log \mu^2} f_{a_1}^{n_F}(x; \mu) = \sum_{a_0} P_{a_1 a_0}^{n_F}(\mu) \otimes f_{a_0}^{n_F}(\mu), \quad (2.3)$$

where \otimes denotes the usual Mellin convolution. In the factors of a convolution product we omit the momentum fractions that are integrated over, and it is understood that the product depends on one momentum fraction (which can be deduced from the context).

As mentioned in the introduction, we consider DPDs with the same factorisation scale μ for both partons. The evolution equation then reads

$$\frac{d}{d \log \mu^2} F_{a_1 a_2}^{n_F}(x_1, x_2, y; \mu) = \sum_{b_1} P_{a_1 b_1}^{n_F}(\mu) \otimes_1 F_{b_1 a_2}^{n_F}(y; \mu) + \sum_{b_2} P_{a_2 b_2}^{n_F}(\mu) \otimes_2 F_{a_1 b_2}^{n_F}(y; \mu) \quad (2.4)$$

with separate Mellin convolutions

$$P \otimes_1 F = \int_{x_1}^1 \frac{dz}{z} P(z) F\left(\frac{x_1}{z}, x_2\right), \quad P \otimes_2 F = \int_{x_2}^1 \frac{dz}{z} P(z) F\left(x_1, \frac{x_2}{z}\right) \quad (2.5)$$

for each parton momentum fraction. It is understood that convolution products with a subscript 1 or 2 depend on two momentum fractions (x_1 and x_2 in the present case).

We write the perturbative expansion of the evolution kernels as

$$P_{a_1 a_0}^{n_F}(z; \mu) = \sum_{k=0}^{\infty} [a_s^{n_F}(\mu)]^{k+1} P_{a_1 a_0}^{n_F(k)}(z), \quad (2.6)$$

where

$$a_s^{n_F}(\mu) = \frac{\alpha_s^{n_F}(\mu)}{2\pi} \quad (2.7)$$

and $\alpha_s^{n_F}$ is the strong coupling constant for n_F flavours renormalised in the $\overline{\text{MS}}$ scheme. The scale dependence of the coupling reads

$$\frac{d}{d \log \mu^2} a_s^{n_F}(\mu) = \frac{\beta^{n_F}(a_s^{n_F}(\mu))}{2\pi} \quad (2.8)$$

with

$$\frac{\beta^{n_F}(a_s^{n_F})}{2\pi} = -\frac{\beta_0^{n_F}}{2} (a_s^{n_F})^2 + \mathcal{O}((a_s^{n_F})^3) \quad (2.9)$$

and

$$\beta_0^{n_F} = \frac{11}{3} C_A - \frac{4}{3} T_F n_F, \quad (2.10)$$

where $C_A = N_c$ for N_c colours, and $T_F = 1/2$.

At LO, the n_F dependence of the DGLAP kernel for gluon splitting resides only in β_0 :

$$P_{gg}^{n_F(0)}(z) = \tilde{P}_{gg}^{(0)}(z) + \frac{\beta_0^{n_F}}{2} \delta(1-z). \quad (2.11)$$

Corresponding relations hold for polarised gluons, with different functions $\tilde{P}_{\Delta g \Delta g}^{(0)}$ and $\tilde{P}_{\delta g \delta g}^{(0)}$ for longitudinal and linear gluon polarisation, but the same term $\beta_0^{n_F} \delta(1-z)/2$ in all cases. For all other parton channels, the LO coefficients $P_{a_1 a_0}^{(0)}$ are n_F independent.

2.2 Flavour matching

We refer to changing the number of active flavours as “flavour matching”. When matching from n_F to $n_F + 1$ active flavours, we call the first n_F flavours “light” and the $(n_F + 1)$ st flavour Q “heavy”.

The matching relation for the strong coupling is

$$a_s^{n_F}(\mu) = \sum_{k=0}^{\infty} [a_s^{n_F+1}(\mu)]^{k+1} A_{\alpha}^{n_F(k)}(m_Q; \mu), \quad (2.12)$$

where m_Q is the mass of the heavy quark. The LO and NLO coefficients are n_F independent and read

$$A_{\alpha}^{(0)} = 1, \quad A_{\alpha}^{(1)}(m_Q; \mu) = \frac{\Delta\beta_0}{2} \log \frac{\mu^2}{m_Q^2} \quad (2.13)$$

with

$$\Delta\beta_0 = \beta_0^{n_F+1} - \beta_0^{n_F} = -\frac{4}{3} T_F. \quad (2.14)$$

One readily verifies that (2.13) is consistent with the scale dependence of $a_s(\mu)$ given by equations (2.8) to (2.10). The higher-order coefficients $A_\alpha^{n_F(2)}$ and $A_\alpha^{n_F(3)}$ can be found in [47].

The matching relation for PDFs reads

$$f_{a_1}^{n_F+1}(x; \mu) = \sum_{a_0} A_{a_1 a_0}^{Q, n_F}(m_Q; \mu) \otimes f_{a_0}^{n_F}(\mu) \quad (2.15)$$

with

$$A_{a_1 a_0}^{Q, n_F}(z, m_Q; \mu) = \sum_{k=0}^{\infty} [a_s^{n_F+1}(\mu)]^k A_{a_1 a_0}^{Q, n_F(k)}(z, m_Q; \mu). \quad (2.16)$$

As is customary, we expand the matching kernels A^{Q, n_F} in $a_s^{n_F+1}$ rather than in $a_s^{n_F}$. The matching coefficients in (2.16) contain explicit logarithms:

$$A_{a_1 a_0}^{Q, n_F(k)}(z, m_Q; \mu) = \sum_{\ell=0}^{k-1} \log^\ell \frac{\mu^2}{m_Q^2} A_{a_1 a_0}^{Q, n_F[k, \ell]}(z). \quad (2.17)$$

At LO, the matching kernels have the simple form

$$A_{a_1 a_0}^{Q(0)}(z) = \delta_{a_1 l}^{n_F} \delta_{a_1 a_0} \delta(1-z), \quad (2.18)$$

where

$$\delta_{al}^{n_F} = \begin{cases} 1 & \text{if } a \text{ is one of the } n_F \text{ light flavours} \\ 0 & \text{otherwise} \end{cases} \quad (2.19)$$

enforces the condition (2.2). The NLO matching kernels are n_F independent and can be written as

$$A_{a_1 a_0}^{Q(1)}(z, m_Q; \mu) = \left[P_{a_1 a_0}^{n_F+1(0)}(z) - P_{a_1 a_0}^{n_F(0)}(z) \right] \log \frac{\mu^2}{m_Q^2}, \quad (2.20)$$

where we recall the convention specified in equation (2.1). This implies $A_{a_1 a_0}^{Q(1)} = 0$ if a_1 or a_0 is a light quark or antiquark. In the other channels, we have

$$A_{Qg}^{Q(1)}(z, m_Q; \mu) = P_{gg}^{(0)}(z) \log \frac{\mu^2}{m_Q^2} = T_F \left[z^2 + (1-z)^2 \right] \log \frac{\mu^2}{m_Q^2}, \quad (2.21)$$

$$A_{gg}^{Q(1)}(z, m_Q; \mu) = \frac{\Delta\beta_0}{2} \delta(1-z) \log \frac{\mu^2}{m_Q^2}, \quad (2.22)$$

for unpolarised partons, as well as

$$A_{\Delta Q \Delta g}^{Q(1)}(z, m_Q; \mu) = P_{\Delta q \Delta g}^{(0)}(z) \log \frac{\mu^2}{m_Q^2} = T_F \left[z^2 - (1-z)^2 \right] \log \frac{\mu^2}{m_Q^2}, \quad (2.23)$$

and

$$A_{\Delta g \Delta g}^{Q(1)} = A_{\delta g \delta g}^{Q(1)} = A_{gg}^{Q(1)} \quad (2.24)$$

for polarised ones. Note that there is no transition from linearly polarised gluons to transversely polarised quarks, i.e. $A_{\delta Q \delta g}^{Q(1)} = 0$. The two-loop matching coefficients $A^{Q(2)}$ for unpolarised partons can be found in references [48–51]. They are all independent of n_F .

Flavour matching for DPDs proceeds in full analogy to the PDF case and reads

$$F_{a_1 a_2}^{n_F+1}(x_1, x_2, y; \mu) = \sum_{b_1} A_{a_1 b_1}^{Q, n_F}(m_Q; \mu) \otimes_1 F_{b_1 a_2}^{n_F}(y; \mu) + \sum_{b_2} A_{a_2 b_2}^{Q, n_F}(m_Q; \mu) \otimes_2 F_{a_1 b_2}^{n_F}(y; \mu). \quad (2.25)$$

One way to see this is to rewrite the matching equation (2.15) for PDFs as a matching relation between the twist-two operators that define PDFs with $n_F + 1$ or n_F active flavours. DPDs are defined in terms of the same twist-two operators, containing the product of an operator for parton a_1 and an operator for parton a_2 at relative transverse distance y . This readily implies the matching relation (2.25) as a generalisation of (2.15), just as the renormalisation group equation for the twist-two operators implies the evolution equation (2.4) for DPDs as a generalisation of the DGLAP equation (2.3) for PDFs.

2.3 DPDs at short distance

As we just mentioned, DPDs are defined as the matrix elements of the product between two twist-two operators that are separated by a distance y in the transverse plane. In the limit where this distance y is much smaller than a typical hadronic scale, one can perform an operator product expansion and thus express DPDs in terms of short-distance coefficients and matrix elements of single operators with definite twist. The leading operators have twist two, and their matrix elements are PDFs. This corresponds to the first term in the decomposition $F = F^{\text{spl}} + F^{\text{intr}}$ we already mentioned in the introduction. From now on, we focus on this term and omit the superscript “spl” for brevity. A detailed account of its properties can be found in [52, 53], where the associated short-distance coefficients (called “DPD splitting kernels”) are computed up to NLO for unpolarised massless partons.

The general form of the splitting formula for DPDs with n_F massless flavours reads

$$F_{a_1 a_2}^{n_F}(x_1, x_2, y; \mu) = \frac{1}{\pi y^2} \sum_{a_0} V_{a_1 a_2, a_0}^{n_F}(y; \mu) \otimes_{12} f_{a_0}^{n_F}(\mu), \quad (2.26)$$

where

$$V_{12} \otimes f = \int_{x_1+x_2}^1 \frac{dz}{z^2} V\left(\frac{x_1}{z}, \frac{x_2}{z}\right) f(z) \quad (2.27)$$

is a generalised Mellin convolution depending on two momentum fractions. A useful relation is

$$D \otimes_{12} [C \otimes f] = [D \otimes_{12} C] \otimes_{12} f, \quad (2.28)$$

where D depends on two momentum fractions and C and f depend on one momentum fraction.

The DPD splitting kernels can be expanded in the strong coupling as

$$V_{a_1 a_2, a_0}^{n_F}(z_1, z_2, y; \mu) = \sum_{k=1}^{\infty} [a_s^{n_F}(\mu)]^k V_{a_1 a_2, a_0}^{n_F(k)}(z_1, z_2, y; \mu) \quad (2.29)$$

with coefficients of the form

$$V_{a_1 a_2, a_0}^{n_F(k)}(z_1, z_2, y; \mu) = \sum_{\ell=0}^{k-1} \log^\ell \frac{\mu^2}{\mu_y^2} V_{a_1 a_2, a_0}^{n_F[k, \ell]}(z_1, z_2). \quad (2.30)$$

Here we have introduced the mass scale corresponding to the distance y ,

$$\mu_y = \frac{b_0}{y}, \quad (2.31)$$

where $b_0 = 2e^{-\gamma_E} \approx 1.12$ with the Euler-Mascheroni constant γ_E .

The LO splitting kernels are n_F independent and have the kinematic constraint

$$V_{a_1 a_2, a_0}^{(1)}(z_1, z_2) = \delta(1 - z_1 - z_2) V_{a_1 a_2, a_0}^{(1)}(z_1), \quad (2.32)$$

where the function V on the right-hand side depends on only one momentum fraction. With this constraint, the general form (2.26) turns into

$$F_{a_1 a_2}^{n_F}(x_1, x_2, y; \mu) = \frac{a_s^{n_F}(\mu)}{\pi y^2} V_{a_1 a_2, a_0}^{(1)}\left(\frac{x_1}{x_1 + x_2}\right) \frac{f_{a_0}^{n_F}(x_1 + x_2; \mu)}{x_1 + x_2} + \mathcal{O}((a_s^{n_F})^2). \quad (2.33)$$

The functions $V_{a_1 a_2, a_0}^{(1)}(z)$ are equal to the LO DGLAP kernels $P_{a_1 a_0}^{(0)}(z)$ with all plus-distributions and $\delta(1 - z)$ terms removed. The structure of the DPD splitting kernels at NLO (i.e. at order a_s^2) will be discussed at the beginning of section 5.

The relations from (2.26) to (2.33) hold if the partons a_1 and a_2 are unpolarised or polarised.

3 Schemes for treating heavy quarks in splitting DPDs

As discussed in the introduction, the computation of a DPS cross section requires the double parton luminosities (1.1), which involve DPDs for all distances y above a value of order $1/\mu$, where μ is the typical scale of the hard-scattering processes. The DPDs need to be evolved to this scale, starting from a scale at which they can either be computed (for small y) or modelled (for large y). In the present section, we discuss how to treat massive quarks in different regions of small y .

Before doing so, let us briefly discuss the transition from small to large y . For small y and massless partons, one should compute the DPDs at a scale proportional to μ_y given in (2.31), since this avoids large logarithms in the coefficients (2.30) of the splitting formula (2.26). For large y , it is natural to model the DPDs at a scale in the GeV region, which must be large enough to use the perturbative expansion of the DGLAP kernels when evolving to higher scales. To interpolate between the two regimes, one may take the starting scale for DPD evolution proportional to

$$\mu_{y^*} = \frac{b_0}{y^*(y)} \quad \text{with } y^*(y) \rightarrow \begin{cases} y & \text{for } y \rightarrow 0 \\ y_{\max} & \text{for } y \rightarrow \infty \end{cases} \quad (3.1)$$

which tends to μ_y for small y and to $\mu_{\min} = b_0/y_{\max}$ for large y . In the numerical study of section 4, we will take $\mu_{\min} = 1 \text{ GeV}$ and the functional form

$$y^*(y) = \frac{y}{(1 + y^p/y_{\max}^p)^{1/p}}. \quad (3.2)$$

With $p = 2$, this function is widely used in the phenomenology of transverse-momentum dependent parton distributions. We will instead take the form with $p = 4$, which tends more rapidly to μ_y for small y . A rather similar function was used in [54].

3.1 Splitting kernels including mass effects

The DPD splitting formula (2.26) is applicable if all quark masses in the perturbative splitting process can be neglected. The corresponding LO kernels are given in reference [6] for all polarisations, and the unpolarised NLO kernels can be found in [52, 53]. This version of the splitting formula is appropriate if the characteristic mass scale $\mu_y = b_0/\mu$ of the splitting is much bigger than the masses of the active quark flavours in the DPD.

If μ_y is much larger than the masses of the first n_F quark flavours but similar in size to the mass m_Q of the $n_F + 1$ st flavour, then the latter should be treated as massive in the computation of the $1 \rightarrow 2$ splitting kernels V . In this case, we can use the splitting formula

$$F_{a_1 a_2}^{n_F+1}(x_1, x_2, y; \mu) = \frac{1}{\pi y^2} \sum_{a_0} V_{a_1 a_2, a_0}^{Q, n_F}(y, m_Q; \mu) \otimes_{12} f_{a_0}^{n_F}(\mu) \quad (3.3)$$

with a perturbative expansion

$$V_{a_1 a_2, a_0}^{Q, n_F}(z_1, z_2, y, m_Q; \mu) = \sum_{k=1}^{\infty} [a_s^{n_F+1}(\mu)]^k V_{a_1 a_2, a_0}^{Q, n_F(k)}(z_1, z_2, y, m_Q; \mu). \quad (3.4)$$

The label n_F on V^Q indicates the number of flavours that are treated as massless. Notice that only the n_F light quark flavours are taken as active in the PDF on the r.h.s. of (3.3), i.e. the heavy flavour Q only appears in the splitting kernel. In analogy to the flavour matching kernels (2.16), we expand the massive splitting kernels in $a_s^{n_F+1}$.

At LO one finds only one channel where heavy quarks can be produced by the splitting, namely $g \rightarrow Q\bar{Q}$. The corresponding kernels can readily be obtained by extending the calculation in section 5.2.2 of reference [6]. We find

$$\begin{aligned} V_{Q\bar{Q},g}^{Q(1)}(z_1, z_2, y, m_Q) &= T_F (ym_Q)^2 \left[(z_1^2 + z_2^2) K_1^2(ym_Q) + K_0^2(ym_Q) \right] \delta(1 - z_1 - z_2), \\ V_{\Delta Q \Delta \bar{Q},g}^{Q(1)}(z_1, z_2, y, m_Q) &= T_F (ym_Q)^2 \left[-(z_1^2 + z_2^2) K_1^2(ym_Q) + K_0^2(ym_Q) \right] \delta(1 - z_1 - z_2), \\ V_{\delta Q \delta \bar{Q},g}^{Q(1)}(z_1, z_2, y, m_Q) &= T_F (ym_Q)^2 \left[-2z_1 z_2 K_1^2(ym_Q) \right] \delta(1 - z_1 - z_2), \end{aligned} \quad (3.5)$$

where $K_i(w)$ denotes the modified Bessel functions of the second kind. Kernels with exactly one observed heavy flavour are zero at this order, whereas kernels with only light flavours are equal to their massless counterparts,

$$V_{a_1 a_2, a_0}^{Q(1)}(z_1, z_2, y, m_Q) = V_{a_1 a_2, a_0}^{(1)}(z_1, z_2) \quad \text{if } a_1 \text{ and } a_2 \text{ are light.} \quad (3.6)$$

The situation at NLO is significantly more involved and will be analysed in section 5.

Consider now the unpolarised $g \rightarrow Q\bar{Q}$ kernel from (3.5) in the limits $\mu_y \ll m_Q$ and $\mu_y \gg m_Q$. In the first case — which corresponds to $y \gg 1/m_Q$ — the massive kernel vanishes exponentially,

$$V_{Q\bar{Q},g}^{Q(1)}(z_1, z_2, y, m_Q) \xrightarrow{\mu_y \ll m_Q} y m_Q \exp(-2ym_Q) \xrightarrow{y \rightarrow \infty} 0, \quad (3.7)$$

so that the production of heavy quarks is strongly suppressed. In the second case — which corresponds to $y \ll 1/m_Q$ — one obtains

$$V_{Q\bar{Q},g}^{Q(1)}(z_1, z_2, y, m_Q) \xrightarrow{\mu_y \gg m_Q} V_{Q\bar{Q},g}^{(1)}(z_1, z_2) + \mathcal{O}((ym_Q)^2 \log^2(ym_Q)). \quad (3.8)$$

Analogous limiting expressions hold for polarised quarks, except that for transverse polarisation the corrections to the small y limit are of order $(ym_Q)^2 \log(ym_Q)$. As one expects, the massive kernels approach the massless ones for $\mu_y \gg m_Q$, with power corrections in the small parameter ym_Q . Notice that the massless LO kernel on the right-hand side of (3.8) does not depend on the number of active flavours, but the coupling a_s it is multiplied with in the perturbative expansion (2.29) does.

Two heavy flavours If μ_y is comparable in size to both m_c and m_b , one may want to treat both charm and bottom quarks as massive when computing the $1 \rightarrow 2$ splitting. The DPD with five active flavours is then given by

$$F_{a_1 a_2}^5(x_1, x_2, y; \mu) = \frac{1}{\pi y^2} \sum_{a_0} V_{a_1 a_2, a_0}^{cb}(y, m_c, m_b; \mu) \otimes_{12} f_{a_0}^3(\mu) \quad (3.9)$$

with the perturbative expansion

$$V_{a_1 a_2, a_0}^{cb}(z_1, z_2, y, m_c, m_b; \mu) = \sum_{k=1}^{\infty} [a_s^5(\mu)]^k V_{a_1 a_2, a_0}^{cb}(z_1, z_2, y, m_c, m_b; \mu). \quad (3.10)$$

For brevity, we do not indicate that V^{cb} assumes the presence of 3 light quark flavours.

At LO, the only nonzero kernels for observed heavy flavours are

$$\begin{aligned} V_{c\bar{c}, g}^{cb(1)}(z_1, z_2, y, m_c, m_b) &= V_{Q\bar{Q}, g}^{Q(1)}(z_1, z_2, y, m_c), \\ V_{b\bar{b}, g}^{cb(1)}(z_1, z_2, y, m_c, m_b) &= V_{Q\bar{Q}, g}^{Q(1)}(z_1, z_2, y, m_b), \end{aligned} \quad (3.11)$$

and their polarised counterparts, whereas for observed light flavours one has $V_{a_1 a_2, a_0}^{cb(1)} = V_{a_1 a_2, a_0}^{Q(1)}$.

3.2 Schemes for one massive flavour

In this subsection, we consider a setting with n_F light flavours and one heavy flavour Q . The DPD for $n_F + 1$ active flavours is characterised by three mass scales: the scale Λ of nonperturbative interactions, the scale μ_y associated with the distance between the two observed partons, and the mass of the heavy quark, which satisfies $m_Q \gg \Lambda$. The DPD factorises in different ways depending on the size of μ_y .

For $\mu_y \sim \Lambda$, the dynamics for the production of light flavours is purely nonperturbative and encoded in the n_F flavour DPD F^{n_F} . The DPD for $n_F + 1$ active flavours, including the production of heavy quarks, is then given by flavour matching for each of the two partons and given by equation (2.25).

For $\mu_y \gg \Lambda$, the dynamics at nonperturbative scales is contained in PDFs for the n_F light flavours, and we can distinguish three different factorisation regimes.

1. For $\mu_y \ll m_Q$, the dynamics at scales $\sim \mu_y$ is contained in the DPD splitting kernel V^{n_F} that describes the transition from the parton in the PDF to two light partons in an n_F flavour DPD. The dynamics at scales $\sim m_Q$ is contained in the flavour matching kernels for the transition from F^{n_F} to F^{n_F+1} . This corresponds to factorised graphs as shown in figure 1(a).
2. For $\mu_y \sim m_Q$, splitting and heavy-quark excitation take place at the same scale, and the transition from the light parton in the PDF to the observed partons of the DPD is described by the massive splitting kernel V^{Q, n_F} introduced in the previous subsection. The structure of the corresponding graphs is given in figure 1(b).
3. For $\mu_y \gg m_Q$, the quark mass effects are contained in the matching kernel for the transition from PDFs f^{n_F} to PDFs f^{n_F+1} . The $1 \rightarrow 2$ splitting happens at much higher scales μ_y and is described by the massless splitting kernel V^{n_F+1} . The factorised graphs have the form of figure 1(c).

In section 5.3 we will use the preceding analysis to derive the limiting forms of V^{Q, n_F} for small and for large y . In the following, we discuss two schemes to compute the DPD in the full range of perturbative y . We will briefly comment on the transition to nonperturbative y in section 3.3.

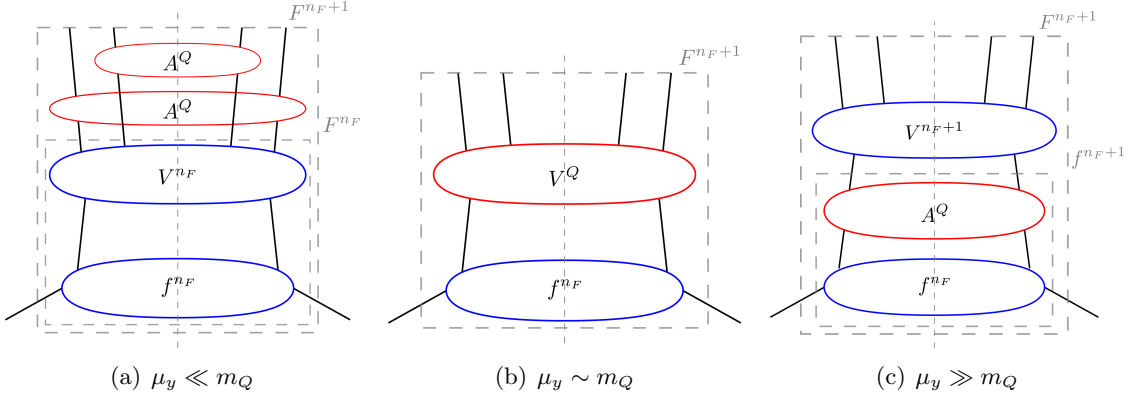


Figure 1: The factorisation regimes for an $n_F + 1$ flavour DPD in different regions of $\mu_y \gg \Lambda$. Kernels with superscript Q are computed with the heavy flavour Q treated as massive, whereas kernels with superscripts n_F and $n_F + 1$ are computed for n_F or $n_F + 1$ massless quark flavours, respectively. For brevity, we omit the superscript n_F in A^Q and V^Q .

3.2.1 Scheme with massless splitting kernels

We start with a simplified scheme in which only the splitting formula (2.26) for massless quarks is used. Not surprisingly, this requires rather coarse approximations. One may nevertheless want to use such a scheme, e.g. because at NLO accuracy only massless splitting kernels are presently available.

In this purely massless scheme, one directly switches from the description of figure 1(a) to the one of figure 1(c) at a scale $\mu_y = b_0/y = \gamma m_Q$. The choice of the scheme parameter γ will be discussed in section 4.2.1; we anticipate that values $\gamma \sim 1$ are most appropriate.

For $\mu_y < \gamma m_Q$, the splitting DPD is computed for n_F massless flavours from an n_F flavour PDF. This is done at a renormalisation scale

$$\mu_{\text{split}} \sim \mu_y \quad (3.12)$$

to avoid large logarithms spoiling the perturbative expansion of the splitting kernel. The DPD is then evolved to the scale

$$\mu_Q \sim m_Q, \quad (3.13)$$

where flavour matching of the DPD from n_F to $n_F + 1$ active flavours is performed. The corresponding formulae read

$$\begin{aligned}
 F_{a_1 a_2}^{n_F}(y; \mu_{\text{split}}) &= \frac{1}{\pi y^2} \sum_{a_0} V_{a_1 a_2, a_0}^{n_F}(y; \mu_{\text{split}}) \otimes_{12} f_{a_0}^{n_F}(\mu_{\text{split}}), \\
 F_{a_1 a_2}^{n_F+1}(y; \mu_Q) &= \sum_{b_1, b_2} A_{a_1 b_1}^{Q, n_F}(m_Q; \mu_Q) \otimes_1 A_{a_2 b_2}^{Q, n_F}(m_Q; \mu_Q) \otimes_2 F_{b_1 b_2}^{n_F}(y; \mu_Q) \\
 &\quad \text{for } \mu_y < \gamma m_Q. \quad (3.14)
 \end{aligned}$$

For $\mu_y > \gamma m_Q$, the splitting DPD is computed for $n_F + 1$ massless flavours from an $n_F + 1$ flavour PDF:

$$F_{a_1 a_2}^{n_F+1}(y; \mu_{\text{split}}) = \frac{1}{\pi y^2} \sum_{a_0} V_{a_1 a_2, a_0}^{n_F+1}(y; \mu_{\text{split}}) \otimes_{12} f_{a_0}^{n_F+1}(\mu_{\text{split}}) \quad \text{for } \mu_y > \gamma m_Q \quad (3.15)$$

with μ_{split} as in (3.12). The $n_F + 1$ flavour DPD at any other scale is then obtained by evolution from the starting conditions in (3.14) or (3.15). The transition from n_F to $n_F + 1$

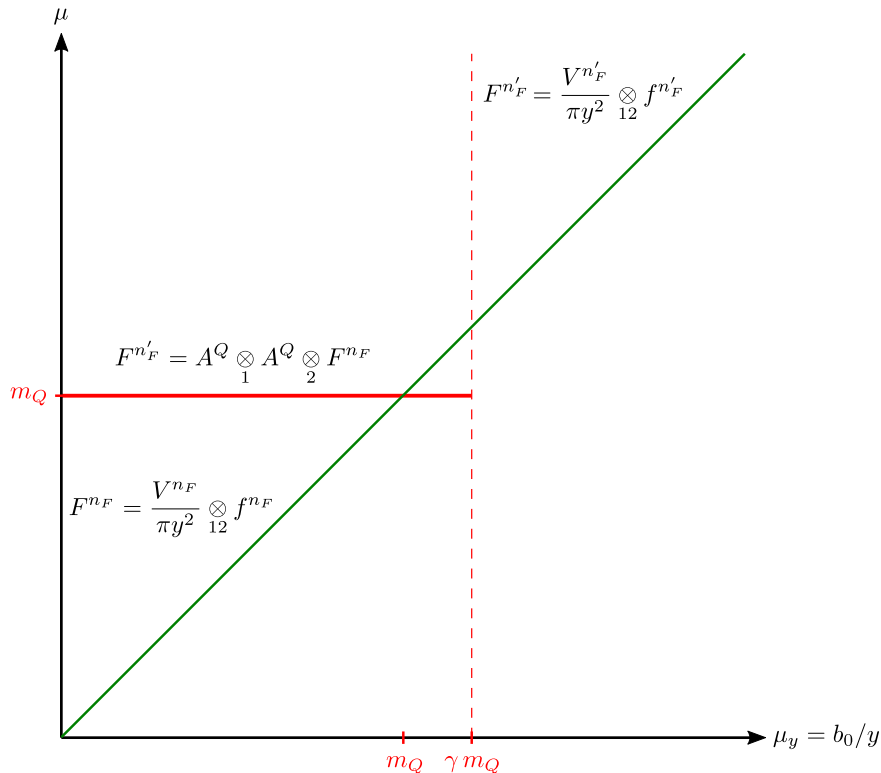


Figure 2: Illustration of the scheme with only massless splitting kernels. The green line indicates the scale $\mu_{\text{split}} = \mu_y$ at which the DPD splitting formulae are evaluated, and the solid red line indicates the scale $\mu_Q = m_Q$ used for DPD flavour matching. For brevity, we write $n'_F = n_F + 1$ and omit the superscript n_F in A^Q . The region of nonperturbatively small μ_y is not included in the plot (i.e. the zero point is suppressed on the axes for μ_y and μ).

flavours in the PDF is obtained by flavour matching:

$$f_{a_0}^{n_F+1}(\mu_Q) = \sum_{b_0} A_{a_0 b_0}^{Q, n_F}(m_Q; \mu_Q) \otimes f_{b_0}(\mu_Q). \quad (3.16)$$

Here and in the following it is understood that flavour matching for the strong coupling is also performed at the scale μ_Q . A graphical representation of this scheme is given in figure 2.

The approach just described has an obvious shortcoming. It lacks the heavy-quark contributions that can be produced by splitting for $\mu_y < \gamma m_Q$, and it neglects the effects of finite m_Q in the splitting kernels for $\mu_y > \gamma m_Q$, even though these effects can only be neglected for $\mu_y \gg m_Q$. An indication of these shortcomings is that the DPDs for some flavour combinations have large unphysical discontinuities at $\mu_y = \gamma m_Q$, as we will see in section 4.1.1. Nevertheless, we will show in section 4.2.1 that, after one integrates over y to obtain a double parton luminosity (1.1), the massless scheme can actually give a fair approximation of the more realistic scheme presented next.

3.2.2 Scheme with massive splitting kernels

We now consider the case where the massive splitting kernels are used. For the transition between the three regimes shown in figure 1, we introduce two scales αm_Q and βm_Q with $\alpha \ll 1$ and $\beta \gg 1$. For $\mu_y < \alpha m_Q$ or $\mu_y > \beta m_Q$, it is appropriate to use the two-step factorisation

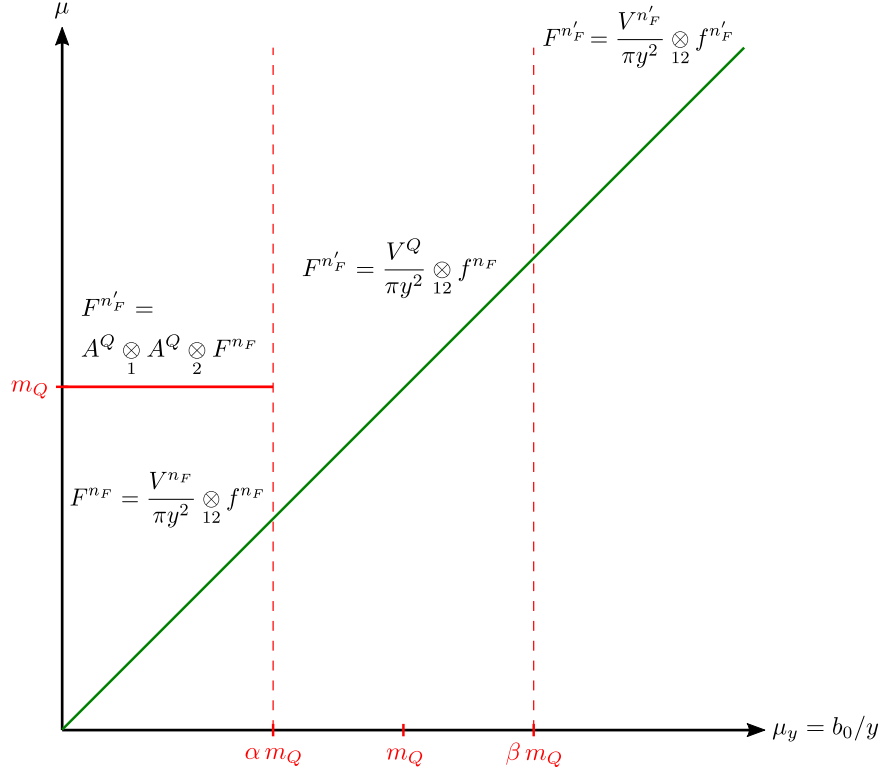


Figure 3: As figure 2, but for the scheme with massless and massive splitting kernels. For brevity, we write $n'_F = n_F + 1$ and omit the superscript n_F in A^Q and V^Q .

of figure 1(a) or figure 1(c), respectively. In the intermediate region $\alpha m_Q < \mu_y < \beta m_Q$, one uses the massive splitting formula (3.3).

The choice of the scheme parameters α and β is a matter of compromise. To minimise the errors inherent in the two-step factorisation schemes, one should take α small and β large enough. On the other hand, the splitting kernels V^{Q,n_F} in the intermediate regime contain logarithms $\log(\mu/m_Q)$ and $\log(\mu/\mu_y)$ at higher orders in a_s , which cannot be kept small for any choice of renormalisation scale μ if the interval from α to β becomes too large.

The scheme just described is represented in figure 3. The splitting DPD is computed from

$$\begin{aligned}
 F_{a_1 a_2}^{n_F}(y; \mu_{\text{split}}) &= \frac{1}{\pi y^2} \sum_{a_0} V_{a_1 a_2, a_0}^{n_F}(y; \mu_{\text{split}}) \otimes_{12} f_{a_0}^{n_F}(\mu_{\text{split}}), \\
 F_{a_1 a_2}^{n_F+1}(y; \mu_Q) &= \sum_{b_1, b_2} A_{a_1 b_1}^{Q, n_F}(m_Q; \mu_Q) \otimes_1 A_{a_2 b_2}^{Q, n_F}(m_Q; \mu_Q) \otimes_2 F_{b_1 b_2}^{n_F}(y; \mu_Q) \\
 &\quad \text{for } \mu_y < \alpha m_Q, \quad (3.17)
 \end{aligned}$$

from

$$F_{a_1 a_2}^{n_F+1}(y; \mu_{\text{split}}) = \frac{1}{\pi y^2} \sum_{a_0} V_{a_1 a_2, a_0}^{Q, n_F}(y, m_Q; \mu_{\text{split}}) \otimes_{12} f_{a_0}^{n_F}(\mu_{\text{split}}) \quad \text{for } \alpha m_Q < \mu_y < \beta m_Q, \quad (3.18)$$

and from

$$F_{a_1 a_2}^{n_F+1}(y; \mu_{\text{split}}) = \frac{1}{\pi y^2} \sum_{a_0} V_{a_1 a_2, a_0}^{n_F+1}(y; \mu_{\text{split}}) \otimes_{12} f_{a_0}^{n_F+1}(\mu_{\text{split}}) \quad \text{for } \mu_y > \beta m_Q \quad (3.19)$$

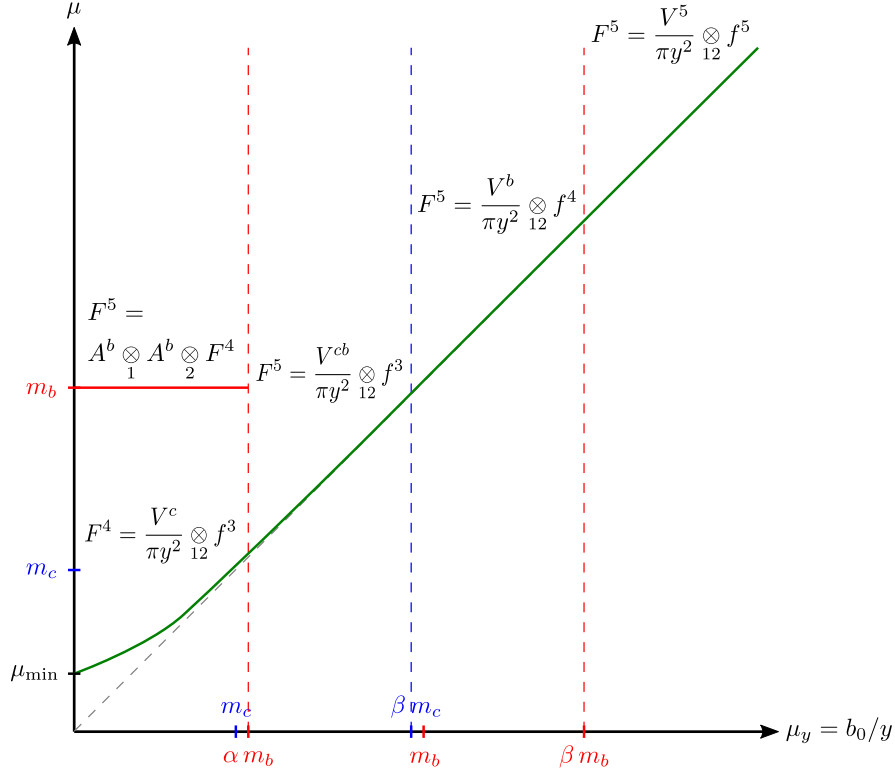


Figure 4: Illustration of the massive scheme for charm and bottom quarks. The green line indicates the splitting scale $\mu_{\text{split}} = \mu_{y^*}$ specified in equation (3.1) and below, and the solid red line indicates the flavour matching scale $\mu_b = m_b$.

with f^{n_F+1} given by (3.16). In all cases, we take renormalisation scales $\mu_{\text{split}} \sim \mu_y$ and $\mu_Q \sim m_Q$ as before. We will explain in section 5.6 why we prefer the choice $\mu_{\text{split}} \sim \mu_y$ in the massive kernels V^{Q,n_F} , where one may alternatively consider scales that depend on m_Q or on both y and m_Q .

3.3 Two heavy flavours (charm and bottom)

For two quark masses that are far apart, such as m_b and m_t , the schemes described above can easily be combined sequentially. However, the masses m_c and m_b are not well separated, and there is a region of y where it is appropriate to keep both of them in the $1 \rightarrow 2$ splitting kernels.

A scheme that takes this into account is shown in figure 4. The general idea remains the same as in the case of a single heavy flavour, with the main difference being that now there is a regime where both the c and b quarks are treated as massive. Notice that this scheme does *not* include a separate region $\mu_y < \alpha m_c$ where the charm quark would be absent in the $1 \rightarrow 2$ splitting process and generated by flavour matching from F^3 to F^4 . This is because for $\alpha \ll 1$, the value of αm_c is not large compared with nonperturbative scales. The $n_F = 4$ splitting DPD is thus computed with the massive kernel $V^{c,3} = V^{Q,3}$.

In addition, the figure explicitly shows that for low μ_y the splitting is to be computed at the modified scale μ_{y^*} of equation (3.1) rather than at μ_y , in order to keep scales in the perturbative region. Moreover, for values of y where μ_{y^*} differs appreciably from μ_y , the perturbative splitting formula for DPDs loses its validity. One way to deal with this issue is described in section 4.1.

The computation of the DPD at perturbative values of y thus proceeds as follows:

$$\begin{aligned}
F_{a_1 a_2}^4(y; \mu_{\text{split}}) &= \frac{1}{\pi y^2} \sum_{a_0} V_{a_1 a_2, a_0}^{c,3}(y, m_c; \mu_{\text{split}}) \otimes_{12} f_{a_0}^3(\mu_{\text{split}}), \\
F_{a_1 a_2}^5(y; \mu_b) &= \sum_{b_1, b_2} A_{a_1 b_1}^{b,4}(m_b; \mu_b) \otimes_1 A_{a_2 b_2}^{b,4}(m_b; \mu_b) \otimes_2 F_{b_1 b_2}^4(y; \mu_b) \quad \text{for } \mu_y < \alpha m_b \quad (3.20)
\end{aligned}$$

with $\mu_{\text{split}} \sim \mu_{y^*}$ and $\mu_b \sim m_b$,

$$F_{a_1 a_2}^5(y; \mu_{\text{split}}) = \frac{1}{\pi y^2} \sum_{a_0} V_{a_1 a_2, a_0}^{cb}(y, m_c, m_b; \mu_{\text{split}}) \otimes_{12} f_{a_0}^3(\mu_{\text{split}}) \quad \text{for } \alpha m_b < \mu_y < \beta m_c, \quad (3.21)$$

$$F_{a_1 a_2}^5(y; \mu_{\text{split}}) = \frac{1}{\pi y^2} \sum_{a_0} V_{a_1 a_2, a_0}^{b,4}(y, m_b; \mu_{\text{split}}) \otimes_{12} f_{a_0}^4(\mu_{\text{split}}) \quad \text{for } \beta m_c < \mu_y < \beta m_b, \quad (3.22)$$

and

$$F_{a_1 a_2}^5(y; \mu_{\text{split}}) = \frac{1}{\pi y^2} \sum_{a_0} V_{a_1 a_2, a_0}^5(y; \mu_{\text{split}}) \otimes_{12} f_{a_0}^5(\mu_{\text{split}}) \quad \text{for } \mu_y > \beta m_b. \quad (3.23)$$

In equations (3.21) to (3.23) one may use either $\mu_{\text{split}} \sim \mu_y$ or $\mu_{\text{split}} \sim \mu_{y^*}$. The PDFs in (3.22) and (3.23) are obtained from f^3 by flavour matching at the appropriate scales.

4 Numerical studies with LO splitting kernels

We now present numerical studies of the schemes introduced in the previous section. Since the massive $1 \rightarrow 2$ splitting kernels are at present only known at leading order, we limit ourselves to that order. The initialisation and scale evolution of the splitting DPDs are performed with the CHILIPDF library [55]. Unless stated otherwise, scale evolution and flavour matching of DPDs, PDFs, and α_s are all performed at LO, with flavor matching done at $\mu_Q = m_Q$. We restrict ourselves to unpolarised partons.

To cover effects from all three heavy quarks, we consider DPDs evolved to the scale $\mu = Q$ at momentum fractions associated with one of the settings

$$n_F = 5, \quad Q = 25 \text{ GeV}, \quad \sqrt{s} = 14 \text{ TeV}, \quad (4.1)$$

$$n_F = 6, \quad Q = 1 \text{ TeV}, \quad \sqrt{s} = 100 \text{ TeV}, \quad (4.2)$$

where Q is the invariant mass of the system produced in each of the hard-scattering processes, and \sqrt{s} is the c.m. energy of the proton-proton collision. Examples of corresponding DPS processes are double dijet production at the LHC for the first setting and double $t\bar{t}$ production at a future hadron collider for the second one. In both cases, Q is significantly larger than the mass of the heaviest active parton in the DPD, so that in the hard-scattering cross section all active partons may be treated as massless.

Given the special interest of like-sign W production for DPS studies [15, 21, 56–61], we also considered the setting

$$n_F = 5, \quad Q = m_W, \quad \sqrt{s} = 14 \text{ TeV}. \quad (4.3)$$

We did not find any features in this setting that are not also present in the one of equation (4.1) and therefore refer to appendix A for its discussion.

4.1 Splitting DPDs

We start by looking at the splitting DPDs. For each of the three settings just discussed, the parton momentum fractions x_1 and x_2 are chosen such that the final-state system corresponding to each hard scatter is produced at central rapidity, i.e.

$$x_1 = x_2 = Q/\sqrt{s}. \quad (4.4)$$

As discussed in section 3.3, we initialise the splitting DPDs at the scale $\mu_{\text{split}} = \mu_{y^*}$, where μ_{y^*} is specified by (3.1) with minimal value $\mu_{\text{min}} = 1 \text{ GeV}$ and by (3.2) with power $p = 4$. In addition, we modify the perturbative splitting formula by multiplying with an exponential damping factor,

$$F_{a_1 a_2}(x_1, x_2, y; \mu) = \exp\left[\frac{-y^2}{4h_{a_1 a_2}}\right] \frac{a_s(\mu)}{\pi y^2} V_{a_1 a_2, a_0}\left(\frac{x_1}{x_1 + x_2}\right) \frac{f_{a_0}(x_1 + x_2; \mu)}{x_1 + x_2}, \quad (4.5)$$

where V is either $V^{(1)}$ or $V^{Q(1)}$. For the damping constants, we take

$$h_{gg} = 4.66 \text{ GeV}^{-2}, \quad h_{gq} = h_{qg} = 5.86 \text{ GeV}^{-2}, \quad h_{qq} = 7.06 \text{ GeV}^{-2}. \quad (4.6)$$

The exponential gives a more realistic behaviour at nonperturbative y while not significantly affecting the perturbative region. For a motivation of the values in (4.6) we refer to section 9.2.1 of reference [13].

For the PDFs in the splitting formula, we take the default LO set of the MSHT20 parametrisation [62], with the associated values $\alpha_s(m_Z) = 0.13$ for the strong coupling and

$$m_c = 1.4 \text{ GeV}, \quad m_b = 4.75 \text{ GeV}, \quad m_t = 172.5 \text{ GeV} \quad (4.7)$$

for the quark masses. We also produced plots for LO sets from HERAPDF2.0 and NNPDF4.0 [63, 64] and find them to be quite similar to the ones for MSHT20.¹ In particular, they lead us to the same conclusions regarding the values of our scheme parameters α , β , and γ .

The focus of our attention is the y dependence of the DPDs evolved to scale μ for different parton combinations. We will plot against $\mu_y = b_0/y$ rather than y , in order to facilitate comparison with the graphs in figures 2 to 4. Let us recall that we need the DPDs for μ_y up to order μ when computing DPS observables.

For a given number n_F of active flavours, we expect that the DPDs are smooth functions of y (and hence of μ_y), since y corresponds to a space-like distance between different fields, and there are no physical production thresholds associated with such a distance. In both the massless and the massive schemes we introduced earlier, we will however find discontinuities at the transition points between regimes where different approximations are made in computing the DPDs. While this is unavoidable, we regard it as desirable to minimise such discontinuities. We will use this as our default criterion to select the parameters α and β in the massive scheme.

4.1.1 Massless scheme

To begin with, we discuss the DPDs in the massless scheme of section 3.2.1, where the splitting DPDs are initialised for $n_F = 3, 4, 5$ or 6 active flavours as μ_y increases, with transition points at γm_c , γm_b , and γm_t . The qualitative features we wish to discuss depend weakly on γ , and we find it sufficient to show plots with $\gamma = 1$ in the following.

In figure 5 we show the DPDs for the jet production setting at $\mu = 25 \text{ GeV}$ introduced above. We see in figure 5(a) that the $c\bar{c}$ distribution has a discontinuity at $\mu_y = \gamma m_c$. This

¹Specifically, we used the sets named MSHT201o_as130, HERAPDF20_LO_EIG, and NNPDF40_lo_pch_as_01180 in the LHAPDF interface [65].

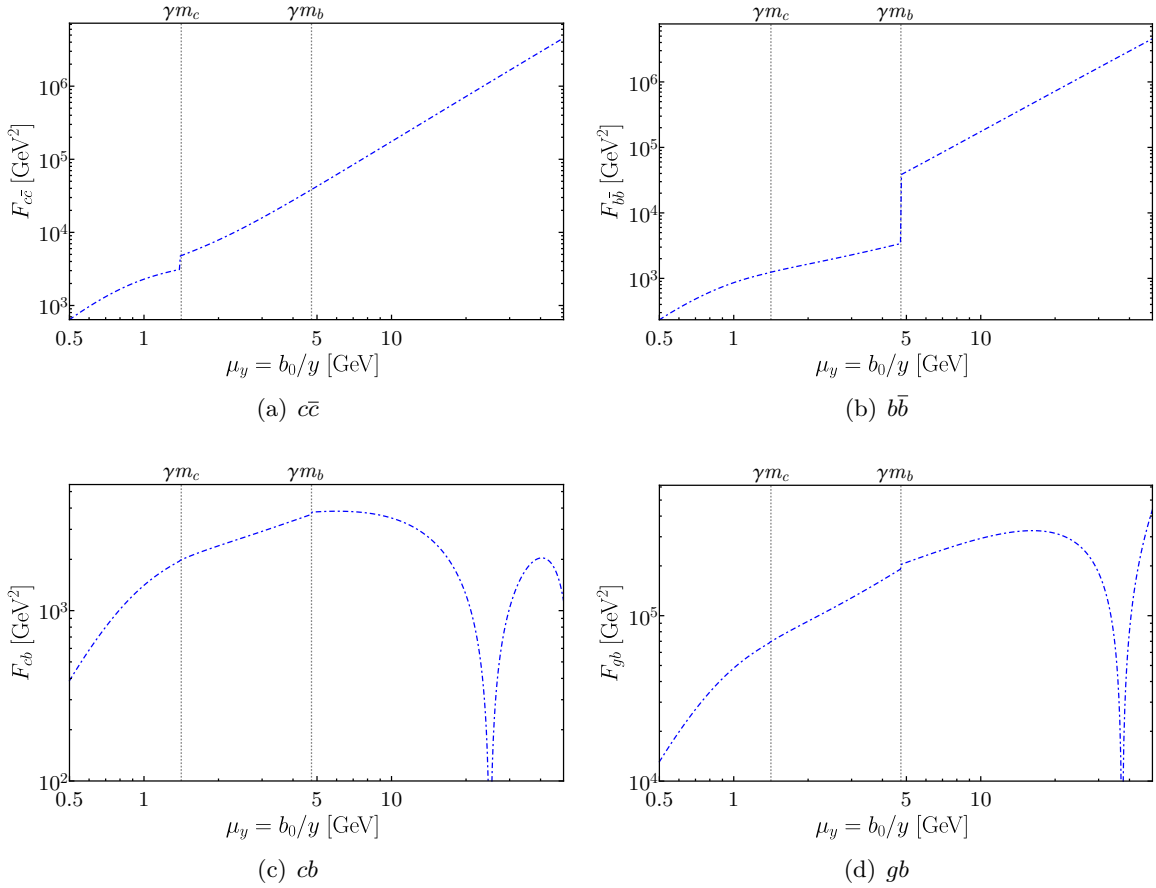


Figure 5: $n_F = 5$ splitting DPDs at $\mu = 25$ GeV for the setting (4.1), computed in the purely massless scheme of section 3.2.1 with $\gamma = 1$. The momentum fractions are $x_1 = x_2 \approx 1.8 \times 10^{-3}$ according to (4.4). Here and in similar figures $|F_{a_1 a_2}|$ is shown.

is readily understood: above this value, charm is treated as massless and $F_{c\bar{c}}$ can be directly produced by $g \rightarrow c\bar{c}$ splitting. Below this value, charm is only produced by evolution above the flavour matching scale $\mu_c = m_c$. For $F_{c\bar{c}}$ this requires two $g \rightarrow c\bar{c}$ splittings in the evolution chain. The discussion of $F_{b\bar{b}}$, shown in 5(b), proceeds in full analogy. The discontinuity is even stronger in this case.

A very different behaviour is seen for the cb distribution in figure 5(c). This parton combination is not produced by direct splitting at LO, but only by scale evolution, which explains the zero crossing at $\mu_y = \mu = 25$ GeV, where no evolution takes place. Above this value, the DPD is actually negative, because one has to evolve backwards from μ_y to μ . To understand the tiny discontinuity of the distribution at γm_b , we note that above this value $F_{b\bar{b}}$ is directly produced by splitting (see figure 5(b)), so that F_{cb} is produced more abundantly by evolution. The corresponding effect at γm_c is too small to be visible in the plot. We remark in passing that when the $1 \rightarrow 2$ splitting is evaluated at NLO, the cb channel can directly be produced by $c \rightarrow cb$ and $b \rightarrow cb$ for $\mu_y > \gamma m_b$, so that one can expect a more pronounced discontinuity in that case.

As an example for a channel with one observed heavy flavour, we show the gb distribution in figure 5(d). We see a small discontinuity at $\mu_y = \gamma m_b$, above which F_{gb} can be produced directly by $b \rightarrow gb$ splitting, or by one evolution step from $F_{b\bar{b}}$. The fact that the discontinuity is not very pronounced suggests that the dominant contribution in this region comes from the

evolution of F_{gg} via a $g \rightarrow b$ splitting. Indeed, one finds that F_{gg} is larger than $F_{b\bar{b}}$ by more than a factor 100 around $\mu_y = \gamma m_b$.

For DPDs with only light flavours, we find a smooth behaviour at the transition points in μ_y , as one may expect. The behaviour of the $n_F = 6$ DPDs in the $t\bar{t}$ setting (4.2) is analogous to the one just discussed and therefore not shown here.

4.1.2 Massive scheme

We now investigate the scheme where massive splitting kernels are used along with massless ones. DPDs with $n_F = 5$ are computed as laid out in section 3.3. DPDs with $n_F = 6$ are obtained from these by flavour matching if $\mu_y < \alpha m_t$, whereas for $\mu_y > \alpha m_t$ the prescription of section 3.2.2 is used. We computed distributions with different scheme parameters, namely $\alpha = 1/2, 1/3, 1/4$ and $\beta = 2, 3, 4$, and will compare a subset of these in the following. We do not consider smaller α or larger β in order to avoid large logarithms in the intermediate mass region, as explained in section 3.2.2.

Let us first look at distributions in setting (4.1), beginning with $F_{b\bar{b}}$ shown in figures 6(a) and 6(b). Instead of the large discontinuity at γm_b in the massless scheme, the massive scheme has a much smaller discontinuity at αm_b and a tiny one at βm_b . The tiny jump at βm_b is due to switching from massive to massless DPD splitting kernels, which according to (3.8) is a small effect, and to changing from a 4 to a 5 flavour gluon density in the splitting formula. Quantitatively, we find that this jump is somewhat smaller for $\beta = 2$ than for $\beta = 4$. The discontinuity at αm_b can also be ascribed to two effects. For μ_y above this value, $b\bar{b}$ can be produced by direct splitting, although the massive splitting kernels are exponentially suppressed at $\mu_y \ll m_b$ according to (3.7). Furthermore, the $b\bar{b}$ distribution is initialised at scale μ_y to the right of αm_b , whereas to the left of this point it can be produced by evolution only above the flavour matching scale $\mu_b = m_b$, i.e. with a shorter evolution path towards the final scale μ . Quantitatively, we find that the absolute size of the discontinuity is smaller for $\alpha = 1/4$ than for $\alpha = 1/2$. Among the scheme parameters we considered, the mildest discontinuities for the $b\bar{b}$ distribution are thus obtained for the combination $\alpha = 1/4$ and $\beta = 2$.

We now turn to the gb distribution shown in figures 6(c) and 6(d), which has only small discontinuities in the massless scheme. In the massive scheme, a discontinuity appears at $\mu_y = \alpha m_b$, and its absolute size varies only weakly with α . To explain this discontinuity, we recall that gb can be produced by one evolution step from the very large gg distribution. Just to the right of the discontinuity, this evolution starts at scale $\mu_y \approx \alpha m_b$, whereas just to the left it starts only at $\mu_b = m_b$. This large difference in evolution length is absent in the massless scheme, where the transition happens at $\mu_y = \gamma m_b$ with $\gamma \sim 1$.

A second (and perhaps more intriguing) feature of the gb distribution in the massive scheme is the significant discontinuity at $\mu_y = \beta m_b$, which strongly increases with β . To understand this behaviour, let us compare how gb can be produced in the massive scheme for the region $\beta m_c < \mu_y < \beta m_b$ and in the massless scheme for $\mu_y > \gamma m_b$ (which coincides with the massive scheme for $\mu_y > \beta m_b$). In the massless scheme, all production modes shown in figure 7 contribute for $\mu_y > \gamma m_b$ and are evaluated with massless $1 \rightarrow 2$ splitting kernels. The PDFs in the splitting formula are evaluated for 5 flavours, and the b quark PDF has been obtained from a four-flavour gluon PDF by flavour matching and subsequent evolution as illustrated in the lower box of figure 7(a). For the contributions in figures 7(b) and 7(c), evolution is necessary to produce the final gb distribution, as indicated by the DGLAP splitting in the upper boxes. This implies that these contributions vanish if the $1 \rightarrow 2$ splitting is evaluated at the target scale, i.e. for $\mu_y = \mu = 25 \text{ GeV}$. As one approaches this point, the direct splitting contribution in figure 7(a) therefore becomes dominant. In

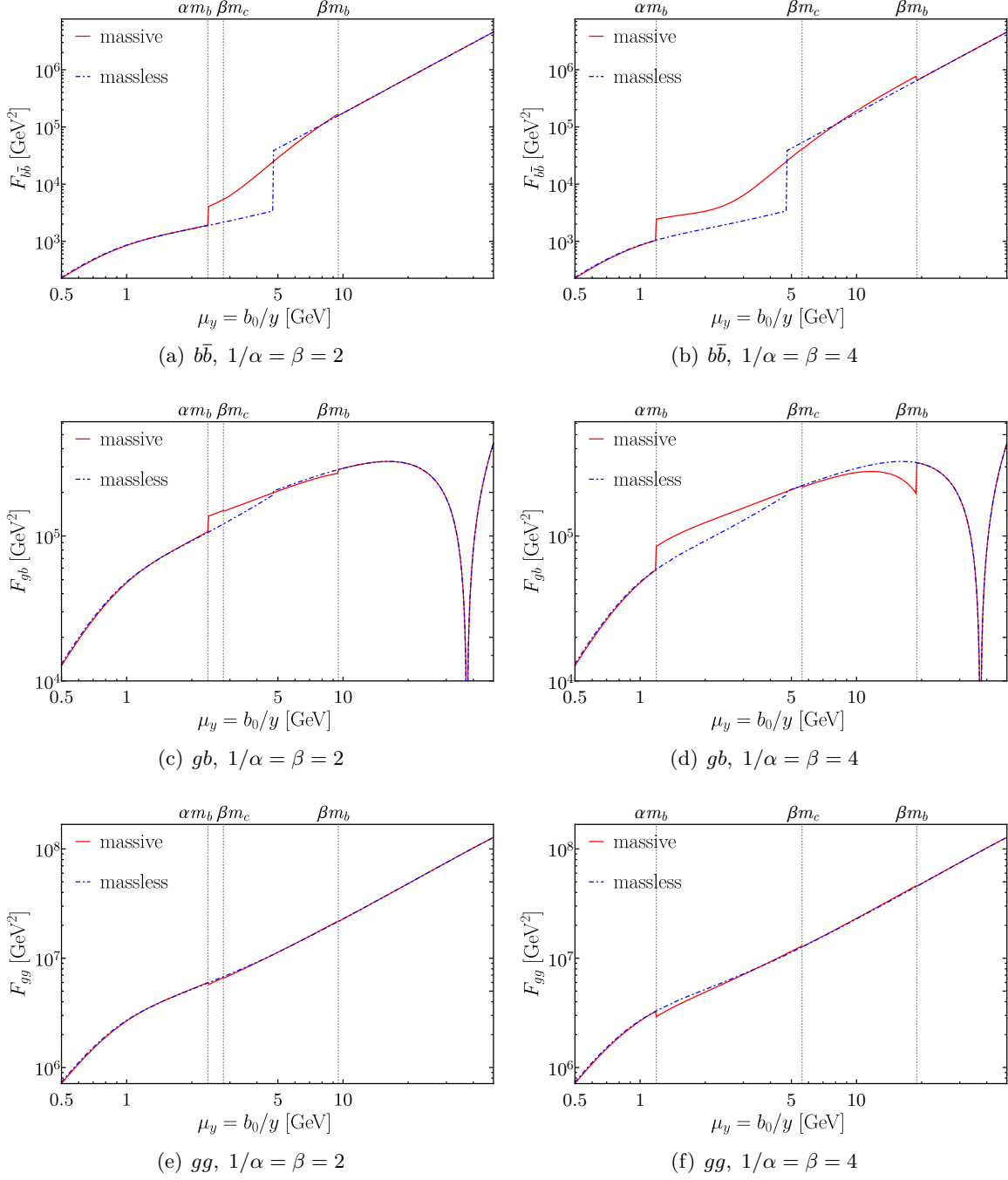


Figure 6: $n_F = 5$ splitting DPDs at $\mu = 25$ GeV for the setting (4.1). Solid lines are for the massive scheme of section 3.3, and dashed lines are for the massless scheme with $\gamma = 1$ (already shown in figure 5).

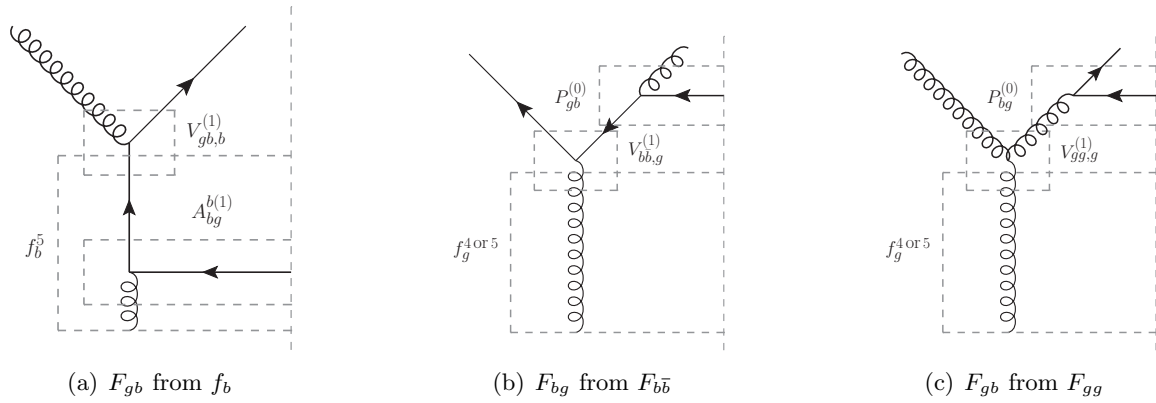


Figure 7: Production modes of F_{gb} for $\mu_y > \gamma m_b$ in the massless scheme and for $\beta m_c < \mu_y < \beta m_b$ in the massive scheme. For $\mu_y > \beta m_b$ the two schemes coincide. Horizontal parton lines correspond to unobserved spectators. In panel (b) F_{bg} is shown for clarity of presentation — from this F_{gb} is readily obtained by swapping the two partons. In the same panel, $V^{(1)}$ must be replaced by $V^{b(1)}$ for $\beta m_c < \mu_y < \beta m_b$ in the massive scheme.

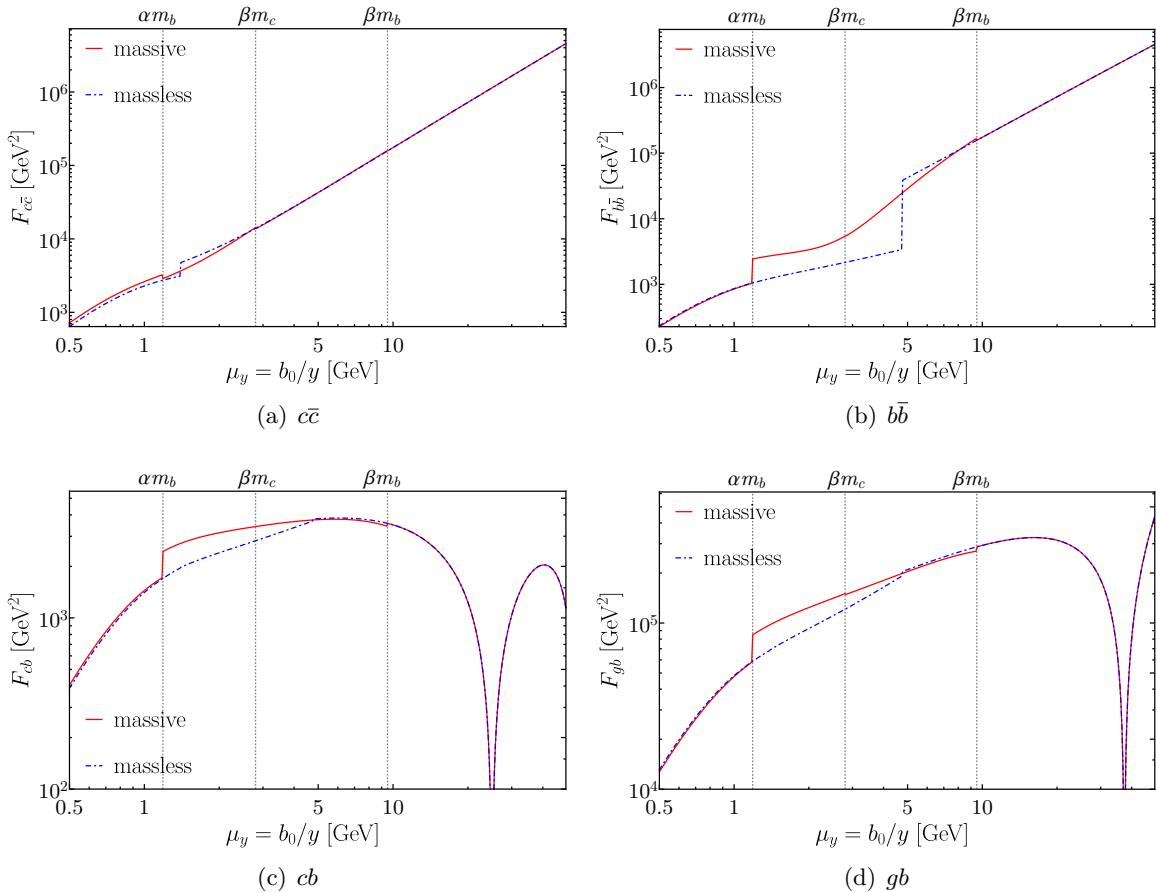


Figure 8: $n_F = 5$ splitting DPDs at $\mu = 25$ GeV for the setting (4.1). Solid lines are for the massive scheme of section 3.3 with our preferred values $\alpha = 1/4$ and $\beta = 2$, and dashed lines are for the massless scheme with $\gamma = 1$.

the massive scheme, the PDFs in the splitting formula are evaluated for four flavours for $\beta m_c < \mu_y < \beta m_b$, so that only the modes in figures 7(b) and 7(c) — now evaluated with four-flavour PDFs and massive $1 \rightarrow 2$ splitting kernels — contribute to the gb distribution. This explains why the discrepancies between the massless and massive scheme become larger the closer one comes to $\mu_y = \mu = 25 \text{ GeV}$ (for any $\beta \leq 25 \text{ GeV}/m_b$).

At which value of β should one switch between the two regions within the massive scheme? For the contribution in figure 7(c), the two regions differ only by the number of active flavours in the gluon distribution, which is a higher-order effect. The contribution in figure 7(b) is evaluated more precisely for $\mu_y < \beta m_b$, because mass effects are included in the kernel for $g \rightarrow b\bar{b}$. For equal momentum fractions of b and \bar{b} , the massive kernel differs from the massless one by more than 100% if $\mu_y = m_b$, but for $\mu_y \geq 2m_b$ the difference is less than 15%. Most importantly, the contribution of figure 7(a) is missing for $\mu_y < \beta m_b$ if one works with LO kernels, which becomes a serious deficiency if β is too large. Our preferred choice is therefore $\beta = 2$, which we already favoured in the description of the $b\bar{b}$ distribution. Notice that the shortcoming of the massive scheme for larger values of β should be mitigated if one could work with splitting kernels at NLO, which include the process $g \rightarrow gb$ of figure 7(a). This provides a particular motivation to study the massive NLO kernels in sections 5 and 8.

The features of the cb distribution in the massive scheme are similar to the gb case, including a discontinuity at βm_b that grows with β (but is less pronounced than for gb). The explanation of this finding is similar to the one just presented. For the $c\bar{c}$ and gc distributions, we find only tiny discontinuities in the massive scheme. We recall that there is no transition point αm_c in this case.

The two-gluon distribution, shown in the bottom row of figure 6, differs only a little between the massive and the massless schemes. Nevertheless, we can see a small discontinuity at αm_b , which is more pronounced for smaller α . Visibly, it matters that to the left of this point, gluons evolve with $n_F = 4$ flavours up to the scale $\mu_b = m_b$ and with $n_F = 5$ flavours above, whereas to the right of this point, they evolve with $n_F = 5$ starting at the initialisation scale μ_y . Similar small discontinuities are seen in DPDs for light quark flavours, showing their sensitivity to the gluon distribution during evolution. Of course, the presence of these small discontinuities in the massive scheme does *not* lead us to conclude that it is less realistic than the massless one (which makes more drastic approximations). Clearly, the absence of discontinuities in the y dependence does not guarantee that an approximation for the DPDs is very precise.

To avoid the largest discontinuities across different parton channels for the dijet production setting, we choose $\alpha = 1/4$ and $\beta = 2$ as our preferred scheme parameters. In figure 8 we show the corresponding DPDs for the same parton combinations that we already presented in figure 5 for the massless scheme.

To see whether the same parameters give a good description in other situations, we show in figure 9 the $t\bar{t}$ and gt distributions for the $t\bar{t}$ production setting (4.2). The pattern of discontinuities in the massive scheme is the same as the one we see in figure 6 for b quarks, confirming our above choice of parameters. Remarkably, the discontinuity of the $t\bar{t}$ distribution amounts to almost two orders of magnitude at $\mu_y = \gamma m_t$ in the massless scheme, and to more than one order of magnitude in the massive scheme with $\alpha = 1/2$. DPDs for our preferred scheme parameters are shown in figure 10. It is remarkable that the discontinuities of the $b\bar{b}$ and cb distributions at αm_b are not entirely washed out by evolution to the much larger final scale 1 TeV.

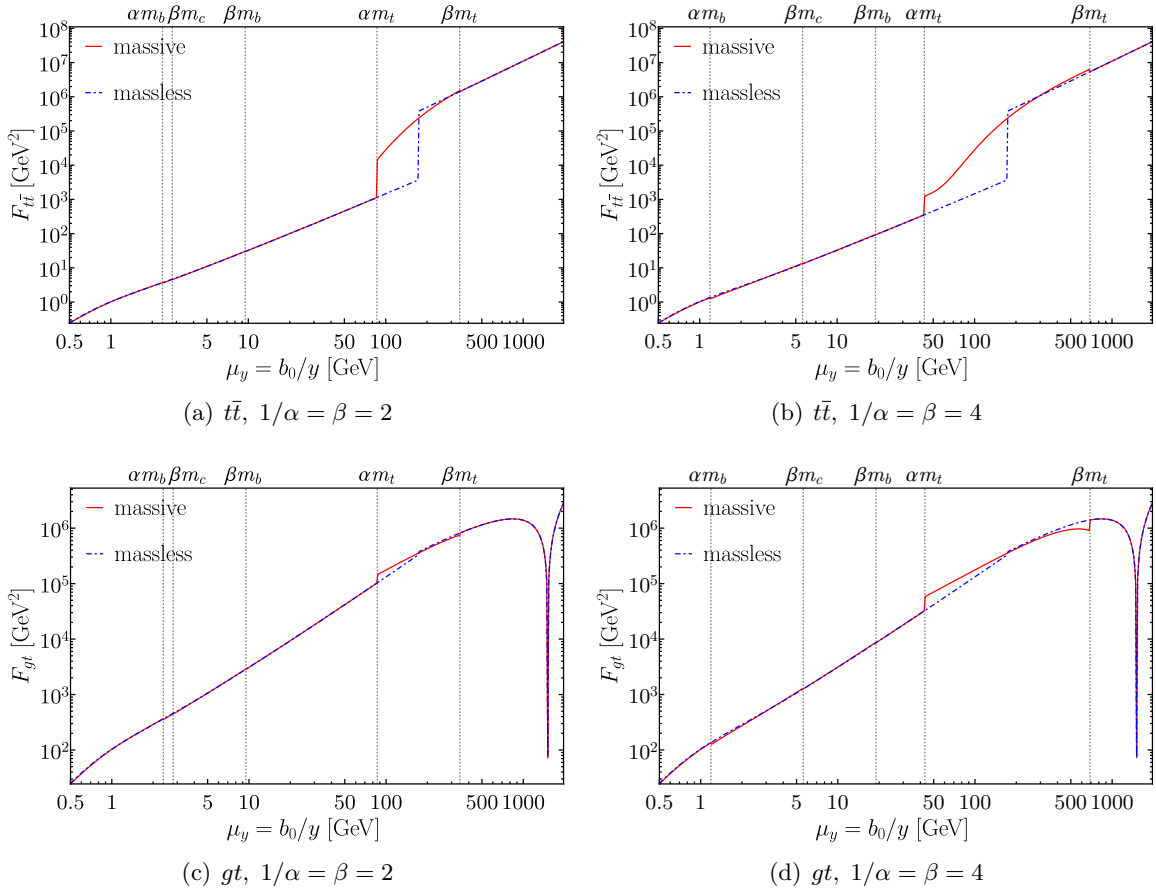


Figure 9: $n_F = 6$ splitting DPDs at $\mu = 1$ TeV for the setting (4.2). Solid lines are for the massive scheme with $1/\alpha = \beta$, and dashed lines are for the massless scheme with $\gamma = 1$. The momentum fractions are $x_1 = x_2 = 10^{-2}$ according to (4.4).

4.2 Double parton luminosities

So far our focus has been on the DPDs and their y dependence. This dependence is not directly observable in DPS processes, where DPDs only appear in integrals over y . As already mentioned in the introduction, the relevant quantities are double parton luminosities

$$\begin{aligned} \mathcal{L}_{a_1 a_2 b_1 b_2}(x_{1a}, x_{2a}, x_{1b}, x_{2b}; \mu, \nu) \\ = \int d^2 y \theta(y - b_0/\nu) F_{a_1 a_2}^{n_F}(x_{1a}, x_{2a}, y; \mu) F_{b_1 b_2}^{n_F}(x_{1b}, x_{2b}, y; \mu), \end{aligned} \quad (4.8)$$

where we express the lower cutoff on y in terms of a momentum scale ν following [13]. We always set $\nu = \mu$ in this section, except for figures 11 and 12.

We evaluate these luminosities at parton momentum fractions that correspond to a kinematic setting where the system produced in the first and second hard scattering has rapidity Y and $-Y$, respectively. For equal invariant mass Q of both systems, this corresponds to

$$x_{1a} = x_{2b} = \frac{Q}{\sqrt{s}} \exp(Y), \quad x_{2a} = x_{1b} = \frac{Q}{\sqrt{s}} \exp(-Y). \quad (4.9)$$

At this point, we recall that the splitting DPDs F^{spl} discussed so far are the leading contribution in a small-distance expansion that contains also an “intrinsic” contribution F^{intr} .

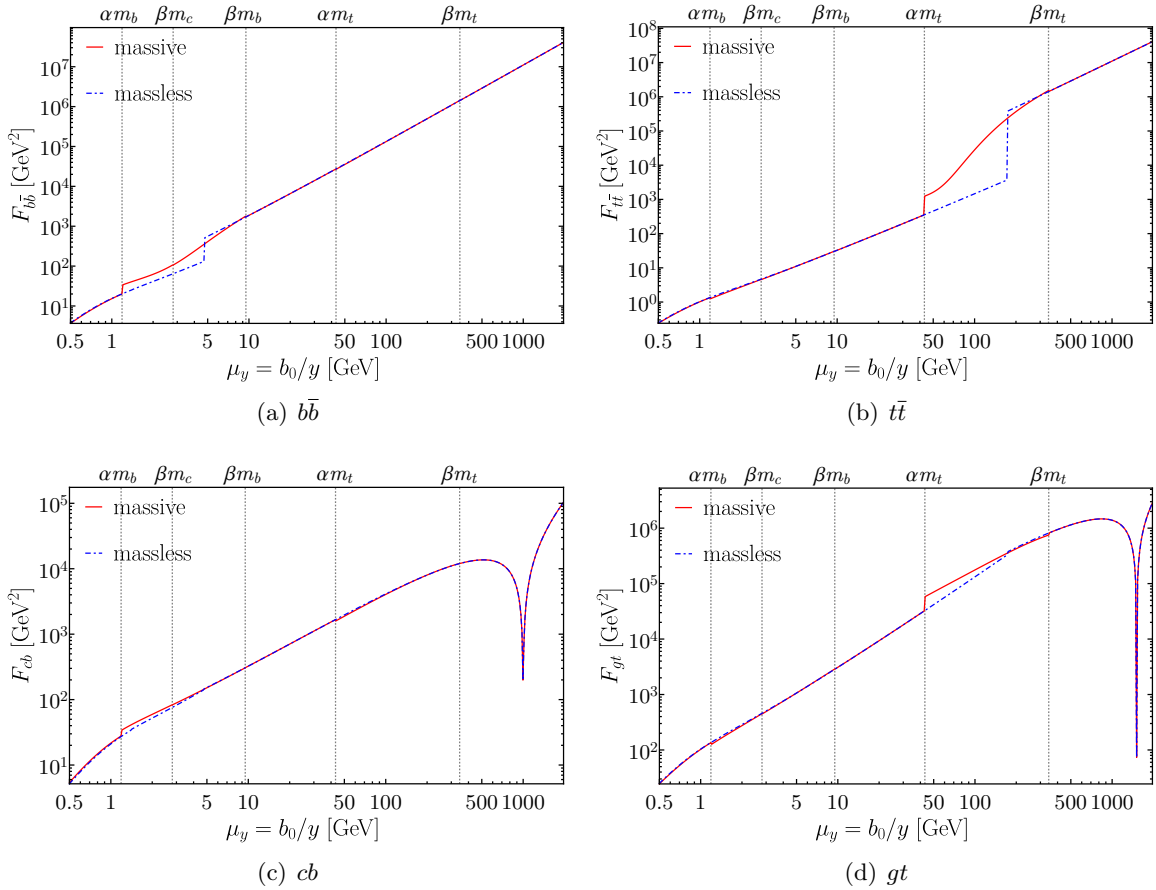


Figure 10: $n_F = 6$ splitting DPDs at $\mu = 1$ TeV for the setting (4.2). Solid lines are for the massive scheme of section 3.3 with our preferred values $\alpha = 1/4$ and $\beta = 2$, and dashed lines are for the massless scheme with $\gamma = 1$.

While subleading in y , this contribution can be important for parton combinations where the splitting DPD is small, and it is generally growing more strongly when the parton momentum fractions decrease.

Following section 9.2.1 of [13], we model the intrinsic contribution as

$$F_{a_1 a_2}^{\text{intr}}(x_1, x_2, y; \mu_0) = \frac{1}{4\pi h_{a_1 a_2}} \exp\left[\frac{-y^2}{4h_{a_1 a_2}}\right] \frac{(1-x_1-x_2)^2}{(1-x_1)^2(1-x_2)^2} f_{a_1}(x_1; \mu_0) f_{a_2}(x_2; \mu_0) \quad (4.10)$$

with $\mu_0 = 1$ GeV. The normalised Gaussian with the widths given in equation (4.6) is used to model the y dependence of the DPDs, and the x_1 and x_2 dependent prefactor ensures a sensible behaviour of the DPDs as the momentum fractions approach the kinematic threshold $x_1 + x_2 \rightarrow 1$. The ansatz (4.10) is made for $n_F = 3$ active flavours, and flavour matching is used to obtain the DPDs for higher n_F .

We note that the distinction between a splitting and an intrinsic part of the DPD is unambiguously defined only in the small y limit; for large y we simply define our DPD model as the sum of the regularised splitting form (4.5) and the intrinsic term (4.10) (after evolving them to a common scale). We emphasise that this model has not been tuned against data and is likely too simplistic, but we estimate that it contains enough realistic features for the studies that will follow.

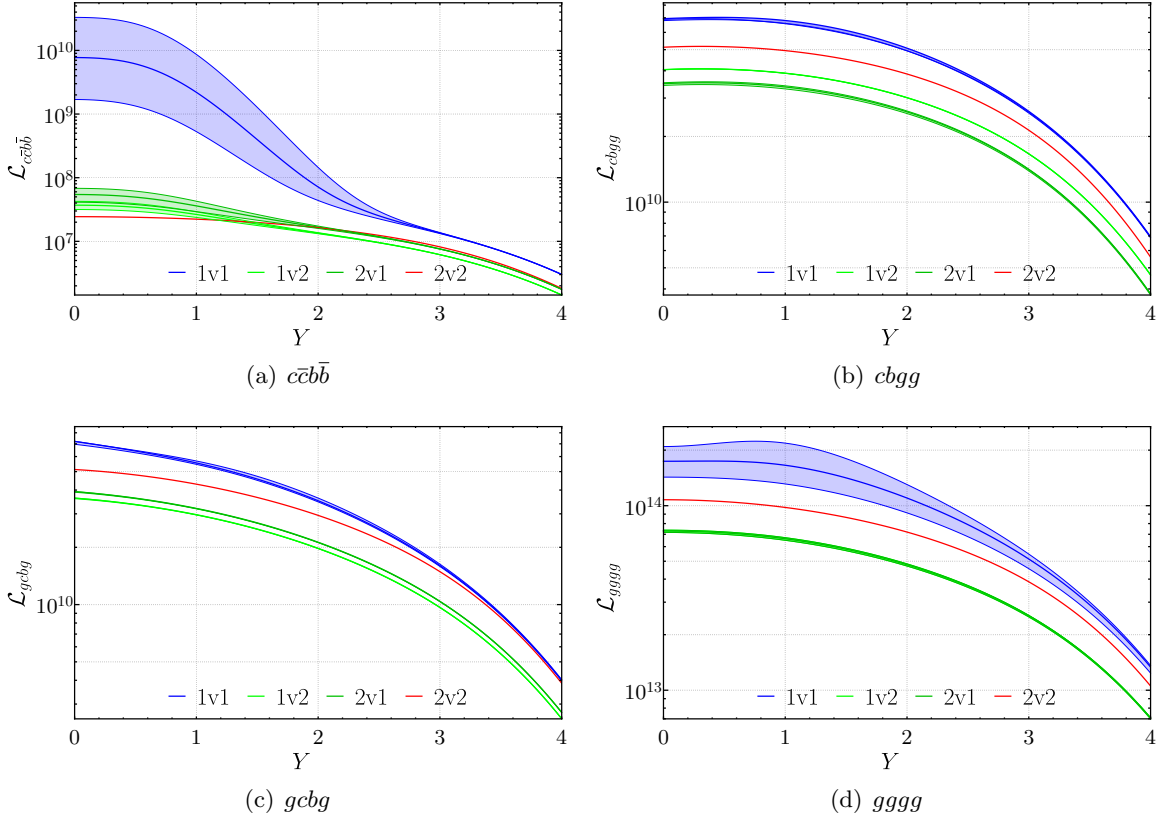


Figure 11: Double parton luminosities at $\mu = 25$ GeV for the dijet production setting, computed in the massive scheme of section 3.3 with $\alpha = 1/4$ and $\beta = 2$. The momentum fractions in the DPDs are specified by equations (4.1) and (4.9). Central values correspond to a cutoff parameter $\nu = \mu$, and bands to the variation of ν between $\mu/2$ and 2μ .

The decomposition $F^{\text{spl}} + F^{\text{intr}}$ induces a decomposition of the double parton luminosity (4.8) into four contributions:

$$\begin{aligned}
 \mathcal{L}_{a_1 a_2 b_1 b_2}^{1v1} &= \int d^2 y F_{a_1 a_2}^{\text{spl}} F_{b_1 b_2}^{\text{spl}}, & \mathcal{L}_{a_1 a_2 b_1 b_2}^{2v2} &= \int d^2 y F_{a_1 a_2}^{\text{intr}} F_{b_1 b_2}^{\text{intr}}, \\
 \mathcal{L}_{a_1 a_2 b_1 b_2}^{1v2} &= \int d^2 y F_{a_1 a_2}^{\text{spl}} F_{b_1 b_2}^{\text{intr}}, & \mathcal{L}_{a_1 a_2 b_1 b_2}^{2v1} &= \int d^2 y F_{a_1 a_2}^{\text{intr}} F_{b_1 b_2}^{\text{spl}},
 \end{aligned} \tag{4.11}$$

where the arguments and integration boundaries are the same as in equation (4.8). The superscripts “1v1”, “1v2” etc. follow the nomenclature introduced in [10].

In figure 11, we show the different contributions to $\mathcal{L}_{c\bar{c}b\bar{b}}$, \mathcal{L}_{cbgg} , \mathcal{L}_{gcbg} , and \mathcal{L}_{gggg} for the dijet production setting (4.1). We see that the 1v1 and 2v2 contributions are of comparable size, except for $\mathcal{L}_{c\bar{c}b\bar{b}}$, where the 1v1 contribution is dominant for small and intermediate values of the rapidity Y . The luminosity for four gluons is by far the largest one.

For the $t\bar{t}$ production setting (4.2), the mass scheme dependence is most pronounced for DPDs containing top quarks, so that we expect significant mass effects for the luminosities $\mathcal{L}_{t\bar{t}t\bar{t}}$ and $\mathcal{L}_{gtg\bar{t}}$ shown in figure 12. We see that for both channels, the 1v1 contribution dominates in the full Y range considered.

At this point, we recall that the luminosities shown here need to be combined with luminosities that correspond to the double counting subtraction terms in the overall cross section. The importance of these terms, which we will not investigate in this work, can be estimated

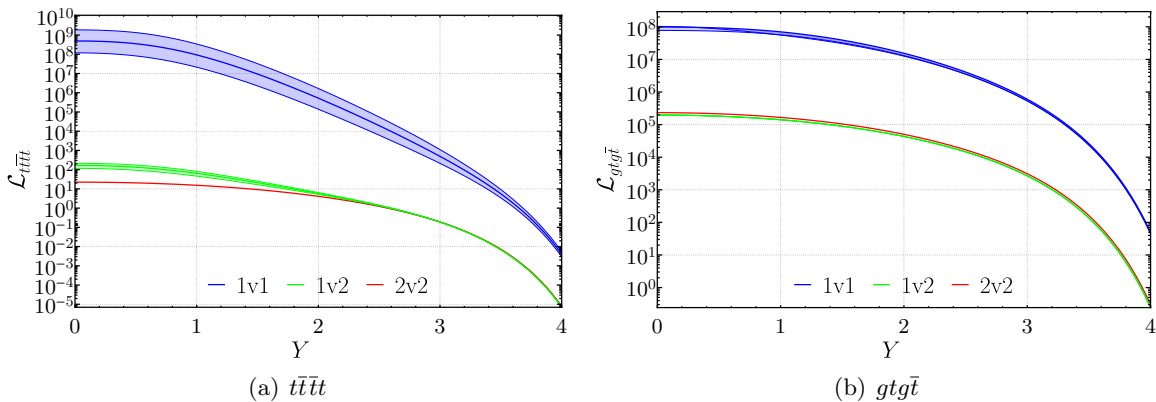


Figure 12: As figure 11 but at $\mu = 1$ TeV for the $t\bar{t}$ production setting (4.2). The 2v1 luminosities are not shown here, because they are almost indistinguishable from the 1v2 ones.

by varying the lower cut-off of the y integration. This is because the dependence on this cut-off approximately cancels between DPS and the subtraction terms, up to perturbative orders that are beyond the accuracy of the calculation. A detailed discussion is given in sections 6.2 and 9.2 of [13]. The largest variation with ν seen in figures 11 and 12 appears in the 1v1 contributions to $c\bar{c}b\bar{b}$, $g\bar{g}g\bar{g}$, and $t\bar{t}t\bar{t}$ at low Y . One can hence expect the double counting subtraction to be most important in these cases.

Given the very different y dependence of F^{spl} and F^{intr} , the dominant region of y in the partial luminosities (4.11) in general differs appreciably between the 1v1 and the 1v2 or 2v1 terms. We can therefore expect corresponding differences in the sensitivity of these terms to details of the heavy-flavour treatment. The 2v2 contribution is of course independent of how heavy quarks are treated in the splitting DPDs.

4.2.1 Dependence on the scheme parameters

We now study how the double parton luminosities depend on the scheme parameters — α and β in the massive scheme and γ in the massless one. To this end, we consider the ratios

$$r(\beta) = \frac{\mathcal{L}_{\text{massive}}(1/\alpha = \beta)}{\mathcal{L}_{\text{massive}}(\alpha = 1/4, \beta = 2)}, \quad r(\gamma) = \frac{\mathcal{L}_{\text{massless}}(\gamma)}{\mathcal{L}_{\text{massive}}(\alpha = 1/4, \beta = 2)}, \quad (4.12)$$

whose denominator is evaluated with our preferred values in the massive scheme (see figures 11 and 12). Within the massive scheme, we plot $r(\beta)$ for a range of values $\beta = 2, 3, 4$ where logarithms in the massive splitting formula remain of moderate size. For the massless scheme, we plot $r(\gamma)$ with $\gamma = 1/2, 1, 2$. We discard values $\gamma < 1/2$, for which quarks are treated as massless in the splitting at scales much below their mass, as well as values $\gamma > 2$, for which direct $g \rightarrow Q\bar{Q}$ splitting is omitted at splitting scales much larger than m_Q .

In figure 13 we show ratios for the different contributions to $\mathcal{L}_{c\bar{c}b\bar{b}}$ in the dijet production setting. Generally, deviations from unity are larger in the massless scheme than in the massive one (note however that different parameters are varied in the two cases). Furthermore, the ratios show a pronounced Y dependence in many cases. If the $b\bar{b}$ pair is produced by splitting (figures 13(a) and 13(c)), the largest deviations are slightly below 30% in the massive scheme and slightly above in the massless one. Deviations are smaller if only the $c\bar{c}$ pair originates from splitting (figure 13(b)). This is in line with the weak scheme dependence we observed for $F_{c\bar{c}}$ in figure 8(a).

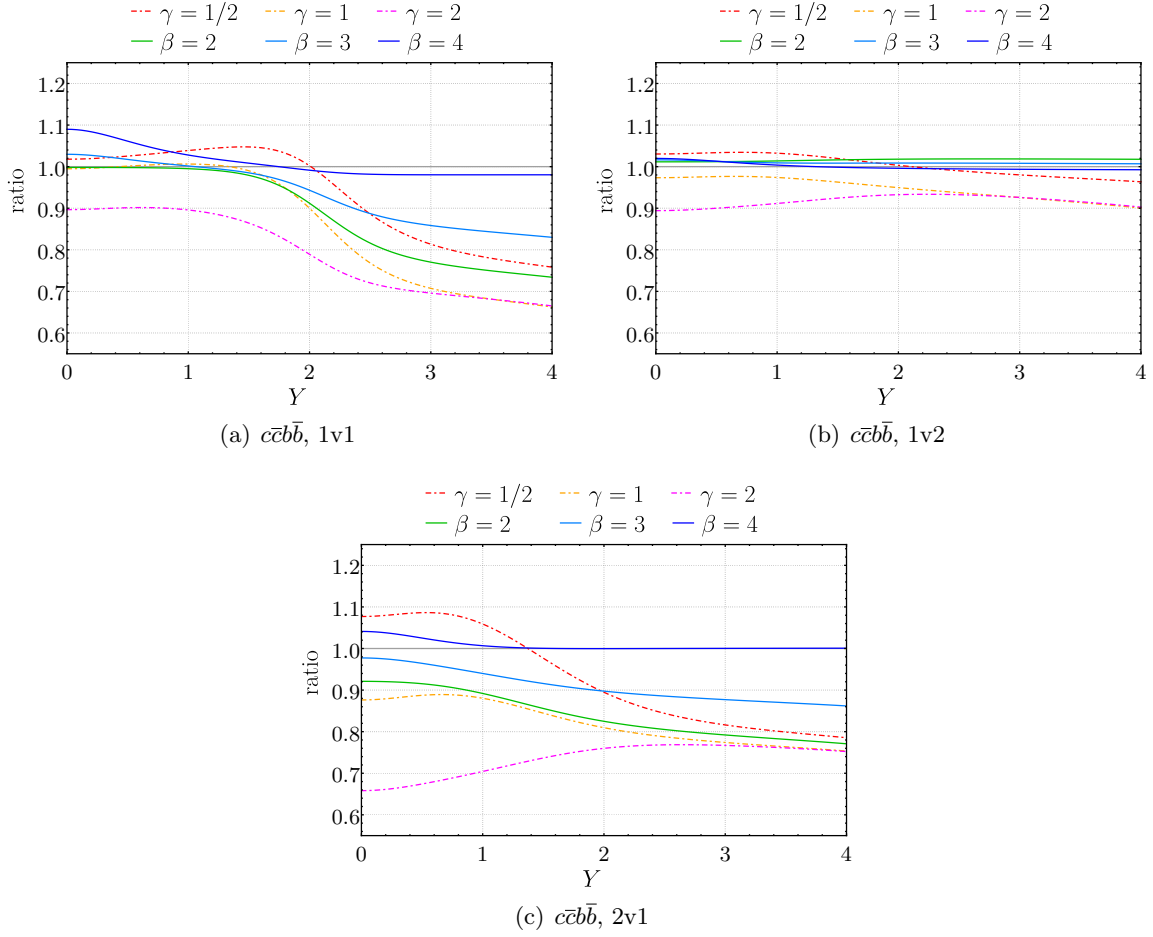


Figure 13: Double parton luminosity ratios (4.12) for $c\bar{c}b\bar{b}$ in the dijet production setting (4.1) with $\nu = \mu = 25$ GeV. Solid (dashed) lines correspond to the numerator computed in the (massless) scheme.

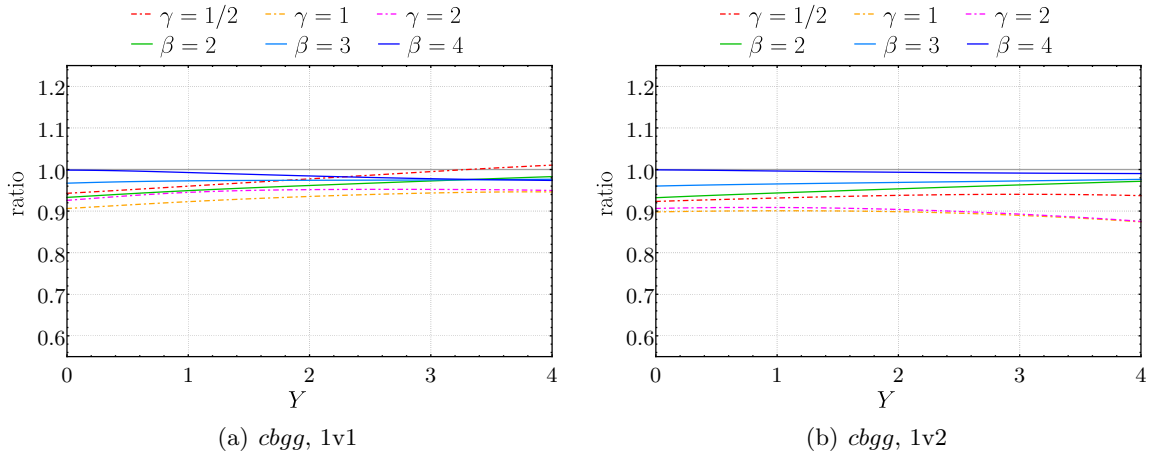


Figure 14: As figure 13, but for the $cbgg$ luminosity. The ratios for the 2v1 contribution deviate from unity by at most 4% and are not shown here.

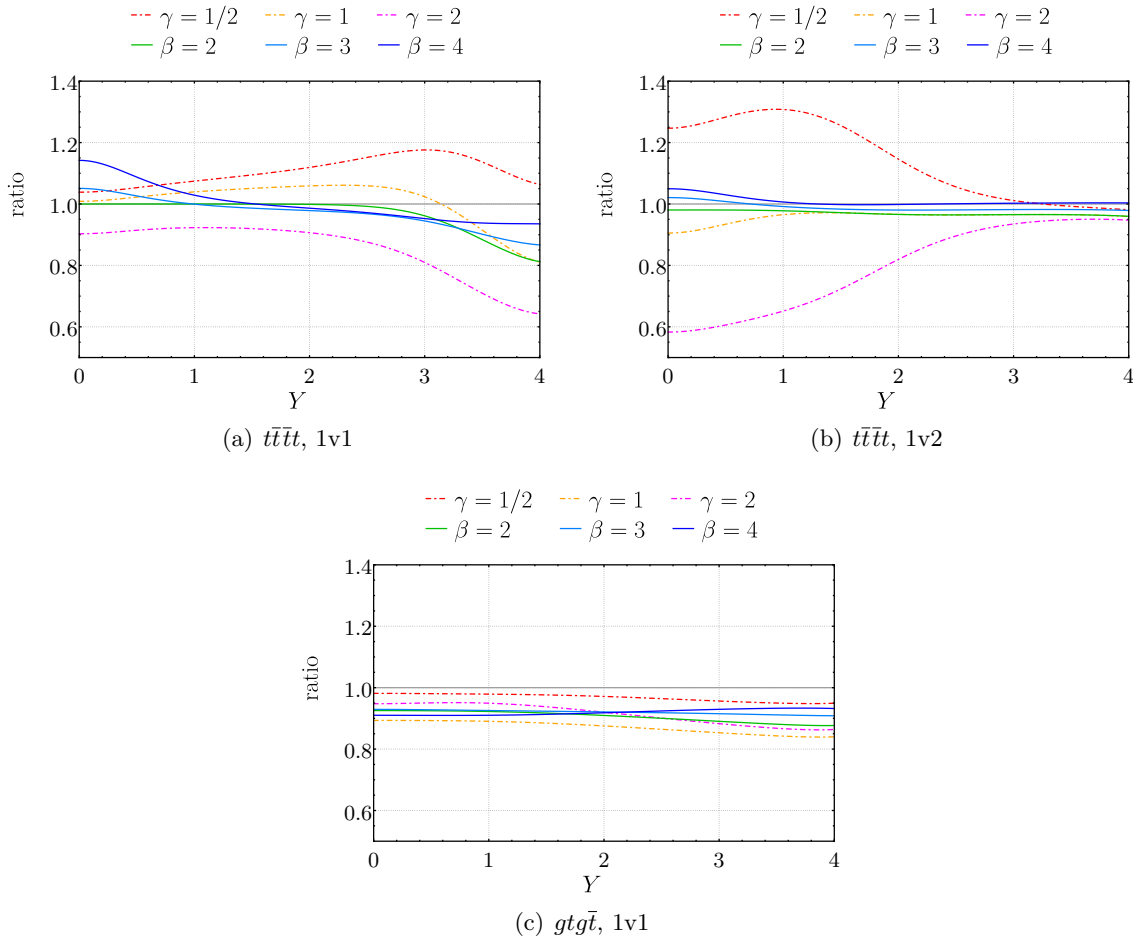


Figure 15: As figure 13, but for selected contributions to the $t\bar{t}t\bar{t}$ and $gtg\bar{t}$ luminosities at $\mu = 1$ TeV for the setting (4.2). The 1v2 and 2v1 contributions to $t\bar{t}t\bar{t}$ are identical to each other. Deviations of the ratio from unity are tiny for the 1v2 and 2v1 contributions to $gtg\bar{t}$ and not shown here.

We now turn to the channels in figure 11 for which the heavy flavours are not directly produced by $1 \rightarrow 2$ splitting. An example is the $cbgg$ channel shown in figure 14. Again, the deviations of the ratios from unity are somewhat larger in the massless scheme than in the massive one, but they remain below 15% in both cases. Deviations in the $gcbg$ luminosity are not larger than those shown for $cbgg$. In the $gggg$ channel, we find a parameter deviations of at most 6%, which originate in the small but visible scheme dependence we observed for F_{gg} in figure 6.

Plots for the $t\bar{t}$ production setting (4.2) are shown in figure 15. Deviations for the $t\bar{t}t\bar{t}$ luminosity reach at most 20% in the massive and at most 40% in the massless scheme. For the $gtg\bar{t}$ channel, effects are smaller in either scheme, and for $gggg$ they do not exceed 1%.

In both settings, we thus find that the largest scheme dependence arises for parton combinations that can directly be produced by $1 \rightarrow 2$ splitting in both DPDs. Results in the massive scheme depend on α and β at the level of at most 30%.

One may ask whether there is a choice of γ in the massless scheme that typically gives the best agreement with the more realistic results in the massive scheme. Whilst for $c\bar{c}b\bar{b}$ luminosities in figure 12, ratios closest to unity are obtained for $\gamma = 1/2$, the preferred value for the $gtg\bar{t}$ luminosities in figure 12 is between $1/2$ and 1. Values below $1/2$ or above 2 would

not improve the global agreement. For $1/2 \leq \gamma \leq 1$ the luminosities in the massless scheme approximately reproduce the ones in the massive scheme with $\alpha = 1/4$ and $\beta = 2$. Typical deviations reach 30% in either direction and can depend strongly on Y , i.e. on the momentum fractions in the DPDs.

4.2.2 Splitting scale variation

To estimate the importance of higher-order corrections in the DPD splitting formulae (2.26) and (3.3), one may vary the scale μ_{split} at which they are evaluated before the DPD is evolved to the final scale μ (with flavour matching at an intermediate scale if appropriate). It is customary to vary the renormalisation scale in a fixed-order formula by a factor of 2 around its central value. We modify this to

$$\min(\mu_{\min}, \mu_{y^*}/2) \leq \mu_{\text{split}} \leq 2\mu_{y^*}, \quad (4.13)$$

which avoids renormalisation scales below $\mu_{\min} = 1 \text{ GeV}$. This results in an asymmetric scale variation for $\mu_{y^*} < 2\mu_{\min}$, which translates to $y > 0.57 \text{ GeV}^{-1}$ with our choice of $y^*(y)$. In the following, we study the impact of this scale variation on double parton luminosities in the massive scheme with $\alpha = 1/4$ and $\beta = 2$.

Starting with the dijet production setting, we show in figure 16 the splitting scale dependence for the same luminosities that were given in figure 11. The variation of the 1v1 terms is far greater than for the 1v2 and 2v1 terms, which is not surprising because the former involve two splitting DPDs and the latter only one. We also observe that the bands are more asymmetric for the sum of the 1v2 and 2v1 terms than for 1v1. This is because the former receive important contributions from the region $y > 0.57 \text{ GeV}$ where the scale variation (4.13) becomes asymmetric. In the channels $cbgg$, $gcbg$, and $gggg$, the scale variation is of considerable size and depends rather weakly on Y . By contrast, the scale variation of for $c\bar{c}b\bar{b}$ is very weak at low Y but large at high Y . An explanation for this remarkable feature is given in appendix A.

The splitting scale dependence of double parton luminosities in the $t\bar{t}$ production setting is shown in figure 17 and shows similarities to the cases just discussed. In the 1v1 terms, we find a large scale variation for $gtg\bar{t}$ at all Y and for $t\bar{t}t\bar{t}$ at high Y .

4.2.3 Variation of the flavour matching scale

Apart from the DPD splitting scale μ_{split} , the evaluation of DPDs in the schemes of section 3 involve a second scale choice, namely for the scale μ_Q at which flavour matching is performed for DPDs, PDFs, and α_s . It is therefore natural to study the impact of varying this scale as well. In analogy to (4.13), we vary the matching scale in the interval

$$\min(\mu_{\min}, m_Q/2) \leq \mu_Q \leq 2m_Q \quad \text{for } Q = c, b, t, \quad (4.14)$$

where the minimum-prescription on the l.h.s. is relevant for the charm quark mass.

In the following, we also compare results with flavour matching evaluated either at LO or at NLO. For the default choice $\mu_Q = m_Q$, this makes no difference, since all one-loop flavour matching kernels are zero at that point. For different scale choices, this is no longer the case. We note that computing A^Q at NLO but V and V^Q at LO corresponds to order α_s in all kernels appearing in the factorised graphs of figure 1. Of course, the overall accuracy remains at LO with such a hybrid choice.

Notice that not only the computation of the splitting DPDs involves flavour matching, but also the evaluation of the intrinsic part F^{intr} . The latter is initialised for $n_F = 3$ flavours

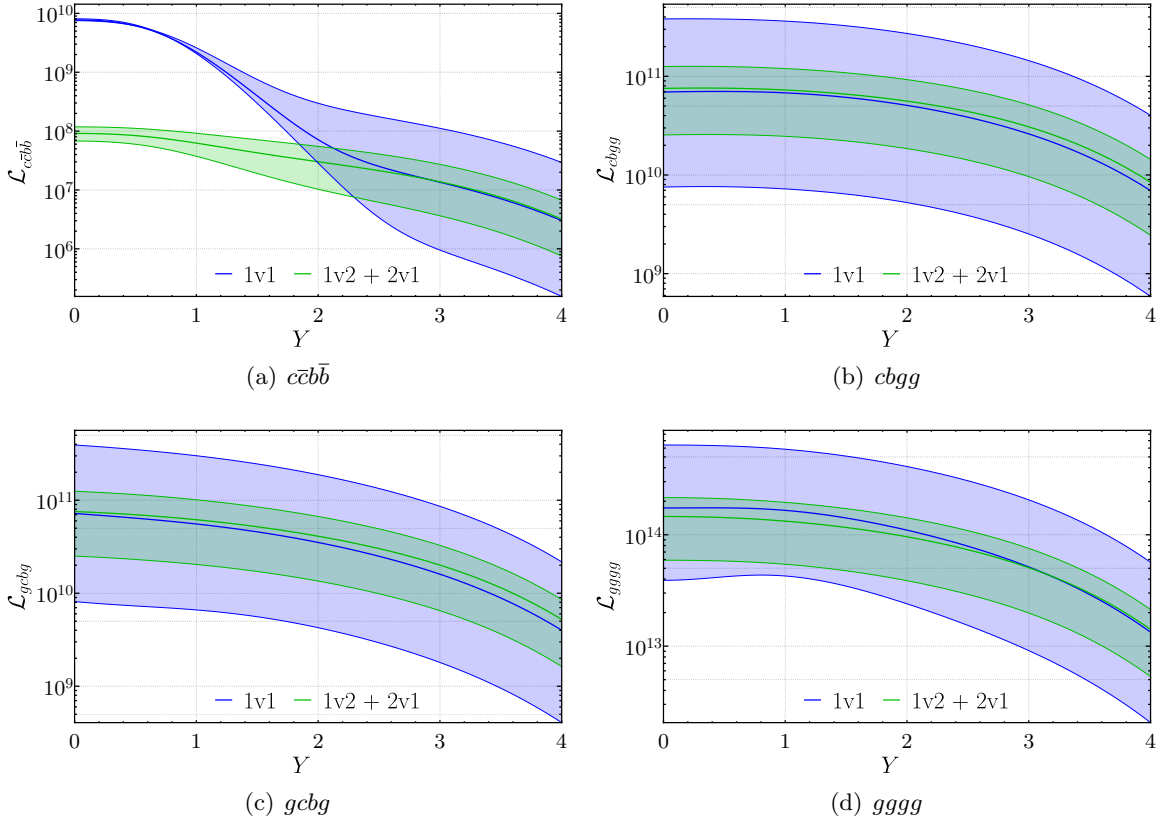


Figure 16: Splitting scale variation of the double parton luminosities shown in figure 11 for the dijet production setting. Central curves are for $\mu_{\text{split}} = \mu_{y^*}$, and bands correspond to the variation specified in (4.13). Notice that the $1v2$ and $2v1$ contributions have been added.

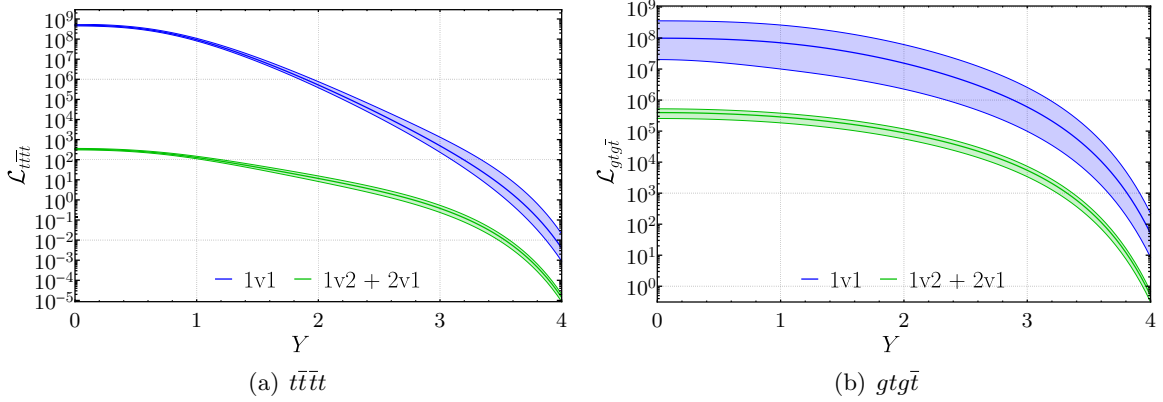


Figure 17: As figure 16, but for the luminosities shown in figure 12 for the $t\bar{t}$ production setting.

for all y and thus requires several steps of DPD flavour matching in our settings with $n_F = 5$ or 6 for dijet or $t\bar{t}$ production, respectively.

The matching scale dependence of luminosities in the dijet production setting is shown in figure 18. With LO flavour matching we find large scale uncertainties, except in $\mathcal{L}_{c\bar{c}b\bar{b}}^{1v1}$ at

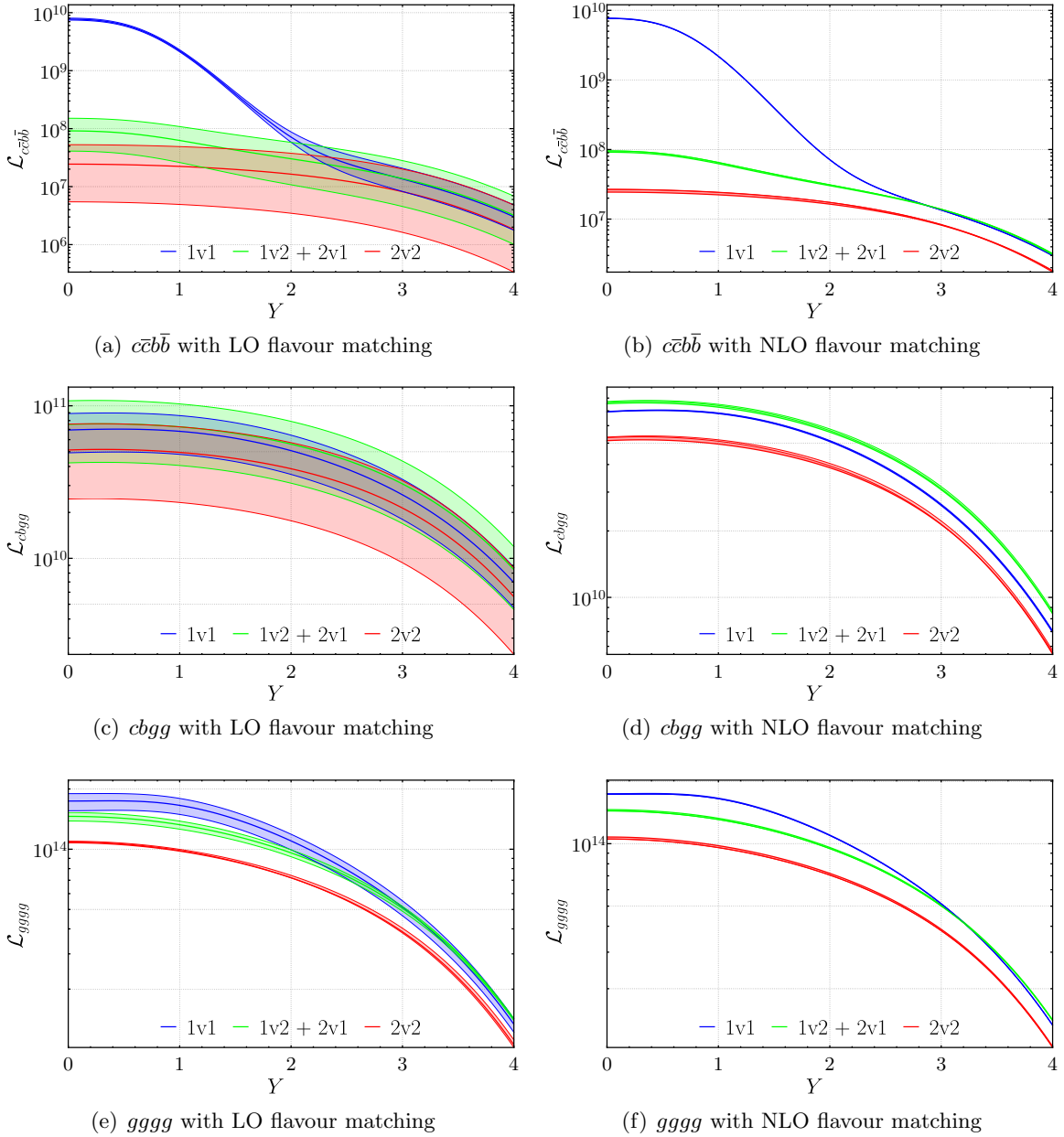


Figure 18: Dependence on the flavour matching scale of the double parton luminosities shown in figure 11 for the dijet production setting. Central curves are for $\mu_Q = m_Q$, and bands correspond to the variation specified in (4.14). Flavour matching (of DPDs, PDFs, and α_s) is performed at LO in the panels on the left and at NLO in the panels on the right.

low or intermediate Y and in the $gggg$ channel. Not surprisingly, the effects are largest for terms where the observed heavy partons can only be produced by flavour matching, such as the $2v2$ contributions to $c\bar{c}b\bar{b}$ and $cbgg$. The scale dependence is greatly reduced when flavour matching is performed at NLO, with small variations in all channels and in the full Y range.

Corresponding plots for the $t\bar{t}$ production setting can be seen in figure 19 and show a very similar picture. At LO, the scale variation for the $2v2$ terms is huge, in particular for the $t\bar{t}t\bar{t}$ channel, whereas only small variations are found in all cases at NLO.

Since the scale variation at NLO is very small, we expect that higher-order graphs as-

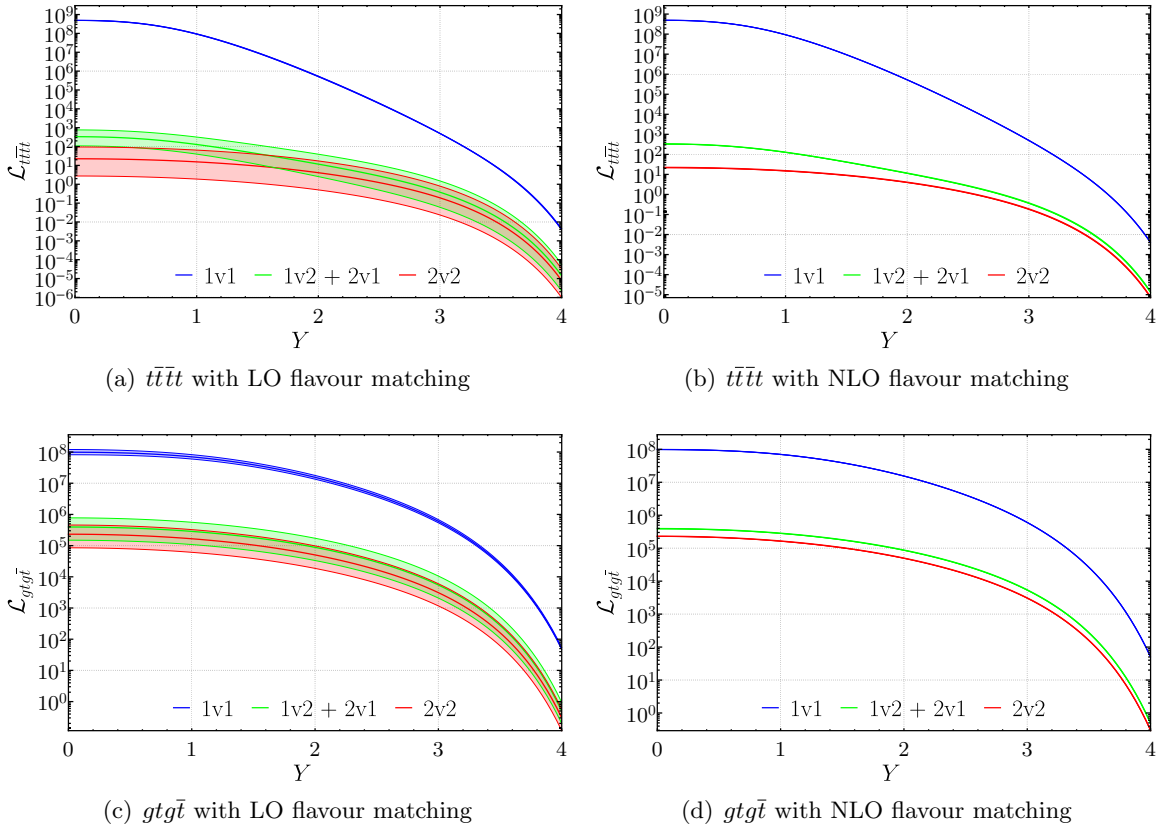


Figure 19: As figure 18, but for the luminosities shown in figure 12 for the $t\bar{t}$ production setting.

sociated with flavour matching will provide only small corrections to the results obtained with $\mu_Q = m_Q$ (at LO or NLO). This is in stark contrast to the higher-order corrections to DPD splitting, where based on the scale variation exercise, we must expect very substantial corrections to the leading-order results.

5 Massive splitting kernels at NLO

The large variation of LO splitting DPDs reported in the previous section provides a strong motivation for evaluating the splitting kernels at NLO accuracy, i.e. at two loops. For massless kernels and unpolarised partons, this has been achieved in [52, 53], and the extension of these calculations to polarisation is rather straightforward. By contrast, the massive splitting kernels are only known at LO (see equations (3.5) and (3.6)). To compute them at NLO is well beyond the scope of the present work. Instead, we derive their limiting behaviour for small and large y , as well as their dependence on n_F and on the renormalisation scale μ . In a later section, we will also show which constraints follow from the DPD sum rules [1, 66] for unpolarised partons.

From now on it is understood that PDFs f^{n_F} , DPDs F^{n_F} , the splitting kernels V^{n_F} and V^{Q,n_F} , and the flavour matching kernels A^{Q,n_F} are to be evaluated at the following arguments:

$$f_{a_0}^{n_F} \equiv f_{a_0}^{n_F}(x; \mu), \quad (5.1)$$

$$F_{a_1 a_2}^{n_F} \equiv F_{a_1 a_2}^{n_F}(x_1, x_2, y; \mu), \quad (5.2)$$

$$V_{a_1 a_2, a_0}^{Q, n_F} \equiv V_{a_1 a_2, a_0}^{Q, n_F}(z_1, z_2, y, m_Q; \mu), \quad (5.3)$$

$$V_{a_1 a_2, a_0}^{n_F} \equiv V_{a_1 a_2, a_0}^{n_F}(z_1, z_2, y; \mu), \quad (5.4)$$

$$A_{a_1 a_0}^{Q, n_F} \equiv A_{a_1 a_0}^{Q, n_F}(z, m_Q; \mu), \quad (5.5)$$

unless indicated otherwise. Notice our convention to use momentum fraction arguments x , x_1 , x_2 in distributions and z , z_1 , z_2 in kernels.

5.1 Two-loop splitting graphs with massive quarks

Some properties of the NLO massive splitting kernels follow directly from the Feynman graphs for the associated splitting process. Let us briefly review these and point out in which ones massive quark lines appear. We distinguish between ‘‘LO channels’’ with splitting processes that are already possible at LO ($g \rightarrow q\bar{q}$, $q \rightarrow qg$, $g \rightarrow gg$, and $g \rightarrow Q\bar{Q}$) and ‘‘NLO channels’’, which first appear at two-loop order ($q \rightarrow Q\bar{Q}$, $g \rightarrow Qg$, $q \rightarrow Qq$, $q \rightarrow \bar{Q}q$, and corresponding channels with q or q' instead of Q). Recall that we denote light flavours by q and q' and heavy ones by Q . In detail, we have

1. $g \rightarrow q\bar{q}$. The graphs without heavy-quark lines are given in figures 1(h)-1(k) and 3(f)-3(h) of reference [52]. In addition, there are virtual graphs with a heavy-quark loop on one of the incoming gluons, as shown in figure 20(a). In the massless case this diagram does not contribute, because incoming partons are on-shell, and scaleless integrals vanish in dimensional regularisation.
2. $q \rightarrow qg$. Besides the diagrams with massless quarks in figures 1(l)-1(q) and 3(i)-3(m) of [52]), there are virtual graphs with a heavy-quark loop on one of the outgoing gluon lines, cf. figure 20(b).
3. $g \rightarrow gg$. In addition to the massless graphs in figures 1(a)-1(g) and 3(a)-3(m) of [52]), there are virtual graphs with a heavy-quark loop in a vertex or propagator correction to the tree-level graph, as shown in figures 20(c) to 20(e).
4. $g \rightarrow Q\bar{Q}$. The diagrams for this channel correspond to the ones for the massless $g \rightarrow q\bar{q}$ case, with all quark lines replaced by massive quark lines. They are shown in figures 20(f) to 20(h) and 21(a) to 21(d). In addition, there are virtual graphs with a heavy-quark loop on one of the incoming gluon lines, as shown in figure 20(i).
5. $q \rightarrow Q\bar{Q}$. The diagram for this channel is obtained from the one for the massless $q \rightarrow q'\bar{q}'$ kernel by replacing all q' quark lines by massive lines, as depicted in figure 21(k).
6. $g \rightarrow Qg$. The diagrams for this channel correspond to the ones for the massless $g \rightarrow qg$ kernel, again with all quark lines replaced by massive ones. They are shown in figures 21(e) to 21(j).
7. $q \rightarrow Qq$. The diagram for this channel is obtained from the one for the massless $q \rightarrow q'q'$ kernel by replacing all q' quark lines by massive lines, shown in figure 21(l).

The two-loop diagrams for $q \rightarrow \bar{Q}q$ and $q \rightarrow Qq$ are related by charge reversal of the heavy-quark line, which results in

$$V_{\bar{Q}q,q}^{Q(2)} = V_{Qq,q}^{Q(2)}. \quad (5.6)$$

The two-loop graphs for NLO channels with observed light partons do not involve any heavy-quark lines, so that we have $V_{a_1 a_2, a_0}^{Q(2)} = V_{a_1 a_2, a_0}^{(2)}$ for the corresponding parton combinations.

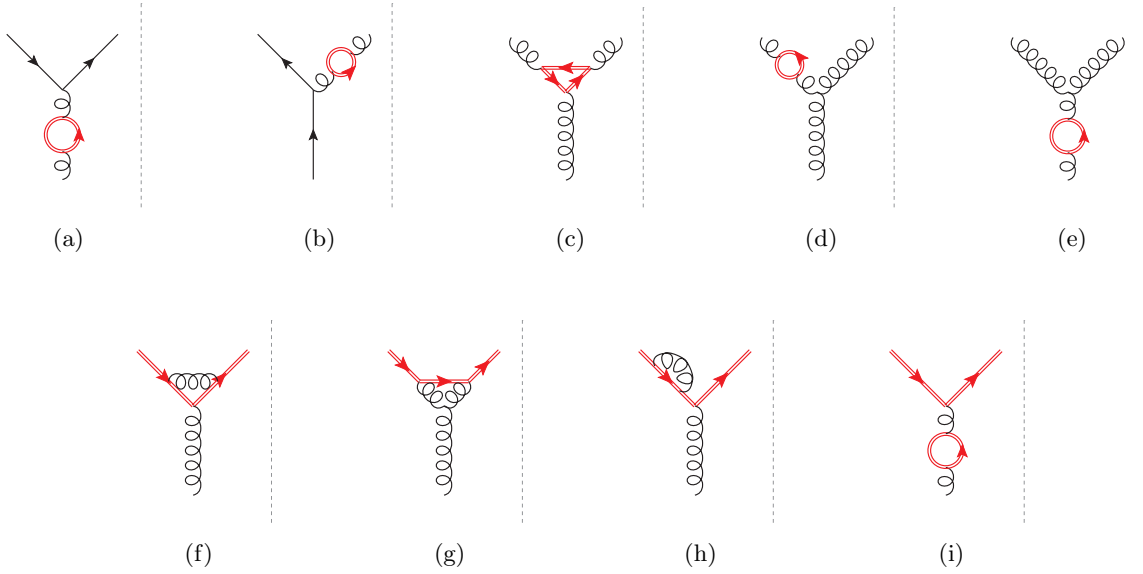


Figure 20: Virtual NLO diagrams for the amplitude that contain heavy-quark lines, indicated by red double lines. The tree graphs in the complex conjugate amplitude are not shown. In Feynman gauge, graphs with eikonal lines are to be added, as specified in figure 4 of [52].

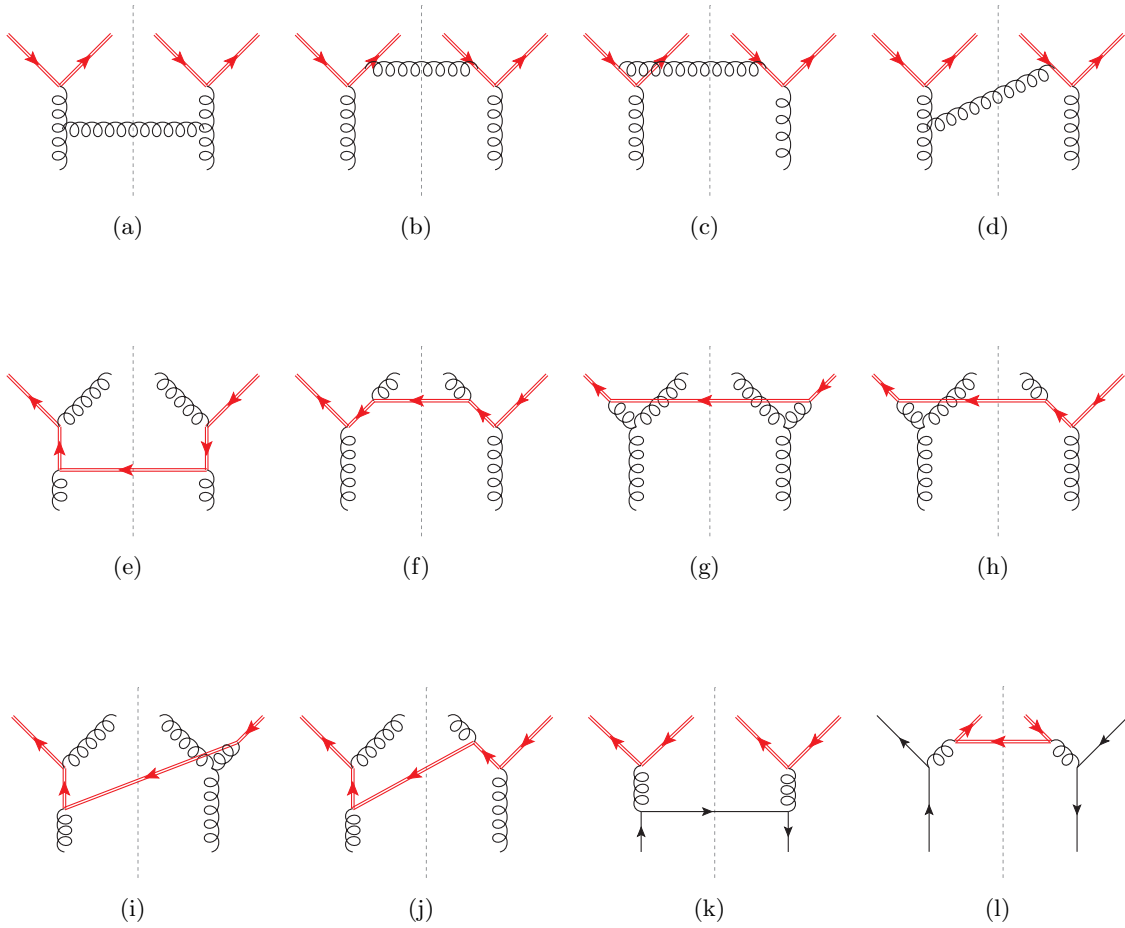


Figure 21: As figure 20, but for real NLO diagrams with heavy quarks.

5.2 Reminders about massless kernels

To begin with, let us recall two properties of the massless two-loop splitting kernels derived in [53, 66].

1. The part $V^{n_F[2,1]}$ of a two-loop kernel that is multiplied by $\log(\mu^2/\mu_y^2)$ can readily be deduced by taking the μ derivative of the splitting formula (2.26) and using the evolution equations for the DPD, PDF, and $a_s(\mu)$. One obtains

$$\begin{aligned} V_{a_1 a_2, a_0}^{n_F[2,1]} &= \sum_{b_1} P_{a_1 b_1}^{n_F(0)} \otimes_1 V_{b_1 a_2, a_0}^{(1)} + \sum_{b_2} P_{a_2 b_2}^{n_F(0)} \otimes_2 V_{a_1 b_2, a_0}^{(1)} \\ &\quad - \sum_{b_0} V_{a_1 a_2, b_0}^{(1)} \otimes_{12} P_{b_0 a_0}^{n_F(0)} + \frac{\beta_0^{n_F}}{2} V_{a_1 a_2, a_0}^{(1)}. \end{aligned} \quad (5.7)$$

2. The n_F dependence of the NLO kernels enters only via quark loops in virtual graphs. This affects the two channels $q \rightarrow qg$ and $g \rightarrow gg$, whereas the NLO kernels for all other channels are n_F independent. The n_F dependence naturally appears via $\beta_0^{n_F}$, see equations (4.17) and (4.23) in [53], and we write

$$V_{a_1 a_2, a_0}^{n_F[2,\ell]} = \tilde{V}_{a_1 a_2, a_0}^{[2,\ell]} + \beta_0^{n_F} V_{a_1 a_2, a_0}^{\beta[2,\ell]} \quad \text{for } (a_1 a_2, a_0) = (qg, q) \text{ and } (gg, g), \quad (5.8)$$

where $\ell = 0, 1$. Since $V^{\beta[2,\ell]}$ originates from virtual graphs, it is proportional to $\delta(1 - z_1 - z_2)$, just as the LO splitting kernels in (2.32). Using (5.7) and the n_F dependence of the LO DGLAP kernels, we can derive that

$$V_{a_1 a_2, a_0}^{\beta[2,1]} = V_{a_1 a_2, a_0}^{(1)} \quad \text{for } (a_1 a_2, a_0) = (qg, q) \text{ and } (gg, g). \quad (5.9)$$

We note that in the expression of (5.7) for $(a_1 a_2, a_0) = (q\bar{q}, g)$ the n_F dependence cancels between the third and fourth terms, owing to the relation (2.11).

The preceding relations also hold if the produced partons a_1 and a_2 are polarised. The first two DGLAP kernels in (5.7) are then polarised, whilst the third one is unpolarised since it refers to the incoming parton a_0 .

5.3 Limiting behaviour for small or large distances

In the limits of small or large y — corresponding to large or small momentum scales μ_y , respectively — the massive splitting kernels can be expressed in terms of massless splitting kernels and flavour matching kernels. This follows from the consistency between the different factorisation regimes in figure 1. If in the intermediate regime (where the massive splitting kernels are used) one takes $\mu_y \gg m_Q$, then one must recover the factorisation regime in which the heavy flavour Q is treated as massless in the $1 \rightarrow 2$ splitting process, whereas for $\mu_y \ll m_Q$ one must recover the regime in which Q decouples in the $1 \rightarrow 2$ splitting. Comparing the DPD splitting formulae for the three regimes (see section 3.2.2) we thus find the following.

For $\mu_y \gg m_Q$ (i.e. in the small- y limit) the massive kernels can be expressed by $n_F + 1$ flavour massless kernels, convoluted with a flavour matching kernel:

$$V_{a_1 a_2, a_0}^{Q, n_F} \xrightarrow{\mu_y \gg m_Q} \sum_{b_0} V_{a_1 a_2, b_0}^{n_F+1} \otimes_{12} A_{b_0 a_0}^{Q, n_F}. \quad (5.10)$$

This corresponds to the right panel in figure 1, where one has first a flavour matching in the PDF and then the $1 \rightarrow 2$ splitting for $n_F + 1$ massless flavours. The $\mathcal{O}(a_s^2)$ term in equation

(5.10) reads

$$V_{a_1 a_2, a_0}^{Q, n_F(2)} \xrightarrow{\mu_y \gg m_Q} \delta_{a_0 l}^{n_F} V_{a_1 a_2, a_0}^{n_F+1(2)} + \sum_{b_0} V_{a_1 a_2, b_0}^{n_F+1(1)} \otimes_{12} A_{b_0 a_0}^{Q(1)} \quad (5.11)$$

with $\delta_{a_0 l}^{n_F}$ defined in (2.19).

For $\mu_y \ll m_Q$ (i.e. in the large- y limit) one has

$$V_{a_1 a_2, a_0}^{Q, n_F} \xrightarrow{\mu_y \ll m_Q} \sum_{b_1, b_2} A_{a_1 b_1}^{Q, n_F} \otimes_1 A_{a_2 b_2}^{Q, n_F} \otimes_2 V_{b_1 b_2, a_0}^{n_F}. \quad (5.12)$$

This corresponds to the left panel in figure 1, where one has a $1 \rightarrow 2$ splitting process for n_F flavours and then DPD flavour matching to $n_F + 1$ flavours. The $\mathcal{O}(a_s^2)$ kernel reads

$$V_{a_1 a_2, a_0}^{Q, n_F(2)} \xrightarrow{\mu_y \ll m_Q} V_{a_1 a_2, a_0}^{n_F(2)} + \sum_{b_1} A_{a_1 b_1}^{Q(1)} \otimes_1 V_{b_1 a_2, a_0}^{(1)} + \sum_{b_2} A_{a_2 b_2}^{Q(1)} \otimes_2 V_{a_1 b_2, a_0}^{(1)} + A_\alpha^{Q(1)} V_{a_1 a_2, a_0}^{(1)}, \quad (5.13)$$

where the term with A_α appears because V^{Q, n_F} is expanded in $a_s^{n_F+1}$ and V^{n_F} in $a_s^{n_F}$.

5.4 Scale dependence

Truncated at NLO, the massive splitting (3.3) formula reads

$$F_{a_1 a_2}^{n_F+1} = \frac{1}{\pi y^2} \sum_{a_0} \left(a_s^{n_F+1} V_{a_1 a_2, a_0}^{Q(1)} \otimes_{12} f_{a_0}^{n_F} + (a_s^{n_F+1})^2 V_{a_1 a_2, a_0}^{Q, n_F(2)} \otimes_{12} f_{a_0}^{n_F} \right) + \mathcal{O}(a_s^3). \quad (5.14)$$

Inserting (5.14) on the l.h.s. of the double DGLAP equation (2.4) gives

$$\begin{aligned} a_s^{n_F+1} \sum_{a_0} \left(\frac{d}{d \log \mu^2} V_{a_1 a_2, a_0}^{Q(1)} \right) \otimes_{12} f_{a_0}^{n_F} + (a_s^{n_F+1})^2 \sum_{a_0} \left[\left(\frac{d}{d \log \mu^2} V_{a_1 a_2, a_0}^{Q(2)} \right) \otimes_{12} f_{a_0}^{n_F} \right. \\ \left. - \frac{\beta_0^{n_F+1}}{2} V_{a_1 a_2, a_0}^{Q(1)} \otimes_{12} f_{a_0}^{n_F} + V_{a_1 a_2, b_0}^{Q(1)} \otimes_{12} \left(P_{b_0 a_0}^{n_F(0)} \otimes f_{a_0}^{n_F} \right) \right] + \mathcal{O}(a_s^3), \end{aligned} \quad (5.15)$$

whilst for the r.h.s. of (2.4) one obtains

$$(a_s^{n_F+1})^2 \left[\sum_{b_1, a_0} P_{a_1 b_1}^{n_F+1(0)} \otimes_1 V_{b_1 a_2, a_0}^{Q(1)} \otimes_{12} f_{a_0}^{n_F} + \sum_{b_2, a_0} P_{a_2 b_2}^{n_F+1(0)} \otimes_2 V_{a_1 b_2, a_0}^{Q(1)} \otimes_{12} f_{a_0}^{n_F} \right] + \mathcal{O}(a_s^3). \quad (5.16)$$

The prefactor $1/(\pi y^2)$ has been omitted in both equations. Using the relation (2.28) for the convolutions with three factors, one derives

$$\frac{d}{d \log \mu^2} V_{a_1 a_2, a_0}^{Q(1)} = 0, \quad \frac{d}{d \log \mu^2} V_{a_1 a_2, a_0}^{Q, n_F(2)} = v_{a_1 a_2, a_0}^{n_F, \text{RGE}} \quad (5.17)$$

with

$$\begin{aligned} v_{a_1 a_2, a_0}^{n_F, \text{RGE}} = \sum_{b_1} P_{a_1 b_1}^{n_F+1(0)} \otimes_1 V_{b_1 a_2, a_0}^{Q(1)} + \sum_{b_2} P_{a_2 b_2}^{n_F+1(0)} \otimes_2 V_{a_1 b_2, a_0}^{Q(1)} \\ - \sum_{b_0} V_{a_1 a_2, b_0}^{Q(1)} \otimes_{12} P_{b_0 a_0}^{n_F(0)} + \frac{\beta_0^{n_F+1}}{2} V_{a_1 a_2, a_0}^{Q(1)}. \end{aligned} \quad (5.18)$$

The first equation in (5.17) confirms the μ independence of the LO kernels given in (3.5) and (3.6). Taking into account the n_F dependence of the LO DGLAP kernels, one obtains the explicit expressions

$$v_{q\bar{q},g}^{\text{RGE}} = V_{q\bar{q},g}^{[2,1]} + \frac{\Delta\beta_0}{2} V_{q\bar{q},g}^{(1)}, \quad (5.19)$$

$$v_{qg,q}^{n_F, \text{RGE}} = V_{qg,q}^{n_F[2,1]} + \Delta\beta_0 V_{qg,q}^{(1)}, \quad (5.20)$$

$$v_{gg,g}^{n_F, \text{RGE}} = V_{gg,g}^{n_F[2,1]} + \frac{3\Delta\beta_0}{2} V_{gg,g}^{(1)}, \quad (5.21)$$

$$v_{Q\bar{Q},g}^{\text{RGE}} = P_{qq}^{(0)} \otimes_1 V_{Q\bar{Q},g}^{Q(1)} + P_{qq}^{(0)} \otimes_2 V_{Q\bar{Q},g}^{Q(1)} - V_{Q\bar{Q},g}^{Q(1)} \otimes_{12} \tilde{P}_{gg}^{(0)} + \frac{\Delta\beta_0}{2} V_{Q\bar{Q},g}^{Q(1)}, \quad (5.22)$$

$$v_{Q\bar{Q},q}^{\text{RGE}} = -V_{Q\bar{Q},g}^{Q(1)} \otimes_{12} P_{gq}^{(0)}, \quad (5.23)$$

$$v_{Qg,g}^{\text{RGE}} = P_{qg}^{(0)} \otimes_1 V_{gg,g}^{(1)} + P_{gq}^{(0)} \otimes_2 V_{Q\bar{Q},g}^{Q(1)}, \quad (5.24)$$

$$v_{Qq,q}^{\text{RGE}} = P_{qg}^{(0)} \otimes_1 V_{gq,q}^{(1)}. \quad (5.25)$$

In (5.19) to (5.21), we used the expression (5.7) of $V^{n_F[2,1]}$, and in (5.22) we made use of the explicit form (2.11) of $P_{gg}^{n_F(0)}$. In accordance with the inspection of the two-loop Feynman graphs, we find that the only kernels with an n_F dependence are those for $q \rightarrow qg$ and $g \rightarrow gg$.

The analogues of equations (5.19) to (5.25) for polarised partons a_1 and a_2 are obtained by replacing the one-loop V kernels on the r.h.s. with their polarised counterparts, as well as the LO DGLAP kernels in the convolutions \otimes_1 and \otimes_2 .

5.5 An explicit parametrisation

We now give an explicit parametrisation of the massive two-loop kernels that incorporates their small- and large- y limits as well as their dependence on μ . It reads

$$\begin{aligned} V_{a_1 a_2, a_0}^{Q, n_F(2)} &= V_{a_1 a_2, a_0}^{n_F[2,0]} + V_{a_1 a_2, a_0}^{n_F[2,1]} \log \frac{m_Q^2}{\mu_y^2} + V_{a_1 a_2, a_0}^I(z_1, z_2, y m_Q) \\ &\quad + k_{11}(y m_Q) \left(V_{a_1 a_2, a_0}^{n_F+1[2,0]} - V_{a_1 a_2, a_0}^{n_F[2,0]} \right) - k_{02}(y m_Q) \left(V_{a_1 a_2, a_0}^{n_F+1[2,1]} - V_{a_1 a_2, a_0}^{n_F[2,1]} \right) \\ &\quad + \log \frac{\mu^2}{m_Q^2} v_{a_1 a_2, a_0}^{n_F, \text{RGE}}(z_1, z_2) \end{aligned} \quad (5.26)$$

with $v^{n_F, \text{RGE}}$ given in (5.18), where we abbreviate

$$k_{ij}(w) = w^2 K_i(w) K_j(w). \quad (5.27)$$

The function $V_{a_1 a_2, a_0}^I$ is μ independent and interpolates between the small and large y limits of the kernels with the properties

$$V_{a_1 a_2, a_0}^I(z_1, z_2, y m_Q) \xrightarrow{y \rightarrow 0} 0, \quad V_{a_1 a_2, a_0}^I(z_1, z_2, y m_Q) \xrightarrow{y \rightarrow \infty} 0. \quad (5.28)$$

For dimensional reasons, it depends on the product of y and m_Q . The functions $k_{11}(y m_Q)$ and $k_{02}(y m_Q)$ in (5.26) can be replaced with other functions that have the same limiting behaviour for $y \rightarrow 0$ and $y \rightarrow \infty$, provided that one makes a corresponding change in V^I . Note that we do not allow for an n_F dependence of V^I . Indeed, the n_F dependence of the two-loop kernels originates from graphs with massless quark loops, and the contribution of these graphs is fully contained in the first two terms and in the last term of (5.26).

To verify that the parametrisation (5.26) has the correct limits for small and for large y , we recall that the modified Bessel functions K_i satisfy

$$\begin{aligned} K_0(w) &\xrightarrow{w \rightarrow 0} \log \frac{b_0}{w}, & K_1(w) &\xrightarrow{w \rightarrow 0} \frac{1}{w}, & K_2(w) &\xrightarrow{w \rightarrow 0} \frac{2}{w^2}, \\ K_i(w) &\xrightarrow{w \rightarrow \infty} 0. \end{aligned} \quad (5.29)$$

As a consequence, one has

$$\begin{aligned} k_{11}(ym_Q) &\xrightarrow{y \rightarrow 0} 1, & k_{02}(ym_Q) &\xrightarrow{y \rightarrow 0} \log \frac{\mu_y^2}{m_Q^2}, \\ k_{ij}(ym_Q) &\xrightarrow{y \rightarrow \infty} 0. \end{aligned} \quad (5.30)$$

Along with the limiting behaviour (5.28) of $V_{a_1 a_2, a_0}^I$, one readily finds that

$$\begin{aligned} V_{a_1 a_2, a_0}^{Q(2)}(z_1, z_2, y, m_Q; m_Q) &\xrightarrow{y \rightarrow 0} V_{a_1 a_2, a_0}^{n_F+1[2,0]} + V_{a_1 a_2, a_0}^{n_F+1[2,1]} \log \frac{m_Q^2}{\mu_y^2} = V_{a_1 a_2, a_0}^{n_F+1(2)}(z_1, z_2, y; m_Q), \\ V_{a_1 a_2, a_0}^{Q(2)}(z_1, z_2, y, m_Q; m_Q) &\xrightarrow{y \rightarrow \infty} V_{a_1 a_2, a_0}^{n_F[2,0]} + V_{a_1 a_2, a_0}^{n_F[2,1]} \log \frac{m_Q^2}{\mu_y^2} = V_{a_1 a_2, a_0}^{n_F(2)}(z_1, z_2, y; m_Q). \end{aligned} \quad (5.31)$$

This agrees with (5.11) and (5.13), given that for $\mu = m_Q$, the LO matching kernels $A^{Q(1)}$ in these equations are zero.

The explicit form of our parametrisation (5.26) for the different channels reads

$$V_{q\bar{q}, g}^{Q(2)} = V_{q\bar{q}, g}^{[2,0]} + V_{q\bar{q}, g}^{[2,1]} \log \frac{\mu^2}{\mu_y^2} + V_{q\bar{q}, g}^I + \frac{\Delta\beta_0}{2} \log \frac{\mu^2}{m_Q^2} V_{q\bar{q}, g}^{(1)}, \quad (5.32)$$

$$\begin{aligned} V_{qg, q}^{Q, n_F(2)} &= V_{qg, q}^{n_F[2,0]} + V_{qg, q}^{n_F[2,1]} \log \frac{\mu^2}{\mu_y^2} + V_{qg, q}^I + k_{11}(ym_Q) \Delta\beta_0 V_{qg, q}^{\beta[2,0]} \\ &\quad + \left[\log \frac{\mu^2}{m_Q^2} - k_{02}(ym_Q) \right] \Delta\beta_0 V_{qg, q}^{(1)}, \end{aligned} \quad (5.33)$$

$$\begin{aligned} V_{gg, g}^{Q, n_F(2)} &= V_{gg, g}^{n_F[2,0]} + V_{gg, g}^{n_F[2,1]} \log \frac{\mu^2}{\mu_y^2} + V_{gg, g}^I + k_{11}(ym_Q) \Delta\beta_0 V_{gg, g}^{\beta[2,0]} \\ &\quad + \left[\frac{3}{2} \log \frac{\mu^2}{m_Q^2} - k_{02}(ym_Q) \right] \Delta\beta_0 V_{gg, g}^{(1)}, \end{aligned} \quad (5.34)$$

$$\begin{aligned} V_{Q\bar{Q}, g}^{Q(2)} &= V_{Q\bar{Q}, g}^I + k_{11}(ym_Q) V_{q\bar{q}, g}^{[2,0]} - k_{02}(ym_Q) V_{q\bar{q}, g}^{[2,1]} \\ &\quad + \log \frac{\mu^2}{m_Q^2} \left[P_{qq}^{(0)} \otimes_1 V_{Q\bar{Q}, g}^{Q(1)} + P_{qq}^{(0)} \otimes_2 V_{Q\bar{Q}, g}^{Q(1)} - V_{Q\bar{Q}, g}^{Q(1)} \otimes_{12} \tilde{P}_{gg}^{(0)} + \frac{\Delta\beta_0}{2} V_{Q\bar{Q}, g}^{Q(1)} \right], \end{aligned} \quad (5.35)$$

$$V_{Q\bar{Q}, q}^{Q(2)} = V_{Q\bar{Q}, q}^I + k_{11}(ym_Q) V_{q'q', q}^{[2,0]} + k_{02}(ym_Q) V_{q\bar{q}, g}^{(1)} \otimes_{12} P_{qq}^{(0)} - \log \frac{\mu^2}{m_Q^2} V_{Q\bar{Q}, g}^{Q(1)} \otimes_{12} P_{qq}^{(0)}, \quad (5.36)$$

$$\begin{aligned} V_{Qg, g}^{Q(2)} &= V_{Qg, g}^I + k_{11}(ym_Q) V_{qg, g}^{[2,0]} - k_{02}(ym_Q) \left[P_{qg}^{(0)} \otimes_1 V_{gg, g}^{(1)} + P_{qg}^{(0)} \otimes_2 V_{q\bar{q}, g}^{(1)} - V_{qg, g}^{(1)} \otimes_{12} P_{qg}^{(0)} \right] \\ &\quad + \log \frac{\mu^2}{m_Q^2} \left[P_{qg}^{(0)} \otimes_1 V_{gg, g}^{(1)} + P_{qg}^{(0)} \otimes_2 V_{Q\bar{Q}, g}^{Q(1)} \right], \end{aligned} \quad (5.37)$$

$$V_{Qq, q}^{Q(2)} = V_{Qq, q}^I + k_{11}(ym_Q) V_{q'q, q}^{[2,0]} - k_{02}(ym_Q) P_{qg}^{(0)} \otimes_1 V_{qg, q}^{(1)} + \log \frac{\mu^2}{m_Q^2} P_{qg}^{(0)} \otimes_1 V_{qg, q}^{(1)}, \quad (5.38)$$

where $\Delta\beta_0$ is defined in (2.14) and $V^{\beta[2,0]}$ in (5.8). In equations (5.36) to (5.38) we have inserted the explicit forms (5.7) of $V^{[2,1]}$ for the relevant channel. The analogues of (5.32) to (5.38) for polarised partons are obtained by replacing the V kernels on the r.h.s. with their polarised counterparts, as well as the DGLAP kernels in the convolutions \otimes_1 and \otimes_2 .

The interpolating function for $g \rightarrow gg$ splitting receives contributions only from virtual graphs with a massive quark loop (see figures 20(c) to 20(e)). It therefore has the form

$$V_{gg,g}^I(z_1, z_2, ym_Q) = \delta(1 - z_1 - z_2) V_{gg,g}^I(z_1, ym_Q), \quad (5.39)$$

where the function on the r.h.s. depends on one instead of two momentum fractions. In section 7.3 we will show that the interpolating function for $g \rightarrow q\bar{q}$ is zero, i.e.

$$V_{q\bar{q},g}^I = 0 \quad (5.40)$$

with corresponding relations for longitudinal or transverse quark polarisation.

We already noted that for NLO channels with light observed partons, the massive two-loop kernels are equal to their massless counterparts. Correspondingly, one finds $V_{a_1 a_2, a_0}^I = 0$ for the relevant parton combinations.

5.6 Large logarithms

For both $\mu_y \ll m_Q$ and $\mu_y \gg m_Q$, the massive splitting kernels involve two physical scales of very different size. The expressions just derived allow us to explicitly investigate the large logarithms that appear at NLO in these limits. Notice that according to (5.30), the function $k_{02}(ym_Q)$ counts as a large logarithm in the limit of small y , whereas this is not the case for $k_{11}(ym_Q)$. Both functions vanish for $\mu_y \ll m_Q$.

From the explicit forms (5.32) to (5.38) it is clear that no choice of μ can remove all large logarithms, not even for light observed partons. In the following we will focus on the scale choice $\mu \sim \mu_y$. This provides an element of continuity between the massive regime and the two regimes with massless DPD splitting kernels in figure 3 — for the latter, μ_y is the only relevant scale in the $1 \rightarrow 2$ splitting process. Moreover, the numerical study in [53] showed that the logarithmic part $V_{gg,g}^{n_F[2,1]}$ of the gluon splitting kernel gives rise to large NLO corrections when the splitting formula is evaluated at scales away from μ_y . In fact, this kernel contains large logarithms in several kinematic limits.

We now discuss the different parton channels in turn.

- **LO channels with observed light partons.** With the choice $\mu \sim \mu_y$ the expressions for all three channels $g \rightarrow q\bar{q}$, $q \rightarrow qg$, and $g \rightarrow gg$ receive logarithmic contributions of the type

$$k \frac{\Delta\beta_0}{2} \log \frac{\mu_y^2}{m_Q^2} V_{a_1 a_2, a_0}^{(1)} \quad (5.41)$$

with $0 \leq k \leq 1$ for $\mu_y \gg m_Q$ and $1 \leq k \leq 3$ for $\mu_y \ll m_Q$. There is hence no kinematic enhancement of the NLO correction relative to the LO result. The prefactor of the logarithm is always negative and at most of size $3|\Delta\beta_0|/2 = 1$. Taking for instance $\mu_y = m_b/4$, we have $a_s^5(\mu_y) \approx 0.066$ and $a_s^5(\mu_y) \log(\mu_y^2/m_b^2) \approx -0.18$.

- **Channels with an observed heavy-quark pair.** In the large- y limit, the NLO kernels $V_{Q\bar{Q},g}^{Q(2)}$ and $V_{Q\bar{Q},q}^{Q(2)}$ go to zero, as does the LO kernel $V_{Q\bar{Q},g}^{Q(1)}$. At two-loop accuracy, the $Q\bar{Q}$ distribution hence decouples for $\mu_y \ll m_Q$.

To analyse the small- y limit, we use the explicit form of $V_{q\bar{q},g}^{[2,1]}$ in equation (5.7), together with the limiting behaviour

$$V_{Q\bar{Q},g}^{Q(1)} \xrightarrow{\mu_y \gg m_Q} V_{q\bar{q},g}^{(1)} \quad (5.42)$$

and the limit of k_{02} given in (5.30). This yields

$$V_{Q\bar{Q},g}^{Q(2)} \xrightarrow{\mu_y \gg m_Q} \log \frac{\mu^2}{\mu_y^2} \left[P_{qq}^{(0)} \otimes_1 V_{q\bar{q},g}^{(1)} + P_{qq}^{(0)} \otimes_2 -V_{q\bar{q},g}^{(1)} \otimes_{12} \tilde{P}_{gg}^{(0)} \right] + \frac{\Delta\beta_0}{2} \log \frac{\mu^2}{m_Q^2} V_{q\bar{q},g}^{(1)} + \dots, \quad (5.43)$$

$$V_{Q\bar{Q},q}^{Q(2)} \xrightarrow{\mu_y \gg m_Q} -\log \frac{\mu^2}{\mu_y^2} V_{q\bar{q},g}^{(1)} \otimes_{12} P_{qq}^{(0)} + \dots, \quad (5.44)$$

where the ellipsis denotes non-logarithmic contributions from $V^I + V^{[2,0]}$. With the choice $\mu \sim \mu_y$ one thus finds that $V_{Q\bar{Q},g}^{Q(2)}$ has the same large logarithm as its counterpart $V_{q\bar{q},g}^{Q(2)}$ for light quarks, whilst $V_{Q\bar{Q},q}^{Q(2)}$ has no large logarithm at all.

- **Channels with one observed heavy quark.** In the large- y limit, one has

$$V_{Qg,g}^{Q(2)} \xrightarrow{\mu_y \ll m_Q} \log \frac{\mu^2}{m_Q^2} P_{qg}^{(0)} \otimes_1 V_{gg,g}^{(1)} = A_{Qg}^{Q(1)}(m_Q; \mu) \otimes_1 V_{gg,g}^{(1)}, \quad (5.45)$$

$$V_{Qq,q}^{Q(2)} \xrightarrow{\mu_y \ll m_Q} \log \frac{\mu^2}{m_Q^2} P_{qg}^{(0)} \otimes_1 V_{gq,q}^{(1)} = A_{Qg}^{Q(1)}(m_Q; \mu) \otimes_1 V_{gq,q}^{(1)}, \quad (5.46)$$

so that the production of one heavy quark does *not* decouple in the limit $\mu_y \ll m_Q$. At this point we must remember that we defined the DPDs in the $\overline{\text{MS}}$ renormalisation scheme, which does *not* yield heavy-quark decoupling for scales much smaller than the quark mass, see e.g. [47]. We note in passing that at order a_s^3 , non-decoupling in the limit $\mu_y \ll m_Q$ will also occur in the channel $g \rightarrow Q\bar{Q}$, because the three-loop kernel contains a term $A_{Qg}^{Q(1)} \otimes_1 A_{Qg}^{Q(1)} \otimes_2 V_{gg,g}^{(1)}$ according to (5.12).

For the scale choice $\mu \sim \mu_y$, the two-loop kernels in (5.45) and (5.46) yield splitting DPDs F_{Qg} and F_{Qq} that are negative and enhanced by a large logarithm $\log(\mu_y^2/m_Q^2)$. This is similar to the negative values of the heavy-quark PDF that one obtains when flavour matching at scales $\mu \ll m_Q$. Both in the DPD and in the PDF case, subsequent DGLAP evolution up to the scale m_Q yields a distribution close to zero, provided that $a_s \log(m_Q^2/\mu^2)$ is sufficiently small. Indeed, the large logarithm in (5.45) and (5.46) is then cancelled by a corresponding term with $\log(m_Q^2/\mu^2)$ from DGLAP evolution, and further evolution terms come with at least one more factor of $a_s \log(m_Q^2/\mu^2)$.

Let us now turn to the small- y limit. In this case, we have

$$V_{Qg,g}^{Q(2)} \xrightarrow{\mu_y \gg m_Q} \log \frac{\mu^2}{\mu_y^2} \left[P_{qg}^{(0)} \otimes_1 V_{gg,g}^{(1)} + P_{qg}^{(0)} \otimes_2 V_{q\bar{q},g}^{(1)} \right] + \log \frac{\mu_y^2}{m_Q^2} V_{q\bar{q},g}^{(1)} \otimes_{12} P_{qg}^{(0)} + \dots, \quad (5.47)$$

$$V_{Qq,q}^{Q(2)} \xrightarrow{\mu_y \gg m_Q} \log \frac{\mu^2}{\mu_y^2} P_{qg}^{(0)} \otimes_1 V_{gq,q}^{(1)} + \dots, \quad (5.48)$$

where the ellipsis again denotes non-logarithmic contributions. For the choice $\mu \sim \mu_y$, a large logarithm remains only in the $g \rightarrow Qg$ channel, which can be rewritten as

$$V_{Qg,g}^{Q(2)} \xrightarrow{\mu_y \gg m_Q} V_{q\bar{q},g}^{(1)} \otimes_{12} A_{Qg}^{Q(1)}(m_Q; \mu_y) + \dots \quad \text{for } \mu \sim \mu_y. \quad (5.49)$$

This is just the expression of the graph in figure 7(a). We recall that in section 4.1.2, this was identified as a large missing NLO contribution when the massive splitting scheme is evaluated at LO. It led us to choose a rather low value for the upper limit βm_Q of the μ_y region where massive splitting kernels are used. One might expect that using massive splitting kernels at NLO will mitigate the problem and possibly allow for using larger β . Of course, this should be confirmed by a numerical study, which is beyond the scope of this work.

The preceding discussion, and in particular the relations (5.42) to (5.49) are readily generalised to the case of polarised partons.

6 NLO splitting kernels with two heavy flavours

In the previous section, we analysed the massive NLO $1 \rightarrow 2$ splitting kernels for one heavy flavour Q with mass m_Q . We now extend our analysis to kernels for two massive flavours, which appear in the scheme we laid out in section 3.3. The corresponding LO kernels have been given in section 3.1. In analogy to equations (5.1) to (5.5), it is understood that the massive kernels are taken at arguments

$$V_{a_1 a_2, a_0}^{cb} \equiv V_{a_1 a_2, a_0}^{cb}(z_1, z_2, y, m_c, m_b; \mu) \quad (6.1)$$

unless specified otherwise.

6.1 Expressions in terms of kernels with one heavy flavour

Inspection of the relevant Feynman graphs allows us to obtain the kernels for massive charm and bottom from the ones for a single heavy flavour. We discuss the different types of parton channels in turn.

LO channels with observed light partons. For the LO channels $g \rightarrow gg$, $g \rightarrow q\bar{q}$, and $q \rightarrow qq$, heavy-quark effects arise solely from closed quark loops, as shown in figure 21. Each of these loop graphs is evaluated once for charm and once for bottom, and there are no graphs that involve both heavy flavours.

We now decompose the kernels for three light flavours and one heavy flavour Q as

$$V_{a_1 a_2, a_0}^{Q,3(2)}(m_Q) = V_{a_1 a_2, a_0}^{3(2)} + \Delta V_{a_1 a_2, a_0}^{Q(2)}(m_Q), \quad (6.2)$$

where $V_{a_1 a_2, a_0}^{3(2)}$ is the massless three-flavour NLO kernel and $\Delta V_{a_1 a_2, a_0}^{Q(2)}(m_Q)$ contains the contributions from diagrams with massive quark loops (see figures 20(a) to 20(e)). Each term on the r.h.s. contains the ultraviolet counterterms in the $\overline{\text{MS}}$ scheme for the flavours running in the quark loops. The sum of counterterms for the kernel (6.2) hence corresponds to renormalising the strong coupling for $3 + 1$ flavours, in agreement with (3.4).

According to our discussion of the relevant Feynman graphs, the kernel for three light and two heavy flavours is then given by

$$V_{a_1 a_2, a_0}^{cb(2)}(m_c, m_b) = V_{a_1 a_2, a_0}^{3(2)} + \Delta V_{a_1 a_2, a_0}^{Q(2)}(m_c) + \Delta V_{a_1 a_2, a_0}^{Q(2)}(m_b). \quad (6.3)$$

The sum of the kernels on the r.h.s. contains the ultraviolet counterterms for $3 + 1 + 1$ flavours, which corresponds to the use of a_s^5 in the perturbative expansion (3.10) of V^{cb} .

Combining the two previous equations, we obtain

$$V_{a_1 a_2, a_0}^{cb(2)}(m_c, m_b) = V_{a_1 a_2, a_0}^{Q,3(2)}(m_c) + V_{a_1 a_2, a_0}^{Q,3(2)}(m_b) - V_{a_1 a_2, a_0}^{3(2)}. \quad (6.4)$$

Here and in the following, we explicitly indicate the dependence of kernels on the two quark masses, but omit the arguments z_1, z_2, y and μ .

LO channels with observed heavy partons. In the NLO kernels for $g \rightarrow c\bar{c}$ and $g \rightarrow b\bar{b}$, the two massive quarks enter on a different footing. For definiteness, let us consider the kernel for $g \rightarrow c\bar{c}$, from which the one for $g \rightarrow b\bar{b}$ is readily obtained by interchanging the roles of c and b quarks, i.e.

$$V_{b\bar{b},g}^{cb(2)}(m_c, m_b) = V_{c\bar{c},g}^{cb(2)}(m_b, m_c). \quad (6.5)$$

The kernel $V_{c\bar{c},g}^{cb(2)}$ differs from $V_{c\bar{c},g}^{c(2)}$, where no b quarks appear, by the contribution from the diagram in figure 20(i) with charm in the upper quark lines and bottom in the quark loop. Denoting the contribution of this graph and its ultraviolet counterterm by $v_{c\bar{c},g}^{cb}$, we have

$$V_{c\bar{c},g}^{cb(2)}(m_c, m_b) = V_{c\bar{c},g}^{c(2)}(m_c) + v_{c\bar{c},g}^{cb}(m_c, m_b). \quad (6.6)$$

In section 7.3 we will derive the expression for the kernel resulting from figure 20(a), where the upper lines are for a light quark. The derivation is trivially extended to the case where that quark is massive and yields

$$v_{c\bar{c},g}^{cb}(m_c, m_b) = \frac{\Delta\beta_0}{2} \log \frac{\mu^2}{m_b^2} V_{c\bar{c},g}^{c(1)}(m_c) = V_{c\bar{c},g}^{c(1)}(m_c) \otimes_{12} A_{gg}^{b(1)}(m_b). \quad (6.7)$$

NLO channels with observed heavy partons. These are the channels $q \rightarrow Q\bar{Q}$, $g \rightarrow Qg$, and $q \rightarrow Qq$ with $Q = c, b$. The relevant graphs involve massive lines only for the observed flavour Q , as seen in the second and third rows of figure 21. They are hence not sensitive to the presence of a second heavy quark and read

$$V_{a_1 a_2, a_0}^{cb(2)}(m_c) = V_{a_1 a_2, a_0}^{c(2)}(m_c) \quad \text{for } (a_1 a_2, a_0) = (c\bar{c}, g), (cg, g), (cq, q) \quad (6.8)$$

for produced charm. For produced bottom, one has to replace the flavour labels and the quark mass.

NLO channels with observed light partons. Since the two-loop graphs for these channels do not involve any heavy-quark lines, we have $V_{a_1 a_2, a_0}^{cb(2)} = V_{a_1 a_2, a_0}^{(2)}$ for the corresponding parton combinations, just as in the case of a single heavy flavour.

In the following subsections, we will verify that (6.4), (6.7), and (6.8) have the correct limits for small or large y and the correct dependence on the renormalisation scale.

6.2 Limiting behaviour for small or large distances

For small or large y , the massive splitting kernels with two heavy flavours can be reduced to the convolution of massless splitting kernels with flavour matching kernels, just like in the one-flavour case (section 5.3). This follows from the consistency between the different factorisation regimes in figure 1 for the case that the heavy-quark subprocesses contain two heavy flavours instead of one.

PDF matching for two heavy flavours. Instead of successively matching a three-flavour PDF first to four and then to five active flavours, one may directly match

$$f_{a_1}^5(x; \mu) = \sum_{a_0} A_{a_1 a_0}^{cb}(m_c, m_b; \mu) \otimes f_{a_0}^3(\mu) \quad (6.9)$$

with a perturbative expansion of the kernel in a_s^5 :

$$A_{a_1 a_0}^{cb}(z, m_c, m_b; \mu) = \sum_{k=0}^{\infty} [a_s^5(\mu)]^k A_{a_1 a_0}^{cb(k)}(z, m_c, m_b; \mu). \quad (6.10)$$

For brevity, we do not indicate explicitly that A^{cb} assumes the presence of 3 massless quark flavours. At tree-level, we have

$$A_{a_1 a_0}^{cb(0)} = A_{a_1 a_0}^{Q(0)} = \delta_{a_1 l}^3 \delta_{a_1 a_0} \delta(1-z) \quad (6.11)$$

with $\delta_{a_1 l}^3$ defined in (2.19), whereas at one-loop order the matching coefficients are additive:

$$A_{a_1 a_0}^{cb(1)}(m_c, m_b) = A_{a_1 a_0}^{c(1)}(m_c) + \delta_{a_0 l}^3 A_{a_1 a_0}^{b(1)}(m_b). \quad (6.12)$$

Results for A^{cb} up to three loops can be found in reference [67]. Up to two loops, the coefficients can be obtained from the single-flavour case, as shown in [68].

In full analogy, one can perform two-flavour matching for the strong coupling,

$$a_s^3(\mu) = \sum_{k=0}^{\infty} [a_s^5(\mu)]^{k+1} A_{\alpha}^{cb(k)}(m_c, m_b; \mu), \quad (6.13)$$

with coefficients

$$A_{\alpha}^{cb(0)} = 1, \quad A_{\alpha}^{cb(1)}(m_c, m_b; \mu) = A_{\alpha}^{c(1)}(m_c; \mu) + A_{\alpha}^{b(1)}(m_b; \mu) \quad (6.14)$$

at LO and NLO.

General limiting behaviour. For small y , or more precisely for $\mu_y \gg m_b$, one finds that the two-flavour kernels can be expressed as

$$V_{a_1 a_2, a_0}^{cb} \xrightarrow{y \rightarrow 0} \sum_{b_0} V_{a_1 a_2, b_0}^5 \otimes_{12} A_{b_0 a_0}^{cb}. \quad (6.15)$$

Expanding this in the five-flavour strong coupling a_s^5 gives

$$V_{a_1 a_2, a_0}^{cb(2)} \xrightarrow{y \rightarrow 0} \delta_{a_0 l}^3 V_{a_1 a_2, a_0}^{5(2)} + \sum_{b_0} V_{a_1 a_2, b_0}^{5(1)} \otimes_{12} A_{b_0 a_0}^{cb(1)} \quad (6.16)$$

for the NLO coefficient. In the opposite limit of large y , or more precisely for $\mu_y \ll m_c$, the two-flavour kernels may be expressed as

$$V_{a_1 a_2, a_0}^{cb} \xrightarrow{y \rightarrow \infty} A_{a_1 b_1}^{cb} \otimes_1 A_{a_2 b_2}^{cb} \otimes_2 V_{b_1 b_2, a_0}^3, \quad (6.17)$$

where the $\mathcal{O}(a_s^2)$ term reads

$$V_{a_1 a_2, a_0}^{cb(2)} \xrightarrow{y \rightarrow \infty} V_{a_1 a_2, a_0}^{3(2)} + \sum_{b_1} A_{a_1 b_1}^{cb(1)} \otimes_1 V_{b_1 a_2, a_0}^{3(1)} + \sum_{b_2} A_{a_2 b_2}^{cb(1)} \otimes_2 V_{a_1 b_2, a_0}^{3(1)} + A_{\alpha}^{cb(1)} V_{a_1 a_2, a_0}^{3(1)}. \quad (6.18)$$

We now show that the kernels derived in section 6.1 correctly fulfil these limits, again considering separately the different groups of parton channels.

LO channels with observed light partons. To have the same small- y limit on both sides of the relation (6.4), we need

$$\begin{aligned} & V_{a_1 a_2, a_0}^{5(2)} + \sum_{b_0} V_{a_1 a_2, b_0}^{(1)} \otimes_{12} A_{b_0 a_0}^{cb(1)} \\ & \stackrel{!}{=} \left[V_{a_1 a_2, a_0}^{4(2)} + \sum_{b_0} V_{a_1 a_2, b_0}^{(1)} \otimes_{12} A_{b_0 a_0}^{c(1)} \right] + \left[V_{a_1 a_2, a_0}^{4(2)} + \sum_{b_0} V_{a_1 a_2, b_0}^{(1)} \otimes_{12} A_{b_0 a_0}^{b(1)} \right] - V_{a_1 a_2, a_0}^{3(2)}, \end{aligned} \quad (6.19)$$

where we have used (5.11) and (6.16). To see that this is the case, we use (6.12) and the relation

$$V_{a_1 a_2, a_0}^{5(2)} = 2V_{a_1 a_2, a_0}^{4(2)} - V_{a_1 a_2, a_0}^{3(2)}, \quad (6.20)$$

which holds because $V^{n_F(2)}$ depends linearly on n_F .

For (6.4) to have the correct large- y limit, we need

$$\begin{aligned} & V_{a_1 a_2, a_0}^{3(2)} + \sum_{b_1} A_{a_1 b_1}^{cb(1)} \otimes_1 V_{b_1 a_2, a_0}^{(1)} + \sum_{b_2} A_{a_2 b_2}^{cb(1)} \otimes_1 V_{a_1 b_2, a_0}^{(1)} + A_{\alpha}^{cb(1)} V_{a_1 a_2, a_0}^{(1)} \\ & \stackrel{!}{=} V_{a_1 a_2, a_0}^{3(2)} + \sum_{b_1} \left(A_{a_1 b_1}^{c(1)} + A_{a_1 b_1}^{b(1)} \right) \otimes_1 V_{b_1 a_2, a_0}^{(1)} + \sum_{b_2} \left(A_{a_2 b_2}^{c(1)} + A_{a_2 b_2}^{b(1)} \right) \otimes_1 V_{a_1 b_2, a_0}^{(1)} \\ & + \left(A_{\alpha}^{c(1)} + A_{\alpha}^{b(1)} \right) V_{a_1 a_2, a_0}^{(1)} \end{aligned} \quad (6.21)$$

according to (5.13) and (6.18). Given (6.12) and (6.14), this is indeed fulfilled.

LO channels with observed heavy partons. According to (5.11) and (6.16), the consistency of relation (6.6) in the small- y limit requires

$$V_{c\bar{c}, g}^{(2)} + V_{c\bar{c}, g}^{(1)} \otimes_{12} A_{gg}^{cb(1)} \stackrel{!}{=} V_{c\bar{c}, g}^{(2)} + V_{c\bar{c}, g}^{(1)} \otimes_{12} \left(A_{gg}^{c(1)} + A_{gg}^{b(1)} \right), \quad (6.22)$$

which is satisfied because of (6.12). In the large- y limit, both sides of equation (6.6) tend to zero according to equations (5.13) and (6.18). An analogous analysis applies to $V_{b\bar{b}, g}^{cb(2)}$.

NLO channels with observed heavy partons. For definiteness, we consider again the case of observed charm quarks.

The small- y behaviour given in (5.11) and (6.16) implies that

$$V_{c\bar{c}, q}^{cb(2)} \text{ and } V_{c\bar{c}, q}^{c(2)} \xrightarrow{y \rightarrow 0} V_{q'\bar{q}', q}^{(2)}, \quad V_{c q, q}^{cb(2)} \text{ and } V_{c q, q}^{c(2)} \xrightarrow{y \rightarrow 0} V_{q' q, q}^{(2)}, \quad (6.23)$$

whilst

$$V_{c g, g}^{cb(2)} \xrightarrow{y \rightarrow 0} V_{q g, g}^{(2)} + V_{q g, q}^{(1)} \otimes_{12} A_{c g}^{cb(1)}, \quad V_{c g, g}^{c(2)} \xrightarrow{y \rightarrow 0} V_{q g, g}^{(2)} + V_{q g, q}^{(1)} \otimes_{12} A_{c g}^{c(1)}. \quad (6.24)$$

The consistency of the relation (6.8) with (6.23) is evident, whilst for (6.24) it requires

$$A_{c g}^{cb(1)} \stackrel{!}{=} A_{c g}^{c(1)}. \quad (6.25)$$

This holds due to (6.12) and the fact that $A_{c g}^{b(1)} = 0$.

In the large- y limit, both $V_{c\bar{c}, q}^{cb(2)}$ and $V_{c\bar{c}, q}^{c(2)}$ tend to zero, whilst

$$V_{c a}^{cb(2)} \xrightarrow{y \rightarrow \infty} A_{c g}^{cb(2)} \otimes_1 V_{g a, a}^{(1)}, \quad V_{c a}^{c(2)} \xrightarrow{y \rightarrow \infty} A_{c g}^{c(2)} \otimes_1 V_{g a, a}^{(1)} \quad \text{for } a = g, q \quad (6.26)$$

according to (5.13) and (6.18). The consistency of (6.8) is again ensured by the relation (6.25).

6.3 Scale dependence

The analysis in section 5.4 can be extended to the case of two heavy flavours in a straightforward manner. Starting from

$$F_{a_1 a_2}^5 = \frac{1}{\pi y^2} \sum_{a_0} \left(a_s^5 V_{a_1 a_2, a_0}^{cb(1)} \otimes_{12} f_{a_0}^3 + (a_s^5)^2 V_{a_1 a_2, a_0}^{cb(2)} \otimes_{12} f_{a_0}^3 \right) + \mathcal{O}(a_s^3) \quad (6.27)$$

and adapting the steps that lead from (5.14) to (5.17) and (5.18), one finds the following scale dependence of the massive splitting kernels with two heavy flavours:

$$\frac{d}{d \log \mu^2} V_{a_1 a_2, a_0}^{cb(1)} = 0, \quad (6.28)$$

$$\begin{aligned} \frac{d}{d \log \mu^2} V_{a_1 a_2, a_0}^{cb(2)} &= \sum_{b_1} P_{a_1 b_1}^{5(0)} \otimes_1 V_{b_1 a_2, a_0}^{cb(1)} + \sum_{b_2} P_{a_2 b_2}^{5(0)} \otimes_2 V_{a_1 b_2, a_0}^{cb(1)} \\ &\quad - V_{a_1 a_2, b_0}^{cb(1)} \otimes_{12} P_{b_0 a_0}^{3(0)} + \frac{\beta_0^5}{2} V_{a_1 a_2, a_0}^{cb(1)}. \end{aligned} \quad (6.29)$$

We now show that this is fulfilled by the two-flavour kernels in (6.4), (6.7), and (6.8).

LO channels with observed light partons. The scale dependence of the two-loop kernels for one heavy flavour is given by (5.18), and for the massless kernel with three flavours one has

$$\frac{d}{d \log \mu^2} V_{a_1 a_2, a_0}^{3(2)} = V_{a_1 a_2, a_0}^{3[2,1]} \quad (6.30)$$

with the r.h.s. given in equation (5.7). Inserting this on the r.h.s. of the relation (6.4), one obtains

$$\begin{aligned} \frac{d}{d \log \mu^2} V_{a_1 a_2, a_0}^{cb(2)} &= \sum_{b_1} \left(2P_{a_1 b_1}^{4(0)} - P_{a_1 b_1}^{3(0)} \right) \otimes_1 V_{b_1 a_2, a_0}^{(1)} + \sum_{b_2} \left(2P_{a_2 b_2}^{4(0)} - P_{a_2 b_2}^{3(0)} \right) \otimes_2 V_{a_1 b_2, a_0}^{(1)} \\ &\quad - \sum_{b_0} V_{a_1 a_2, b_0}^{(1)} \otimes_{12} P_{b_0 a_0}^{3(0)} + \frac{1}{2} (2\beta_0^4 - \beta_0^3) V_{a_1 a_2, a_0}^{(1)}. \end{aligned} \quad (6.31)$$

Here we have used that for observed light partons the kernels $V^{Q(1)}$ on the r.h.s. of (5.18) are equal to their massless counterparts $V^{(1)}$. Since $P^{n_F(1)}$ and $\beta_0^{n_F}$ are linear functions of n_F , we have

$$2P_{ab}^{4(0)} - P_{ab}^{3(0)} = P_{ab}^{5(0)}, \quad 2\beta_0^{4(0)} - \beta_0^{3(0)} = \beta_0^{5(0)}, \quad (6.32)$$

so that equation (6.31) reduces to

$$\begin{aligned} \frac{d}{d \log \mu^2} V_{a_1 a_2, a_0}^{cb(2)} &= \sum_{b_1} P_{a_1 b_1}^{5(0)} \otimes_1 V_{b_1 a_2, a_0}^{(1)} + \sum_{b_2} P_{a_2 b_2}^{5(0)} \otimes_2 V_{a_1 b_2, a_0}^{(1)} \\ &\quad - \sum_{b_0} V_{a_1 a_2, b_0}^{(1)} \otimes_{12} P_{b_0 a_0}^{3(0)} + \frac{\beta_0^5}{2} V_{a_1 a_2, a_0}^{(1)}. \end{aligned} \quad (6.33)$$

This is consistent with (6.29), because the LO kernels $V^{cb(1)}$ are equal to $V^{(1)}$ for observed massless partons.

LO channels with observed heavy partons. Using (5.18) and (6.29) together with the fact that the DGLAP kernel $P_{qq}^{(0)}$ does not depend on the number of active flavours, one finds that $V_{c\bar{c},g}^{cb(2)}$ in (6.6) has the correct scale behaviour.

NLO channels with observed heavy partons. For NLO channels, the kernels $V^{Q(1)}$ and $V^{cb(1)}$ on the r.h.s. of (5.18) and (6.29) are zero, leaving only terms with flavour non-diagonal DGLAP kernels, which are independent of n_F . This ensures the correct scale dependence of the kernels $V_{a_1 a_2, a_0}^{cb(2)}$ in (6.8).

6.4 Explicit parametrisation

An explicit parametrisation of the kernels $V^{cb(2)}$ is readily obtained from the relations in section 6.1 and the parametrisation of $V^{Q(2)}$ in section 5.5. For the LO channels, this gives

$$V_{q\bar{q},g}^{cb(2)} = V_{q\bar{q},g}^{[2,0]} + V_{q\bar{q},g}^{[2,1]} \log \frac{\mu^2}{\mu_y^2} + V_{q\bar{q},g}^I(m_c) + V_{q\bar{q},g}^I(m_b) + L(\mu, m_c, m_b) \frac{\Delta\beta_0}{2} V_{q\bar{q},g}^{(1)}, \quad (6.34)$$

$$\begin{aligned} V_{qg,q}^{cb(2)} &= V_{qg,q}^{3[2,0]} + V_{qg,q}^{3[2,1]} \log \frac{\mu^2}{\mu_y^2} + V_{qg,q}^I(m_c) + V_{qg,q}^I(m_b) + \tilde{k}_{11}(y, m_c, m_b) \Delta\beta_0 V_{qg,q}^{\beta[2,0]} \\ &+ \left[L(\mu, m_c, m_b) - \tilde{k}_{02}(y, m_c, m_b) \right] \Delta\beta_0 V_{qg,q}^{(1)}, \end{aligned} \quad (6.35)$$

$$\begin{aligned} V_{gg,g}^{cb(2)} &= V_{gg,g}^{3[2,0]} + V_{gg,g}^{3[2,1]} \log \frac{\mu^2}{\mu_y^2} + V_{gg,g}^I(m_c) + V_{gg,g}^I(m_b) + \tilde{k}_{11}(y, m_c, m_b) \Delta\beta_0 V_{gg,g}^{\beta[2,0]} \\ &+ \left[\frac{3}{2} L(\mu, m_c, m_b) - \tilde{k}_{02}(y, m_c, m_b) \right] \Delta\beta_0 V_{gg,g}^{(1)}, \end{aligned} \quad (6.36)$$

$$\begin{aligned} V_{c\bar{c},g}^{cb(2)} &= V_{c\bar{c},g}^I(m_c) + k_{11}(y m_c) V_{q\bar{q},g}^{[2,0]} - k_{02}(y m_c) V_{q\bar{q},g}^{[2,1]} \\ &+ \log \frac{\mu^2}{m_c^2} \left[P_{q\bar{q}}^{(0)} \otimes_1 V_{c\bar{c},g}^{c(1)}(m_c) + P_{q\bar{q}}^{(0)} \otimes_2 V_{c\bar{c},g}^{c(1)}(m_c) - V_{c\bar{c},g}^{c(1)}(m_c) \otimes_{12} \tilde{P}_{gg}^{(0)} \right] \\ &+ L(\mu, m_c, m_b) \frac{\Delta\beta_0}{2} V_{c\bar{c},g}^{c,(1)}(m_c), \end{aligned} \quad (6.37)$$

$$\begin{aligned} V_{b\bar{b},g}^{cb(2)} &= V_{b\bar{b},g}^I(m_b) + k_{11}(y m_b) V_{q\bar{q},g}^{[2,0]} - k_{02}(y m_b) V_{q\bar{q},g}^{[2,1]} \\ &+ \log \frac{\mu^2}{m_b^2} \left[P_{q\bar{q}}^{(0)} \otimes_1 V_{b\bar{b},g}^{b(1)}(m_b) + P_{q\bar{q}}^{(0)} \otimes_2 V_{b\bar{b},g}^{b(1)}(m_b) - V_{b\bar{b},g}^{b(1)}(m_b) \otimes_{12} \tilde{P}_{gg}^{(0)} \right] \\ &+ L(\mu, m_c, m_b) \frac{\Delta\beta_0}{2} V_{b\bar{b},g}^{b,(1)}(m_b), \end{aligned} \quad (6.38)$$

where we abbreviated

$$L(\mu, m_c, m_b) = \log \frac{\mu^2}{m_c^2} + \log \frac{\mu^2}{m_b^2}, \quad (6.39)$$

$$\tilde{k}_{ij}(y, m_c, m_b) = k_{ij}(y m_c) + k_{ij}(y m_b). \quad (6.40)$$

For definiteness, we have indicated all dependence on the heavy-quark masses and also given the expression for $V_{b\bar{b},g}^{cb(2)}$.

According to (6.8), the kernels $V^{cb(2)}$ for NLO channels are directly obtained from (5.36) to (5.38) by appropriate substitution of parton labels and masses.

Large logarithms. The analysis of logarithms in (6.34) to (6.38) is very similar to the one in section 5.6, with similar conclusions regarding the large logarithms that remain if one chooses $\mu \sim \mu_y$. The most notable change is that for the NLO corrections from massive quark loops, which appear in all LO channels, one needs to replace $\log(\mu_y^2/m_Q^2)$ in (5.41) with the sum of logarithms $\log(\mu_y^2/m_c^2) + \log(\mu_y^2/m_b^2)$.

7 DPD sum rules and massive splitting kernels

In this section we will show that the number and momentum sum rules for unpolarised DPDs [1, 66] imply corresponding sum rules for the massive splitting kernels V^Q . These sum rules are easily verified for the LO results given in (3.5) and (3.6). More importantly, they provide valuable constraints on the interpolating terms V^I in our parametrisation (5.26) of the NLO kernels. Throughout this section, it is understood that all partons are unpolarised unless stated otherwise. As in section 5, we consider n_F light flavours along with one heavy flavour Q .

The DPD sum rules do not directly apply to the distributions $F(x_1, x_2, y)$ we have considered so far. They require an integral of these distributions over all distances \mathbf{y} in the transverse plane, which due to the $1/y^2$ behaviour from perturbative splitting is logarithmically divergent at small y if carried out naively. In [13, 66] it was shown that the sum rules hold if this splitting singularity is renormalised in the $\overline{\text{MS}}$ scheme (with the integral over \mathbf{y} carried out in $2 - 2\epsilon$ dimensions before modified minimal subtraction of the resulting pole at $\epsilon = 0$). Moreover, a matching formula was derived that connects these distributions $F^{\overline{\text{MS}}}(x_1, x_2)$ to the integral of $F(x_1, x_2, y)$ over \mathbf{y} in two dimensions, evaluated with a lower cutoff on y . The corresponding matching kernels were computed in [66] at LO and in [52] at NLO accuracy. For DPDs with $n_F + 1$ active flavours, the matching relation reads

$$F_{a_1 a_2}^{n_F+1, \overline{\text{MS}}}(x_1, x_2; \mu) = \int_{b_0/\nu}^{\infty} d^2 y F_{a_1 a_2}^{n_F+1}(x_1, x_2, y; \mu) + \sum_{a_0} U_{a_1 a_2, a_0}^{n_F+1}(\nu, \mu) \otimes_{12} f_{a_0}^{n_F+1}(\mu), \quad (7.1)$$

where we use the notation

$$\int_{y_0}^{y_1} d^2 y = 2\pi \int_{y_0}^{y_1} dy y \quad (7.2)$$

for an integral over a ring in the \mathbf{y} plane. The ν dependence cancels between the two terms on the r.h.s. of (7.1), up to power corrections in Λ/ν , where Λ is a hadronic scale. We therefore require $\nu \gg \Lambda$. In line with the convention in (5.2), we will suppress arguments and write

$$F_{a_1 a_2}^{n_F, \overline{\text{MS}}} \equiv F_{a_1 a_2}^{n_F, \overline{\text{MS}}}(x_1, x_2, y; \mu) \quad (7.3)$$

in the following. The perturbative expansion of the matching kernels U reads

$$U_{a_1 a_2, a_0}^{n_F}(z_1, z_2; \nu, \mu) = \sum_{k=1}^{\infty} [a_s^{n_F}(\mu)]^k U_{a_1 a_2, a_0}^{n_F(k)}(z_1, z_2; \nu, \mu) \quad (7.4)$$

with

$$U_{a_1 a_2, a_0}^{n_F(k)}(z_1, z_2; \nu, \mu) = \sum_{\ell=0}^{k-1} \log^{\ell} \frac{\mu^2}{\nu^2} U_{a_1 a_2, a_0}^{n_F[k, \ell]}(z_1, z_2). \quad (7.5)$$

In the following derivations, the kernels U will be needed at different values of ν but always the same μ . Using that the ν dependence appears only via the ratio μ/ν in (7.5), we write

$$U_{a_1 a_2, a_0}^{n_F}(\mu/\nu) \equiv U_{a_1 a_2, a_0}^{n_F}(z_1, z_2; \nu, \mu), \quad (7.6)$$

where the separate dependence on μ , due to the factors of $a_s(\mu)$ in (7.4), is suppressed on the l.h.s. The coefficients $U^{n_F[k, \ell]}$ are related to $V^{n_F[k, \ell-1]}$ via

$$U_{a_1 a_2, a_0}^{n_F[k, \ell]} = \frac{1}{\ell} V_{a_1 a_2, a_0}^{n_F[k, \ell-1]} \quad \text{for } \ell \geq 1. \quad (7.7)$$

Details about the U kernels are given in equations (79), (116) and (140) of reference [52]. In the following, we need that the coefficients $U^{[1,0]}$ are n_F independent, whilst $U^{n_F[2,0]}$ has the same type of n_F dependence as $V^{n_F[2,0]}$. In analogy to (5.8), we can hence write

$$U_{a_1 a_2, a_0}^{n_F[2,0]} = \tilde{U}_{a_1 a_2, a_0}^{[2,0]} + \beta_0^{n_F} U_{a_1 a_2, a_0}^{\beta[2,0]} \quad \text{for } (a_1 a_2, a_0) = (qg, q) \text{ and } (gg, g), \quad (7.8)$$

where $U^{\beta[2,0]}$ is proportional to $\delta(1 - z_1 - z_2)$. The kernels in the matching equation (7.1) have been computed only for massless quarks. They are associated with physics at momentum scales above ν , so that in our setting with a heavy flavour Q we can use them if $\nu \gg m_Q$. This is ensured by taking

$$\nu = \beta m_Q \quad \text{with } \beta \gg 1. \quad (7.9)$$

For DPDs with $n_F + 1$ active flavours, the momentum sum rule reads

$$\sum_{a_2} \int_2 X_2 F_{a_1 a_2}^{n_F+1, \overline{\text{MS}}} = (1 - X) f_{a_1}^{n_F+1}, \quad (7.10)$$

and the number sum rule is given by

$$\int_2 F_{a_1 a_{2v}}^{n_F+1, \overline{\text{MS}}} = (N_{a_{2v}} + \delta_{a_1 \bar{a}_2} - \delta_{a_1 a_2}) f_{a_1}^{n_F+1}, \quad (7.11)$$

where $N_{a_{2v}}$ is the number of valence quarks with flavour a_2 in the hadron. The parton label a_{2v} denotes the difference between a_2 and \bar{a}_2 , i.e. we write $F_{a_1 a_{2v}} = F_{a_1 a_2} - F_{a_1 \bar{a}_2}$ for DPDs and likewise for various kernels appearing below. We also use the shorthand notation introduced in reference [66], where integrals over momentum fractions are denoted by

$$\int C = \int dx C(x), \quad \int_2 D = \int dx_2 D(x_1, x_2) \quad (7.12)$$

for functions of one or two momentum fractions. The multiplication with a power of a momentum fraction is indicated by operators X^n and X_2^n , which act as

$$(X^n C)(x) = x^n C(x), \quad (X_2^n D)(x_1, x_2) = x_2^n D(x_1, x_2). \quad (7.13)$$

The integration boundaries in (7.10) and (7.11) are readily inferred from the support properties of the DPDs, and one finds that the x_2 integrations run from 0 to $1 - x_1$ in both sum rules. It is furthermore understood that the left- and right-hand sides of (7.10) and (7.11) still depend on the momentum fraction x_1 , which is not written out explicitly.

In the following calculations, we will use the identities

$$\int_2 X_2^n (C \otimes_2 D) = \left(\int X^n C \right) \left(\int_2 X_2^n D \right), \quad (7.14)$$

$$\int_2 X_2^n (D \otimes_{12} C) = \left(\int_2 X_2^n D \right) \otimes (X^n C) \quad (7.15)$$

derived in section 6.1 of [66], where it is understood that the overall expressions depend on x_1 in both cases.

$f(y)$	1	$\log(m_Q^2/\mu_y^2)$	$k_{11}(ym_Q)$	$k_{02}(ym_Q)$	$k_{00}(ym_Q)$
$I[f]$	$-2\log\alpha + 2\log\beta$	$2\log^2\alpha - 2\log^2\beta$	$-1 + 2\log\beta$	$1 + 2\log^2\beta$	1

Table 1: Integrals $I[f] = \int_{y_\beta}^{y_\alpha} d^2y f(y)/(\pi y^2)$ of functions $f(y)$ that appear in our parametrisation of the splitting kernels. The integration limits are defined in (7.16), and the limits $\alpha \ll 1$ and $\beta \gg 1$ have been taken.

7.1 Sum rules for the massive splitting kernels

The sum rules just spelled out involve an integral over DPDs from the perturbative to the nonperturbative region of y . To make contact with the DPD splitting kernels, we split the integration over y into the two intervals $[y_\beta, y_\alpha]$ and $[y_\alpha, \infty]$, where

$$y_\beta = b_0/(\beta m_Q), \quad y_\alpha = b_0/(\alpha m_Q) \quad (7.16)$$

with $\beta \gg 1$ and $\alpha \ll 1$, and with αm_Q being in the perturbative region.² The lower limit y_β is equal to ν/b_0 with ν given in (7.9). A number of integrals over y that will be used in the following is collected in table 1.

The y integral on the r.h.s. of the matching equation (7.1) can now be written as

$$\int_{y_\beta}^{\infty} d^2y F_{a_1 a_2}^{n_F+1} = \int_{y_\beta}^{y_\alpha} d^2y \frac{1}{\pi y^2} \sum_{a_0} V_{a_1 a_2, a_0}^{Q, n_F} \otimes_{12} f_{a_0}^{n_F} + \sum_{b_1, b_2} A_{a_1 b_1}^{Q, n_F} \otimes_1 A_{a_2 b_2}^{Q, n_F} \otimes_2 \int_{y_\alpha}^{\infty} d^2y F_{b_1 b_2}^{n_F}. \quad (7.17)$$

For $y_\beta \leq y \leq y_\alpha$, we have used the massive DPD splitting formula, whereas for $y > y_\alpha$ we used DPD flavour matching to relate F^{n_F+1} to F^{n_F} . This is in line with the scheme we presented in section 3.2.2, except that for large y one cannot compute F^{n_F} using a splitting formula. We now use the analogue of the matching formula (7.1) for n_F flavours and take $\nu = \alpha m_Q$, which satisfies $\nu \gg \Lambda$ by assumption. This gives

$$\int_{y_\alpha}^{\infty} d^2y F_{b_1 b_2}^{n_F} = F_{b_1 b_2}^{n_F, \overline{\text{MS}}} - \sum_{a_0} U_{b_1 b_2, a_0}^{n_F} \left(\frac{\mu}{\alpha m_Q} \right) \otimes_{12} f_{a_0}^{n_F}. \quad (7.18)$$

Inserting (7.17) and (7.18) into (7.1), we obtain our master formula

$$\begin{aligned} & F_{a_1 a_2}^{n_F+1, \overline{\text{MS}}} \\ &= \sum_{a_0} \left[\int_{y_\beta}^{y_\alpha} d^2y \frac{1}{\pi y^2} V_{a_1 a_2, a_0}^{Q, n_F} \otimes_{12} f_{a_0}^{n_F} + \sum_{b_0} U_{a_1 a_2, b_0}^{n_F+1}(r_\beta) \otimes_{12} A_{b_0 a_0}^{Q, n_F} \right] \otimes_{12} f_{a_0}^{n_F} \\ &+ \sum_{b_1, b_2} A_{a_1 b_1}^{Q, n_F} \otimes_1 A_{a_2 b_2}^{Q, n_F} \otimes_2 \left[F_{b_1 b_2}^{n_F, \overline{\text{MS}}} - \sum_{a_0} U_{b_1 b_2, a_0}^{n_F}(r_\alpha) \otimes_{12} f_{a_0}^{n_F} \right], \end{aligned} \quad (7.19)$$

where for the term going with U^{n_F+1} we have expressed f^{n_F+1} in terms of f^{n_F} and used the relation (2.28) for a triple convolution. For the argument μ/ν of the U kernels (see (7.6)), we have introduced the notation

$$r_\beta = \mu/(\beta m_Q), \quad r_\alpha = \mu/(\alpha m_Q) \quad (7.20)$$

in analogy to (7.16). Using the DPD sum rules for both $F^{n_F+1, \overline{\text{MS}}}$ and $F^{n_F, \overline{\text{MS}}}$ in (7.19), we will obtain sum rules for the massive splitting kernels V^{Q, n_F} .

²These conditions on α cannot be satisfied for $m_Q = m_c$. Since the aim of this section is to derive constraints on the perturbative kernels V^Q for a generic heavy flavour Q , we can consider a value m_Q that is as large as needed for our arguments to hold.

7.1.1 Momentum sum rule

When inserting (7.19) into the momentum sum rule (7.10) for a DPD with $n_F + 1$ active flavours, one needs the expression

$$M_{b_1}^{n_F}(x_1) = \sum_{a_2, b_2} \int_2 X_2 \left(A_{a_2 b_2}^{Q, n_F} \otimes_2 D_{b_1 b_2}^{n_F} \right) = \sum_{a_2, b_2} \left(\int X A_{a_2 b_2}^{Q, n_F} \right) \left(\int_2 X_2 D_{b_1 b_2}^{n_F} \right), \quad (7.21)$$

where D^{n_F} is the expression in square brackets on the last line of (7.19), and where we used (7.14) in the last step. We now use the momentum sum rule for the PDF matching kernels,

$$\sum_{a_2} \int X A_{a_2 b_2}^{Q, n_F} = \delta_{b_2 l}^{n_F}, \quad (7.22)$$

which ensures the consistency of the momentum sum rules for PDFs with n_F and $n_F + 1$ flavours and can readily be checked for the LO and NLO expressions (2.18) and (2.20). This gives

$$M_{b_1}^{n_F}(x_1) = \sum_{b_2} \int_2 X_2 D_{b_1 b_2}^{n_F} = \sum_{b_2} \int_2 X_2 F_{b_1 b_2}^{n_F, \overline{\text{MS}}} - \sum_{b_2, a_0} \int_2 X_2 \left(U_{b_1 b_2, a_0}^{n_F}(r_\alpha) \otimes_{12} f_{a_0}^{n_F} \right), \quad (7.23)$$

where we could drop $\delta_{b_2 l}^{n_F}$ because D^{n_F} is constructed from quantities with n_F flavours. The first term on the r.h.s. of (7.23) is equal to $(1 - X) f_{b_1}^{n_F}$ according to the DPD momentum sum rule for n_F flavours. Putting everything together and using the relations (7.14) and (7.15) for integrals over convolution products, we obtain

$$\begin{aligned} \sum_{a_2} \int_2 X_2 F_{a_1 a_2}^{n_F+1, \overline{\text{MS}}} &= \sum_{a_0, a_2} \left(\int_2 X_2 \int_{y_\beta}^{y_\alpha} d^2 y \frac{1}{\pi y^2} V_{a_1 a_2, a_0}^Q \right) \otimes (X f_{a_0}^{n_F}) \\ &+ \sum_{a_0, a_2, b_0} \left(\int_2 X_2 U_{a_1 a_2, b_0}^{n_F+1}(r_\beta) \right) \otimes (X A_{b_0 a_0}^{Q, n_F}) \otimes (X f_{a_0}^{n_F}) \\ &+ \sum_{b_1} A_{a_1 b_1}^{Q, n_F} \otimes_1 (1 - X) f_{b_1}^{n_F} - \sum_{a_0, b_1, b_2} A_{a_1 b_1}^{Q, n_F} \otimes_1 \left(\int_2 X_2 U_{b_1 b_2, a_0}^{n_F}(r_\alpha) \right) \otimes (X f_{a_0}^{n_F}). \end{aligned} \quad (7.24)$$

The r.h.s. of the DPD momentum sum rule (7.10) for $n_F + 1$ flavours can be expressed in terms of an n_F flavour PDF as

$$\sum_{a_0} (1 - X) (A_{a_1 a_0}^Q \otimes f_{a_0}^{n_F}) = \sum_{a_0} A_{a_1 a_0}^Q \otimes f_{a_0}^{n_F} - \sum_{a_0} (X A_{a_1 a_0}^Q) \otimes (X f_{a_0}^{n_F}) \quad (7.25)$$

and is to be evaluated at momentum fraction x_1 . Using that (7.24) and (7.25) must be equal for any set of PDFs f^{n_F} , we obtain the desired momentum sum rule for the heavy-quark kernels $V_{a_1 a_2, a_0}^Q$:

$$\begin{aligned} \sum_{a_2} \int_2 X_2 \int_{y_\beta}^{y_\alpha} d^2 y \frac{1}{\pi y^2} V_{a_1 a_2, a_0}^Q &= (1 - X) A_{a_1 a_0}^{Q, n_F} \\ &+ \sum_{b_1, a_2} A_{a_1 b_1}^{Q, n_F} \otimes \left(\int_2 X_2 U_{b_1 a_2, a_0}^{n_F}(r_\alpha) \right) - \sum_{a_2, b_0} \left(\int_2 X_2 U_{a_1 a_2, b_0}^{n_F+1}(r_\beta) \right) \otimes (X A_{b_0 a_0}^{Q, n_F}). \end{aligned} \quad (7.26)$$

At LO, the only heavy-quark kernel is $V_{Q\bar{Q},g}^{Q(1)}$, which appears in the sum rule for $a_0 = g$ and $a_1 = Q$. The term of order $a_s^{n_F+1}$ in (7.26) reads

$$\sum_2 X_2 \int_{y_\beta}^{y_\alpha} d^2y \frac{1}{\pi y^2} V_{Q\bar{Q},g}^{Q(1)} = (1-X) A_{Qg}^{Q(1)} - \int_2 X_2 U_{q\bar{q},g}^{(1)}(r_\beta) \quad (7.27)$$

for this channel. With the explicit form (2.21) of $A_{Qg}^{Q(1)}$ and with

$$U_{q\bar{q},g}^{(1)}\left(\frac{\mu}{\nu}\right) = \delta(1-z_1-z_2) T_F \left[(z_1^2+z_2^2) \log \frac{\mu^2}{\nu^2} - 2z_1 z_2 \right], \quad (7.28)$$

the r.h.s. of (7.27) reduces to

$$2 T_F (1-z_1) \left[(z_1^2 + (1-z_1)^2) \log \alpha + (1-z_1) z_1 \right]. \quad (7.29)$$

For the l.h.s. of equation (7.27) one obtains the same expression, using the result (3.5) for the LO splitting kernel and the relevant integral in table 1. This confirms the validity of the momentum sum rules for the massive splitting kernels at LO.

The term of order $(a_s^{n_F+1})^2$ in equation (7.26) is given by

$$\begin{aligned} \sum_{a_2} \int_2 X_2 \int_{y_\beta}^{y_\alpha} d^2y V_{a_1 a_2, a_0}^{Q, n_F(2)} &= (1-X) A_{a_1 a_0}^{Q(2)} \\ &+ \sum_{a_2} \int_2 X_2 \left[U_{a_1 a_2, a_0}^{n_F(2)}(r_\alpha) - U_{a_1 a_2, a_0}^{n_F+1(2)}(r_\beta) \right] + A_\alpha^{(1)} \sum_{a_2} \int_2 X_2 U_{a_1 a_2, a_0}^{(1)}(r_\alpha) \\ &+ \sum_{b_1, a_2} A_{a_1 b_1}^{Q(1)} \otimes_1 \left(\int_2 X_2 U_{b_1 a_2, a_0}^{(1)}(r_\alpha) \right) - \sum_{a_2, b_0} \left(\int_2 X_2 U_{a_1 a_2, b_0}^{(1)}(r_\beta) \right) \otimes \left(X A_{b_0 a_0}^{Q(1)} \right) \end{aligned} \quad (7.30)$$

where we have rewritten the perturbative expansion (7.4) of U^{n_F} in terms of $a_s^{n_F+1}$ using the matching equation (2.12) for the strong coupling. Since all quantities on its r.h.s. are known, (7.30) provides a non-trivial constraint on the massive two-loop splitting kernels.

7.1.2 Number sum rule

In analogy to (7.21), we now need the expression

$$N_{b_1 a_2 v}^{n_F} = \sum_{b_2} \int_2 A_{a_2 v b_2}^{Q, n_F} \otimes_2 D_{b_1 b_2}^{n_F} = \sum_{b_2} \left(\int A_{a_2 v b_2}^{Q, n_F} \right) \left(\int D_{b_1 b_2}^{n_F} \right) \quad (7.31)$$

where D^{n_F} denotes again the expression in square brackets on the last line of (7.19). The number sum rule for the PDF matching kernels reads

$$\int A_{a_2 v b_2}^{Q, n_F} = \delta_{b_2 l}^{n_F} (\delta_{a_2 b_2} - \delta_{\bar{a}_2 b_2}), \quad (7.32)$$

which is easily verified for the LO and NLO expressions (2.18) and (2.20). Inserting this in (7.31) and performing the sum over b_2 , we get

$$N_{b_1 a_2 v}^{n_F}(x_1) = \int_2 D_{b_1 a_2 v}^{n_F} = \int_2 F_{b_1 a_2 v}^{n_F, \overline{\text{MS}}} - \sum_{a_0} \int_2 \left(U_{b_1 a_2 v, a_0}^{n_F}(r_\alpha) \otimes_{12} f_{a_0}^{n_F} \right). \quad (7.33)$$

The first term on the r.h.s. is equal to $(N_{a_{2v}} + \delta_{b_1\bar{a}_2} - \delta_{b_1a_2}) f_{b_1}^{n_F}$ by virtue of the DPD number sum rule for n_F flavours. With this, we obtain

$$\begin{aligned}
\int_2 F_{a_1 a_{2v}}^{n_F+1, \overline{\text{MS}}} &= \sum_{a_0} \left(\int_2 \int_{y_\beta}^{y_\alpha} \frac{1}{\pi y^2} V_{a_1 a_{2v}, a_0}^Q \right) \otimes f_{a_0}^{n_F} \\
&+ \sum_{a_0, b_0} \left(\int U_{a_1 a_{2v}, b_0}^{n_F+1}(r_\beta) \right) \otimes A_{b_0 a_0}^{Q, n_F} \otimes f_{a_0}^{n_F} \\
&+ \sum_{b_1} (N_{a_{2v}} + \delta_{b_1\bar{a}_2} - \delta_{b_1a_2}) A_{a_1 b_1}^{Q, n_F} \otimes_1 f_{b_1}^{n_F} - \sum_{a_0, b_1} A_{a_1 b_1}^{Q, n_F} \otimes_1 \left(\int_2 U_{b_1 a_{2v}, a_0}^{n_F}(r_\alpha) \right) \otimes f_{a_0}^{n_F}.
\end{aligned} \tag{7.34}$$

Expressing the r.h.s. of the number sum rule (7.11) for $n_F + 1$ flavours in terms of a n_F flavour PDF, we get

$$(N_{a_{2v}} + \delta_{a_1\bar{a}_2} - \delta_{a_1a_2}) \sum_{a_0} A_{a_1 a_0}^{Q, n_F} \otimes f_{a_0}^{n_F}. \tag{7.35}$$

Using that (7.34) and (7.35) must be equal, we obtain the number sum rule for the massive splitting kernels:

$$\begin{aligned}
\int_2 \int_{y_\beta}^{y_\alpha} d^2 y \frac{1}{\pi y^2} V_{a_1 a_{2v}, a_0}^{Q, n_F} &= (\delta_{a_1\bar{a}_2} - \delta_{a_1a_2} - \delta_{a_2\bar{a}_0} + \delta_{a_2a_0}) A_{a_1 a_0}^{Q, n_F} \\
&+ \sum_{b_1} A_{a_1 b_1}^{Q, n_F} \otimes \left(\int_2 U_{b_1 a_{2v}, a_0}^{n_F}(r_\alpha) \right) - \sum_{b_2} \left(\int_2 U_{a_1 a_{2v}, b_0}^{n_F+1}(r_\beta) \right) \otimes A_{b_0 a_0}^{Q, n_F}.
\end{aligned} \tag{7.36}$$

Let us explicitly verify this at LO for the kernel $V_{QQv,g}^{Q(1)} = -V_{Q\bar{Q},g}^{Q(1)}$. In this case, the term of order $a_s^{n_F+1}$ in (7.36) reads

$$\int_2 \int_{y_\beta}^{y_\alpha} d^2 y \frac{1}{\pi y^2} V_{Q\bar{Q},g}^{Q(1)} = A_{Qg}^{Q(1)} - \int_2 U_{q\bar{q},g}^{n_F+1(1)}(r_\beta). \tag{7.37}$$

Using the expression (3.5) of the massive splitting kernel together with (2.21) and (7.28), one finds that both sides of this equation evaluate to

$$-2T_F \left[(z_1^2 + z_2^2) \log \alpha - z_1 z_2 \right]. \tag{7.38}$$

The term of order $(a_s^{n_F+1})^2$ in equation (7.36) reads

$$\begin{aligned}
\int_2 \int_{y_\beta}^{y_\alpha} d^2 y \frac{1}{\pi y^2} V_{a_1 a_{2v}, a_0}^{Q, n_F(2)} &= (\delta_{a_1\bar{a}_2} - \delta_{a_1a_2} - \delta_{a_2\bar{a}_0} + \delta_{a_2a_0}) A_{a_1 a_0}^{Q(2)} \\
&+ \int_2 \left[U_{a_1 a_{2v}, a_0}^{n_F(2)}(r_\alpha) - U_{a_1 a_{2v}, a_0}^{n_F+1(2)}(r_\beta) \right] + A_\alpha^{(1)} \int_2 U_{a_1 a_{2v}, a_0}^{(1)}(r_\alpha) \\
&+ \sum_{b_1} A_{a_1 b_1}^{Q(1)} \otimes \left(\int_2 U_{b_1 a_{2v}, a_0}^{(1)}(r_\alpha) \right) - \sum_{b_2} \left(\int_2 U_{a_1 a_{2v}, b_0}^{(1)}(r_\beta) \right) \otimes A_{b_0 a_0}^{Q(1)}
\end{aligned} \tag{7.39}$$

and provides another constraint on the massive NLO splitting kernels.

7.2 Sum rules for the interpolating function V^I

Let us now rewrite the sum rules (7.30) and (7.39) for the two-loop kernels in terms of the interpolating term V^I in our parametrisation (5.26). To this end, it is sufficient to evaluate these sum rules at the scale $\mu = m_Q$, where they simplify considerably. Using (5.26) and the integrals in table 1, we find that the y integral needed in the sum rules reads

$$\int_{y_\beta}^{y_\alpha} d^2y \frac{1}{\pi y^2} V_{a_1 a_2, a_0}^{Q, n_F(2)}(\mu = m_Q) = (1 - 2 \log \alpha) V_{a_1 a_2, a_0}^{n_F[2,0]} + (1 + 2 \log^2 \alpha) V_{a_1 a_2, a_0}^{n_F[2,1]} \\ - (1 - 2 \log \beta) V_{a_1 a_2, a_0}^{n_F+1[2,0]} - (1 + 2 \log^2 \beta) V_{a_1 a_2, a_0}^{n_F+1[2,1]} + v_{a_1 a_2, a_0}^I, \quad (7.40)$$

where we defined

$$\int_{y_\beta}^{y_\alpha} d^2y \frac{1}{\pi y^2} V_{a_1 a_2, a_0}^I(z_1, z_2, y m_Q) = v_{a_1 a_2, a_0}^I(z_1, z_2). \quad (7.41)$$

Since V^I tends to zero for both $y \rightarrow 0$ and $y \rightarrow \infty$, the y integral in (7.41) is finite for $\alpha \rightarrow 0$ and $\beta \rightarrow \infty$ and evaluated in this limit, as are the integrals in table 1.

Momentum sum rule. For $\mu = m_Q$, the momentum sum rule (7.30) simplifies to

$$\sum_{a_2} \int_2 X_2 \int_{y_\beta}^{y_\alpha} d^2y \frac{1}{\pi y^2} V_{a_1 a_2, a_0}^{Q(2)}(\mu = m_Q) = (1 - X) A_{a_1 a_0}^{Q[2,0]} \\ + \sum_{a_2} \int_2 X_2 \left[U_{a_1 a_2, a_0}^{n_F(2)}(\alpha^{-1}) - U_{a_1 a_2, a_0}^{n_F+1(2)}(\beta^{-1}) \right]. \quad (7.42)$$

Here we have replaced the two-loop PDF matching kernel $A^{Q(2)}$ with its non-logarithmic part $A^{Q[2,0]}$, given that the other terms in (2.17) vanish for $\mu = m_Q$. The one-loop matching kernels $A_\alpha^{(1)}$ and $A^{Q(1)}$ are zero at that point.

Inserting (7.40) for the y integral on the l.h.s. of equation (7.42) and the decomposition (7.5) for the two-loop U kernels on its r.h.s., we obtain

$$\sum_{a_2} \int_2 X_2 \left[(1 - 2 \log \alpha) V_{a_1 a_2, a_0}^{n_F[2,0]} + (1 + 2 \log^2 \alpha) V_{a_1 a_2, a_0}^{n_F[2,1]} \right. \\ \left. - (1 - 2 \log \beta) V_{a_1 a_2, a_0}^{n_F+1[2,0]} - (1 + 2 \log^2 \beta) V_{a_1 a_2, a_0}^{n_F+1[2,1]} + v_{a_1 a_2, a_0}^I \right] \\ = (1 - X) A_{a_1 a_0}^{Q[2,0]} + \sum_{a_2} \int_2 X_2 \left(U_{a_1 a_2, a_0}^{n_F[2,0]} - 2 \log \alpha U_{a_1 a_2, a_0}^{n_F[2,1]} + 4 \log^2 \alpha U_{a_1 a_2, a_0}^{n_F[2,2]} \right) \\ - \sum_{a_2} \int_2 X_2 \left(U_{a_1 a_2, a_0}^{n_F+1[2,0]} - 2 \log \beta U_{a_1 a_2, a_0}^{n_F+1[2,1]} + 4 \log^2 \beta U_{a_1 a_2, a_0}^{n_F+1[2,2]} \right). \quad (7.43)$$

Using the relation (7.7) between $U^{[k,\ell]}$ and $V^{[k,\ell-1]}$, we find that all terms depending on α or β cancel and obtain the momentum sum rule

$$\sum_{a_2} \int_2 X_2 v_{a_1 a_2, a_0}^I = (1 - X) A_{a_1 a_0}^{Q[2,0]} + \sum_{a_2} \int_2 X_2 \left(U_{a_1 a_2, a_0}^{n_F[2,0]} - V_{a_1 a_2, a_0}^{n_F[2,0]} - V_{a_1 a_2, a_0}^{n_F[2,1]} \right) \\ - \sum_{a_2} \int_2 X_2 \left(U_{a_1 a_2, a_0}^{n_F+1[2,0]} - V_{a_1 a_2, a_0}^{n_F+1[2,0]} - V_{a_1 a_2, a_0}^{n_F+1[2,1]} \right) \quad (7.44)$$

for the interpolating function v^I . Notice that this relation only depends on one momentum fraction and does not involve any scale or quark mass.

Number sum rule. For $\mu = m_Q$, the number sum rule (7.39) has the form

$$\int_2 \int_{y_\beta}^{y_\alpha} d^2 y \frac{1}{\pi y^2} V_{a_1 a_{2v}, a_0}^{Q, n_F(2)}(\mu = m_Q) = (\delta_{a_1 \bar{a}_2} - \delta_{a_1 a_2} - \delta_{a_2 \bar{a}_0} + \delta_{a_2 a_0}) A_{a_1 a_0}^{Q[2,0]} + \int_2 \left[U_{a_1 a_{2v}, a_0}^{n_F(2)}(\alpha^{-1}) - U_{a_1 a_{2v}, a_0}^{n_F+1(2)}(\beta^{-1}) \right]. \quad (7.45)$$

Following the same steps that lead from (7.42) to (7.43), we obtain

$$\int_2 v_{a_1 a_{2v}, a_0}^I = (\delta_{a_1 \bar{a}_2} - \delta_{a_1 a_2} - \delta_{a_2 \bar{a}_0} + \delta_{a_2 a_0}) A_{a_1 a_0}^{Q[2,0]} + \int_2 \left(U_{a_1 a_{2v}, a_0}^{n_F[2,0]} - V_{a_1 a_{2v}, a_0}^{n_F[2,0]} - V_{a_1 a_{2v}, a_0}^{n_F[2,1]} \right) - \int_2 \left(U_{a_1 a_{2v}, a_0}^{n_F+1[2,0]} - V_{a_1 a_{2v}, a_0}^{n_F+1[2,0]} - V_{a_1 a_{2v}, a_0}^{n_F+1[2,1]} \right). \quad (7.46)$$

7.3 Explicit determination of the NLO kernel for $g \rightarrow q\bar{q}$

The constraints discussed in the previous subsections can be used to fully determine the kernel $V_{q\bar{q},g}^{Q(2)}$ for a gluon splitting into a light $q\bar{q}$ pair. To this end it is crucial to realise that this kernel can be written as

$$V_{q\bar{q},g}^{Q(2)} = V_{q\bar{q},g}^{(2)} + v_{q\bar{q},g}^Q, \quad (7.47)$$

where $V^{(2)}$ is the massless kernel. The term v^Q contains the contributions from the graph in figure 22 and its complex conjugate, together with the $\overline{\text{MS}}$ counterterm of the heavy-quark loop. Since this is a virtual graph with no lines crossing the final-state cut, v^Q includes the momentum conservation constraint $\delta(1 - z_1 - z_2)$, just like the LO splitting kernels (2.32). As indicated in the figure, v^Q factorises into two parts,

$$v_{q\bar{q},g}^Q(z_1, z_2, y, m_Q; \mu) = V_{q\bar{q},g}^{(1)}(z_1, z_2, y, m_Q) g(m_Q; \mu), \quad (7.48)$$

where the upper part is simply given by the LO $g \rightarrow q\bar{q}$ splitting kernel. The function g that represents the lower part cannot depend on y , since this variable is defined in terms of the lines in the upper part of the graph (see section 4.1 of [52] for details). Likewise, g cannot depend on the momentum fractions z_1 and z_2 of the lines in the upper part. It is straightforward to compute it from the renormalised one-loop graph. Here, we show instead how its expression can be obtained from the results we already derived so far.

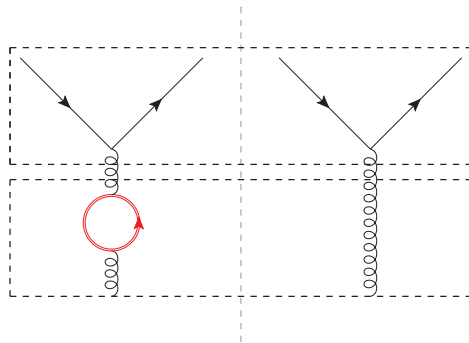


Figure 22: Heavy-quark contribution to $V_{q\bar{q},g}^{Q(2)}$. The heavy quark is indicated by a red double line.

The μ dependence of g is readily obtained from (7.47) and (7.48):

$$\frac{d}{d \log \mu^2} \left(V_{q\bar{q},g}^{(1)} g(\mu) \right) = \frac{d}{d \log \mu^2} \left(V_{q\bar{q},g}^{Q(2)}(\mu) - V_{q\bar{q},g}^{(2)}(\mu) \right) = \frac{\Delta\beta_0}{2} V_{q\bar{q},g}^{(1)}, \quad (7.49)$$

where we indicated only the μ dependence of the functions. In the last step, we used equations (2.30), (5.17), and (5.19). The solution of (7.49) is

$$g(m_Q; \mu) = g_0 + \frac{\Delta\beta_0}{2} \log \frac{\mu^2}{m_Q^2}. \quad (7.50)$$

The integration constant g_0 can be fixed using the number sum rule (7.39) for $V_{q\bar{q},g}^{Q(2)} = -V_{q\bar{q},g}^{(2)}$. Evaluating this sum rule at $\mu = m_Q$, we obtain

$$\int_2 \int_{y_\beta}^{y_\alpha} d^2 y \frac{1}{\pi y^2} \left[V_{q\bar{q},g}^{[2,0]} + \log \frac{m_Q^2}{\mu_y^2} V_{q\bar{q},g}^{[2,1]} + V_{q\bar{q},g}^{(1)} g_0 \right] = \int_2 \left[U_{q\bar{q},g}^{(2)}(\alpha^{-1}) - U_{q\bar{q},g}^{(2)}(\beta^{-1}) \right] \quad (7.51)$$

where we used that $A_{qg}^{Q(2)} = 0$ and that $U_{q\bar{q},g}^{(2)}$ is independent of n_F . The evaluation of both sides proceeds in full analogy to the steps leading from (7.42) to equation (7.43). Using the relation (7.7) between U and V kernels, we find that the sum rule integral over g_0 must be zero. Since g_0 is a constant, this implies

$$g_0 = 0. \quad (7.52)$$

The full expression for $V_{q\bar{q},g}^{Q(2)}$ thus reads

$$V_{q\bar{q},g}^{Q(2)} = V_{q\bar{q},g}^{(2)} + \frac{\Delta\beta_0}{2} \log \frac{\mu^2}{m_Q^2} V_{q\bar{q},g}^{(1)} = V_{q\bar{q},g}^{(2)} + V_{q\bar{q},g}^{(1)} \otimes_{12} A_{gg}^{Q(1)}. \quad (7.53)$$

Comparing this result with the general parametrisation (5.32), we find that the interpolating function $V_{q\bar{q},g}^I$ is zero, as we anticipated in (5.40).

Whilst the sum rules are only valid for unpolarised DPDs, a representation analogous to (7.47) and (7.48) holds also for polarised quarks. Since it involves the same function g for the heavy-quark loop on a gluon line, the result (7.53) generalises to longitudinal or transverse polarisation of the quark and antiquark, with the appropriate V kernels for polarised $g \rightarrow q\bar{q}$ splitting.

8 A model for the unpolarised massive splitting kernels at NLO

In this section, we formulate a model ansatz for the interpolation part V^I of the massive two-loop kernels, which may be used as long as these kernels have not been computed. The interpolating functions must satisfy the limiting behaviour (5.28) at small and large y , which does not provide any constraints on their form at intermediate $y \sim 1/m_Q$. For unpolarised partons, such constraints are provided by the sum rules (7.44) and (7.46) derived in the previous section, which involve an integral over y . We therefore limit our model ansatz to the unpolarised case.

To begin with, we set

$$V_{a_1 a_2, a_0}^I(z_1, z_2, y, m_Q) = k_{00}(y m_Q) v_{a_1 a_2, a_0}^I(z_1, z_2), \quad (8.1)$$

which goes to zero for $y \rightarrow 0$ and $y \rightarrow \infty$, and which is consistent with the normalisation condition (7.41) according to the rightmost entry in table 1. The form (8.1) is inspired by the result for (3.5) of the LO kernels, which contain $k_{00}(ym_Q)$ multiplied by a function of z_1 and z_2 . To be clear, we do *not* expect that the NLO splitting graphs with massive lines yield such a simple factorised form of the y dependence, so that our ansatz is only guided by simplicity at this stage.

8.1 Constraints on the interpolating functions

The factorised ansatz (8.1) allows us to directly use the sum rule constraints (7.44) and (7.46) on the two-parameter functions $v_{a_1 a_2, a_0}^I(z_1, z_2)$. To determine these is not a trivial task, since in general the kernel for given parton labels $(a_1 a_2, a_0)$ appears in different sum rules. In the following we present a sequential construction that ensures that the sum rule constraints are satisfied for all parton channels.

First group: $V_{Q\bar{Q},q}^{Q(2)} + V_{Qq,q}^{Q(2)}$ and $V_{qQ,q}^{Q(2)} + V_{qq,q}^{Q(2)}$

The kernels for the channels $q \rightarrow Q\bar{Q}$, $q \rightarrow Qq$, and $q \rightarrow qq$ have to be treated simultaneously, because they enter together in two distinct momentum sum rules. In addition to these momentum sum rules, one finds three number sum rules for

$$V_{Qv,q}^{Q(2)} = V_{Qq,q}^{Q(2)}, \quad V_{QQv,q}^{Q(2)} = -V_{Q\bar{Q},q}^{Q(2)}, \quad V_{gqv,q}^{Q(2)} = V_{gq,q}^{Q(2)}. \quad (8.2)$$

Sum rule constraints. The momentum sum rules for the interpolating functions read

$$\int_2 X_2 \left(v_{Q\bar{Q},q}^I + v_{Qq,q}^I \right) = (1-X) A_{Qq}^{Q[2,0]} - \int_2 X_2 \left(U_{q'\bar{q}',q}^{[2,0]} - V_{q'\bar{q}',q}^{[2,0]} - V_{q'\bar{q}',q}^{[2,1]} + U_{q'q,q}^{[2,0]} - V_{q'q,q}^{[2,0]} - V_{q'q,q}^{[2,1]} \right), \quad (8.3)$$

$$\int_2 X_2 \left(2v_{qQ,q}^I + v_{qq,q}^I \right) = (1-X) A_{qq}^{Q[2,0]} - 2 \int_2 X_2 \left(U_{qq',q}^{[2,0]} - V_{qq',q}^{[2,0]} - V_{qq',q}^{[2,1]} \right) - \Delta\beta_0 \int_2 X_2 \left(U_{qq,q}^{\beta[2,0]} - V_{qq,q}^{\beta[2,0]} - V_{qq,q}^{(1)} \right), \quad (8.4)$$

where we used (5.8), (5.9) and (7.8) to simplify the difference of V or U kernels for $n_F + 1$ and n_F . In (8.4) we also used $v_{qQ,q}^I + v_{q\bar{Q},q}^I = 2v_{qQ,q}^I$ and corresponding relations for the V and U kernels on the r.h.s. The relevant number sum rules are given by

$$\int_2 v_{Q\bar{Q},q}^I = A_{Qq}^{Q[2,0]} - \int_2 \left(U_{q'\bar{q}',q}^{[2,0]} - V_{q'\bar{q}',q}^{[2,0]} - V_{q'\bar{q}',q}^{[2,1]} \right), \quad (8.5)$$

$$\int_2 v_{Qq,q}^I = A_{Qq}^{Q[2,0]} - \int_2 \left(U_{q'q,q}^{[2,0]} - V_{q'q,q}^{[2,0]} - V_{q'q,q}^{[2,1]} \right), \quad (8.6)$$

$$\int_2 v_{qq,q}^I = A_{qq}^{Q[2,0]} - \Delta\beta_0 \int_2 \left(U_{qq,q}^{\beta[2,0]} - V_{qq,q}^{\beta[2,0]} - V_{qq,q}^{(1)} \right). \quad (8.7)$$

Since the only heavy-quark contribution to $V_{gq,q}^{Q(2)}$ is due to the virtual graph in figure 20(b) and its complex conjugate, the function $v_{gq,q}^I$ includes a factor $\delta(1 - z_1 - z_2)$. It is therefore

uniquely fixed by (8.7) and reads

$$v_{gq,q}^I = \delta(1 - z_1 - z_2) A_{gq}^{Q[2,0]}(z_1) - \Delta\beta_0 \left(U_{gq,q}^{\beta[2,0]} - V_{gq,q}^{\beta[2,0]} - V_{gq,q}^{(1)} \right), \quad (8.8)$$

where for definiteness we have specified the argument of $A_{gq}^{Q[2,0]}$. Given that $v_{gq,q}^I(z_1, z_2) = v_{gq,q}^I(z_2, z_1)$, the momentum sum rule in (8.4) reduces to

$$\int_2 X_2 v_{qQ,q}^I = (1 - X) \left(A_{qq}^{Q[2,0]}(z_1) - A_{qq}^{Q[2,0]}(1 - z_1) \right) - \int_2 X_2 \left(U_{qq',q}^{[2,0]} - V_{qq',q}^{[2,0]} - V_{qq',q}^{[2,1]} \right). \quad (8.9)$$

The next step is to fix $v_{Q\bar{Q},q}^I$ and $v_{Qq,q}^I$. To this end, we make an ansatz

$$v_{Q\bar{Q},q}^I(z_1, z_2) = C_F T_F \sum_i c_i f_i(z_1, z_2), \quad (8.10)$$

$$v_{Qq,q}^I(z_1, z_2) = C_F T_F \sum_i d_i g_i(z_1, z_2), \quad (8.11)$$

$$v_{qQ,q}^I(z_1, z_2) = C_F T_F \sum_i d_i g_i(z_2, z_1), \quad (8.12)$$

where c_i, d_i are numerical coefficients and f_i, g_i are basis functions. We have made the colour factor $C_F T_F$ explicit, which is readily obtained from the Feynman graphs in figures 21(k) and 21(l). The function $v_{Q\bar{Q},q}^I$ must be symmetric under $z_1 \leftrightarrow z_2$, so that we require the same symmetry for the individual basis functions f_i . Of course, (8.12) follows from (8.11).

The set of basis functions f_i and g_i must be large enough to admit a solution of the integral equations (8.3), (8.5), (8.6), and (8.9). As a first attempt, one may take the functions that appear in the corresponding massless kernels, i.e. in $V_{q'\bar{q}',q}^{[2,0]}$ and $V_{q'\bar{q}',q}^{[2,1]}$ for f_i , and in $V_{q'q,q}^{[2,0]}$ and $V_{q'q,q}^{[2,1]}$ for g_i , given that the massive two-loop graphs for these channels have the same topology as their massless counterparts. It turns out that this set is insufficient. We do, however, obtain solution to all constraints when including the functions that appear in $U_{q'\bar{q}',q}^{[2,0]}$ in the set of f_i , and those appearing in $U_{q'q,q}^{[2,0]}$ in the set of g_i . This choice is motivated by the observation that these kernels enter the integral equations in the same manner as the functions v^I . The resulting basis functions are specified in appendix B.

Kinematic constraints. It is plausible to expect that the DPDs computed with massive splitting graphs are not more singular than their massless counterparts in certain kinematical limits. A detailed analysis for the massless case has been given in sections 4.2 to 4.5 of [53] for the limits $x_1 + x_2 \rightarrow 1$, $x_1 + x_2 \ll 1$, $x_1 \ll 1$, and $x_2 \ll 1$.

In the three latter cases, it turns out that individual terms in the massless kernels can be more singular than the sum over all terms. In our ansatz for the massive kernels, we should therefore enforce the same type of cancellation between super-leading terms as happens in the massless case.

To discuss the singular behaviour, it is useful to change variables

$$z_1 = zu, \quad z_2 = z\bar{u} = z(1 - u), \quad (8.13)$$

in the splitting kernels. With the form (2.27) of the convolution \otimes_{12} , one readily finds

$$u = x_1/(x_1 + x_2), \quad \bar{u} = x_2/(x_1 + x_2) \quad (8.14)$$

for the momentum fractions in the splitting DPD.

In the limit of small $x_1 + x_2$, one finds that the convolution of a $1 \rightarrow 2$ kernel with a PDF is enhanced if the kernels grow at least like $\sim z^{-2}$ for small z . Some of the individual basis functions f_i and g_i are in fact more singular than the complete massless kernels, and one finds super-leading terms

$$\sim \frac{\log^2(z)}{z^2}, \quad \sim \frac{\log(z)}{z^2} \quad \text{in some } f_i. \quad (8.15)$$

The massless kernel for $q \rightarrow q'q$ is finite for $z \rightarrow 0$, whilst individual terms in the basis functions behave like

$$\sim \log^2(z), \quad \sim \log(z) \quad \text{in some } g_i. \quad (8.16)$$

In this case, we impose the constraint that the massive splitting kernel should not be more singular for $z \rightarrow 0$ than its massless counterpart, even though this does not enhance the resulting DPD at small $x_1 + x_2$. Requiring that terms of the form shown in (8.15) and (8.16) cancel in (8.10), (8.11), and (8.12) imposes constraints on the coefficients c_i and d_i .

The limits $x_1 \ll 1$ and $x_2 \ll 1$ (with generic values of the other momentum fraction) correspond to $u \ll 1$ and $\bar{u} \ll 1$, respectively. As explained in section 4.4 of [53], a singular behaviour of the splitting DPD for $u \ll 1$ arises from terms in the kernels that grow at least like $1/u$, and from terms with a power of $1 - z_2 = 1 - (1 - u)z$ in the denominator. Inspection of our basis functions reveals that some of them lead to a super-leading behaviour

$$\sim \frac{\log u}{u}, \quad \sim \frac{\log^2 u}{u} \quad (8.17)$$

for the convolution of some g_i with a PDF in the limit $u \ll 1$. Requiring that these terms cancel places additional constraints on the coefficients d_i .

The analysis in [53] also includes the triple Regge limits $x_1 \ll x_1 + x_2 \ll 1$ and $x_2 \ll x_1 + x_2 \ll 1$, which respectively correspond to taking $u \ll 1$ or $\bar{u} \ll 1$ in the small- z limit of the kernels. It turns out that these limits yield no additional constraints for the kernels at hand.

The kinematic requirements just specified, together with the integral equations (8.3), (8.5), (8.6), and (8.9) result in a system of linear equations for the coefficients c_i and d_i . With our choice of basis functions, this system is under-constrained and admits a plethora of solutions. In section 8.2 an algorithm for picking a unique solution will be presented.

Second group: $V_{Q\bar{Q},g}^{Q(2)} + V_{Qg,g}^{Q(2)}$ and $V_{gQ,g}^{Q(2)} + V_{gg,g}^{Q,n_F(2)}$

For the channels $g \rightarrow Q\bar{Q}$, $g \rightarrow Qg$, and $g \rightarrow gg$, one finds again several sum rules that have to be fulfilled simultaneously, namely two momentum sum rules and a number sum rule for

$$V_{QQv,g}^{Q(2)} = -V_{Q\bar{Q},g}^{Q(2)}. \quad (8.18)$$

Sum rule constraints. The momentum sum rules for the interpolating functions read

$$\int_2 X_2 \left(v_{Q\bar{Q},g}^I + v_{Qg,g}^I \right) = (1 - X) A_{Qg}^{Q[2,0]} - \int_2 X_2 \left(U_{q'\bar{q}',g}^{[2,0]} - V_{q'\bar{q}',g}^{[2,0]} - V_{q'\bar{q}',g}^{[2,1]} \right. \\ \left. + U_{qg,g}^{[2,0]} - V_{qg,g}^{[2,0]} - V_{qg,g}^{[2,1]} \right), \quad (8.19)$$

$$\int_2 X_2 \left(2v_{gQ,g}^I + v_{gg,g}^I \right) = (1 - X) A_{gg}^{Q[2,0]} - 2 \int_2 X_2 \left(U_{gg,g}^{[2,0]} - V_{gg,g}^{[2,0]} - V_{gg,g}^{[2,1]} \right) \\ - \Delta\beta_0 \int_2 X_2 \left(U_{gg,g}^{\beta[2,0]} - V_{gg,g}^{\beta[2,0]} - V_{gg,g}^{(1)} \right), \quad (8.20)$$

whilst the number sum rule for $v_{Q\bar{Q},g}^I$ is given by

$$\int_2 v_{Q\bar{Q},g}^I = A_{Qg}^{Q[2,0]} - \int_2 \left(U_{q\bar{q},g}^{[2,0]} - V_{q\bar{q},g}^{[2,0]} - V_{q\bar{q},g}^{[2,1]} \right). \quad (8.21)$$

Our strategy for this case is the same as for the previous one, and we make the ansatz

$$v_{Q\bar{Q},g}^I(z_1, z_2) = C_A T_F \sum_i c_i^A f_i^A(z_1, z_2) + C_F T_F \sum_i c_i^F f_i^F(z_1, z_2), \quad (8.22)$$

$$v_{Qg,g}^I(z_1, z_2) = C_A T_F \sum_i d_i^A g_i^A(z_1, z_2) + C_F T_F \sum_i d_i^F g_i^F(z_1, z_2), \quad (8.23)$$

$$v_{gQ,g}^I(z_1, z_2) = C_A T_F \sum_i d_i^A g_i^A(z_2, z_1) + C_F T_F \sum_i d_i^F g_i^F(z_2, z_1), \quad (8.24)$$

$$v_{gg,g}^I(z_1, z_2) = C_A T_F \sum_i e_i h_i(z_2, z_1), \quad (8.25)$$

where the different colour factors are again deduced from the relevant Feynman graphs. As before, we take as basis functions the terms that appear in the massless kernels $V^{[2,0]}$, $V^{[2,1]}$, and $U^{[2,0]}$ for the relevant parton channel. For f_i^F , we must include additional functions proportional to $(1 - z_1 - z_2)^{-1}$ in order to be able to fulfil all constraints. A simplification occurs for $v_{gg,g}^I$, which includes a factor $\delta(1 - z_1 - z_2)$ according to (5.39). Only basis functions with this structure are therefore needed in (8.25). Details on the resulting set of basis functions are given in appendix B.

Kinematic constraints. As in the previous case, we obtain additional constraints by requiring that the singular behaviour of massive kernels and the resulting splitting DPDs should not be stronger than for their massless counterparts.

For the limit of small $x_1 + x_2$, we find super-leading terms in the small- z behaviour of the basis functions, namely

$$\sim \frac{\log^2(z)}{z^2}, \quad \sim \frac{\log(z)}{z^2} \quad \text{for some } f_i^A \quad (8.26)$$

and

$$\sim \frac{\log^2(z)}{z}, \quad \sim \frac{\log(z)}{z} \quad \text{for some } g_i^A \text{ and } g_i^F. \quad (8.27)$$

We require that these terms cancel in $v_{Q\bar{Q},g}^I$ and $v_{Qg,g}^I$ (and thus also in $v_{gQ,g}^I$).

For the function $v_{Qg,g}^I$, we find further constraints in limits of small x_1 or small x_2 . The convolution of some basis functions g_i^A and g_i^F with a PDF yields super-leading terms

$$\begin{aligned} &\sim \frac{\log^2 u}{u}, && \sim \frac{\log u}{u} && \text{for } u \rightarrow 0, \\ &\sim \frac{\log^2(1-u)}{1-u}, && \sim \frac{\log(1-u)}{1-u} && \text{for } u \rightarrow 1, \end{aligned} \quad (8.28)$$

and we require that these cancel in the convolution of $v_{Qg,g}^I$ with a PDF.

For the same kernel, we also obtain constraints in the triple Regge limit $x_2 \ll x_1 + x_2 \ll 1$, given that some of basis functions show a super-leading behaviour

$$\sim \frac{\log^2(1-u)}{z(1-u)}, \quad \sim \frac{\log(1-u)}{z(1-u)}, \quad \sim \frac{1}{z(1-u)}, \quad (8.29)$$

for $z \rightarrow 0$ and $u \rightarrow 1$. This puts additional constraints on the coefficients d_i^A and d_i^F .

The combination of all sum rules and kinematic constraints leads to a system of linear equations for the coefficients c_i^A , c_i^F , d_i^A , d_i^F , and e_i in equations (8.22) to (8.25) that is under-determined and admits a large number of solutions.

8.2 A particular solution for the kernels

As just stated, the constraints from the sum rules and kinematic limits for the interpolating functions v^I do not uniquely fix the coefficients in our expansion on basis functions. Since we are building a model ansatz, we are free to impose additional requirements. It appears natural to require that the different expansion coefficients do not become too large overall, given that this is true if one expands the massless kernels on the same basis functions.

To turn this into a criterion that leads to a unique solution, let us first build some intuition in a simple toy example. We consider a system with three coefficients c_1 , c_2 , and c_3 and one linear constraint

$$c_3 = Ac_1 + Bc_2 + C, \quad (8.30)$$

where A , B , and C are fixed. In geometric terms, the solutions of this under-determined system form a plane $(c_1, c_2, Ac_1 + Bc_2 + C)$ in the three-dimensional (c_1, c_2, c_3) space. c_1 and c_2 can then be fixed by choosing the point on this plane that has a minimal distance from the origin $(0, 0, 0)$, which in a global sense minimises the size of the coefficients. This point is obtained by minimising the length L of the vector $(c_1, c_2, Ac_1 + Bc_2 + C)$, which is given by

$$L^2 = c_1^2 + c_2^2 + (Ac_1 + Bc_2 + C)^2. \quad (8.31)$$

The minimum of L is obtained by requiring

$$\frac{dL^2}{dc_1} = 0, \quad \frac{dL^2}{dc_2} = 0, \quad (8.32)$$

which yields two more linear constraints for the coefficients c_1 and c_2 .

This approach is readily generalised to the case where one has n coefficients c_1, \dots, c_n and $m < n$ linear constraints. Without loss of generality, one can use the constraints to write the first m coefficients c_1, \dots, c_m as linear combinations of the remaining $n - m$ coefficients c_{m+1}, \dots, c_n , i.e.

$$c_i = f_i(c_{m+1}, \dots, c_n) \quad \text{for } 1 \leq i \leq m. \quad (8.33)$$

The length of the vector (c_1, \dots, c_n) is then given by

$$L^2 = \sum_{i=1}^n c_i^2, \quad (8.34)$$

and the linear constraints that fix the remaining coefficients c_{m+1}, \dots, c_n are

$$\frac{dL^2}{dc_i} = 0, \quad \text{for } m+1 \leq i \leq n. \quad (8.35)$$

The expansion coefficients for the interpolating functions v^I that we obtain with this procedure are given in the ancillary files associated with this paper on the [arXiv](#). We visualise them in figures 23 and 24 and find that they are all of order unity, as desired.

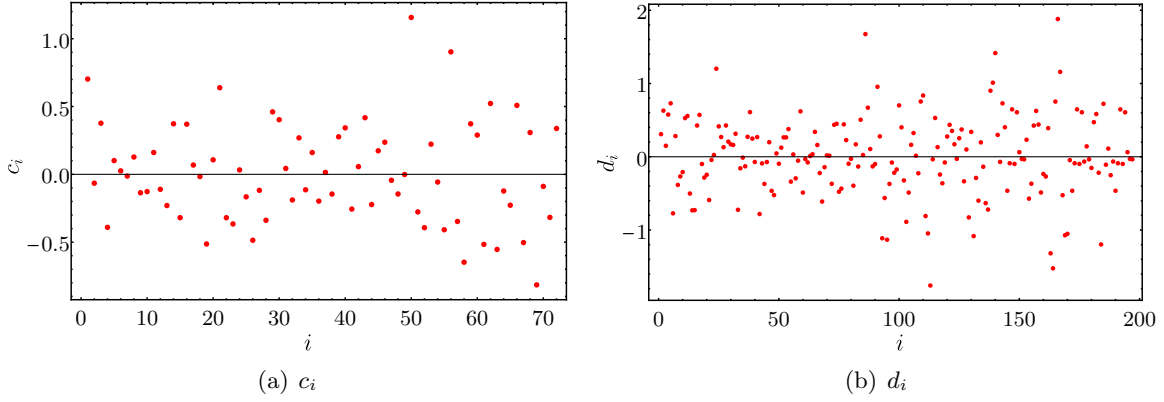


Figure 23: The coefficients c_i and d_i in the expansions (8.10), (8.11), and (8.12), obtained with the criterion of minimal length explained in the text.

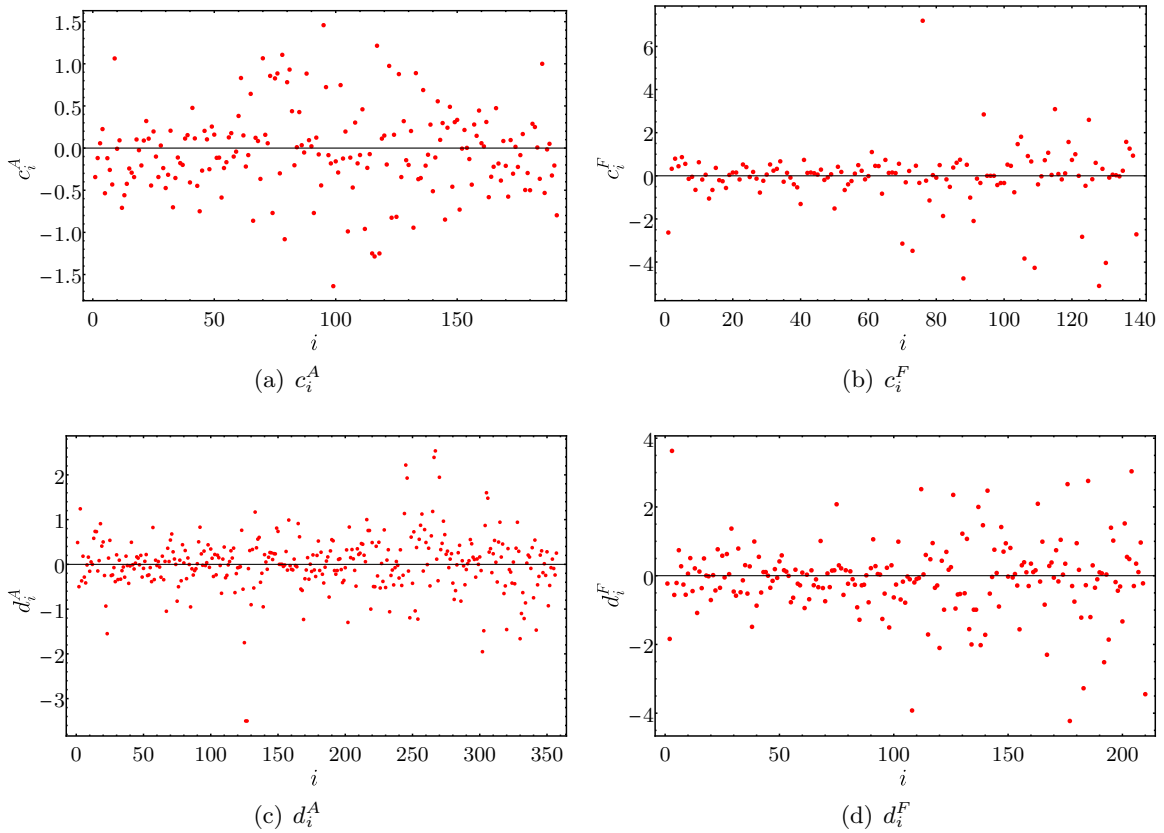


Figure 24: As the previous figure, but for the coefficients c_i^A , c_i^F , d_i^A , and d_i^F in the expansions (8.22), (8.23), and (8.24). Not shown are the three coefficients e_i in (8.25), which have the values $e_1 \approx -1.1$, $e_2 \approx 2.3$, $e_3 \approx -0.45$.

9 Conclusions

We have investigated quark mass effects for the $1 \rightarrow 2$ splitting process in DPDs, which dominates the distributions in the limit of small interparton distances y . Such mass effects should be taken into account if y is comparable to the inverse $1/m_Q$ of a heavy-quark mass. We have set up schemes to compute the splitting part of DPDs in the full range of perturbatively small distances y . In the massive scheme, $1 \rightarrow 2$ splitting kernels including mass effects are used in a y interval around $1/m_Q$. For smaller y , the quark Q is treated as massless in the splitting process, whereas for large y , the DPDs including the heavy flavour are obtained by standard flavour matching, which involves the same matching kernels as flavour matching of PDFs. A graphical representation of these three regimes is given in figure 1. The massive $1 \rightarrow 2$ splitting kernels at LO accuracy can be found in equations (3.5) and (3.6). A simpler, purely massless scheme, is formulated in which only massless $1 \rightarrow 2$ splitting kernels are used. The different schemes are depicted in figures 2 and 3 for a single heavy flavour, and in figure 4 for the combination of charm and bottom quarks.

We numerically studied the different schemes at LO accuracy, focusing on the y dependence of the DPDs and on the double parton luminosities that appear in physical cross sections, both evolved to scales much larger than the masses of the active quarks. This is done using the CHILIPDF library, which we plan to make public in the future. We find a moderate dependence of parton luminosities on the parameters α and β that specify at which y the calculation switches between the three regimes of the massive scheme described above. Luminosities calculated in the massless scheme roughly approximate the massive results if the scheme parameter γ takes values between $1/2$ and 1 , with deviations that can strongly depend on the parton momentum fractions. We furthermore see a substantial dependence of our results on the scale at which the DPDs are computed using the LO splitting formula, which hints at large corrections from higher-order corrections.

Whilst the calculation of massive splitting kernels at NLO is beyond the scope of this work, we derived several properties of these kernels, including their limiting values for small or large y , and their dependence on n_F and the renormalisation scale μ . These properties are encoded in explicit parametrisations, given in (5.32) to (5.40) for one heavy flavour and in (6.34) to (6.38) for charm and bottom. These results hold for all parton polarisations. The non-trivial part of the NLO kernels is described by interpolating kernels $V_{a_1 a_2, a_0}^I$ that depend on two momentum fractions and on ym_Q .

For unpolarised partons, DPDs obey momentum and number sum rules. Using that these must hold for both n_F and $n_F + 1$ active flavours, we derived corresponding sum rules for the massive splitting kernels. Their all-order form is given in equations (7.26) and (7.36), and their NLO part in equations (7.30), (7.39), (7.44), and (7.46). Using these sum rule constraints, we have constructed a model ansatz for the unpolarised massive splitting kernels at two loops.

It would of course be preferable to have an explicit calculation of these kernels. This must be left to future work, as well as a numerical study of the impact on these kernels on DPDs and double parton luminosities. It is to be hoped that this will reduce the large dependence on the splitting scale that we found at LO.

A Numerical studies for W pair production

In sections 4.1 and 4.2 we presented numerical results for the two kinematic settings in (4.1) and (4.2). Here we show and discuss some analogous plots for the setting in (4.3), which corresponds to the production of two W bosons at the LHC. This is because of the phenomenological importance of W -pair production, and it shows to which extent mass effects

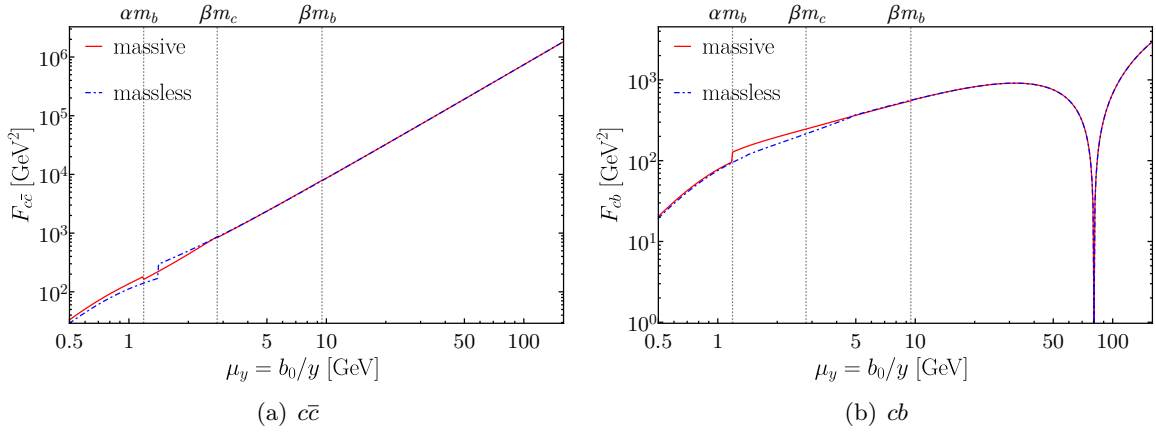


Figure 25: $n_F = 5$ splitting DPDs at $\mu = m_W$ for the W production setting (4.3). Solid lines are for the massive scheme of section 3.3 with our preferred values $\alpha = 1/4$ and $\beta = 2$, and dashed lines are for the massless scheme with $\gamma = 1$. The momentum fractions are $x_1 = x_2 \approx 5.7 \times 10^{-3}$ according to (4.4). Corresponding plots for the dijet production setting are shown in panels (a) and (c) of figure 8.

for charm and bottom persist in DPDs at the scale $\mu = m_W$ and in the associated parton luminosities. Compared with the dijet production setting (4.1), the DPDs in the W production setting are (i) evolved to a higher scale and (ii) evaluated at parton momentum fractions that are larger by a factor $m_W/(25 \text{ GeV}) \approx 3.1$.

As one may expect, discontinuities in the y dependence of the splitting DPDs are generally weaker at $\mu = m_W$ than at $\mu = 25 \text{ GeV}$. This is clearly seen for the cb distribution by comparing figures 25(b) and 8(c). Nonetheless, figure 25 shows that discontinuities for μ_y just above 1 GeV persist even after evolution to the electroweak scale.

For double parton luminosities, we consider the two parton combinations $c\bar{c}b\bar{b}$ and $c\bar{b}\bar{s}c$, which respectively contribute to opposite-sign and like-sign W -pair production. The following plots for $c\bar{c}b\bar{b}$ can be compared with the ones for $c\bar{c}b\bar{b}$ in the dijet production setting, because with splitting, evolution and flavour matching evaluated at LO, DPDs for $\bar{b}b$ and $b\bar{b}$ are identical.

It is therefore not surprising that the qualitative behaviour of the $c\bar{c}b\bar{b}$ luminosity in figure 26(a) is the same as for $c\bar{c}b\bar{b}$ in figure 11(a). In particular, the 1v1 contribution is dominant and has a large ν dependence at low Y . In the $c\bar{b}\bar{s}c$ channel, the ν dependence is very small everywhere, as expected for a parton combination that cannot be directly produced by $1 \rightarrow 2$ splitting.

The scheme dependence of the $c\bar{c}b\bar{b}$ luminosity is shown in figure 27. Compared with the dijet production setting in figure 13, the qualitative behaviour of the ratios is very similar, whilst their deviation from unity is somewhat reduced in most cases. In both settings, the smallest deviations in the massless scheme are obtained for $\gamma = 1/2$.

The dependence of the luminosities on the splitting scale (figure 28) follows the same pattern we found in the two other settings. For $c\bar{c}b\bar{b}$, which can be produced directly by gluon splitting in both DPDs, the scale variation is weak at low Y and grows towards large Y . By contrast, a strong scale variation with little Y dependence is seen for $c\bar{b}\bar{s}c$, just like in panels (b) to (d) of figure 16. The band for the sum of 1v2 and 2v1 contributions is quite asymmetric in figure 28(b), which indicates important contributions from large y also in this setting.

For the matching scale dependence, we observe large effects in figure 29 when flavour

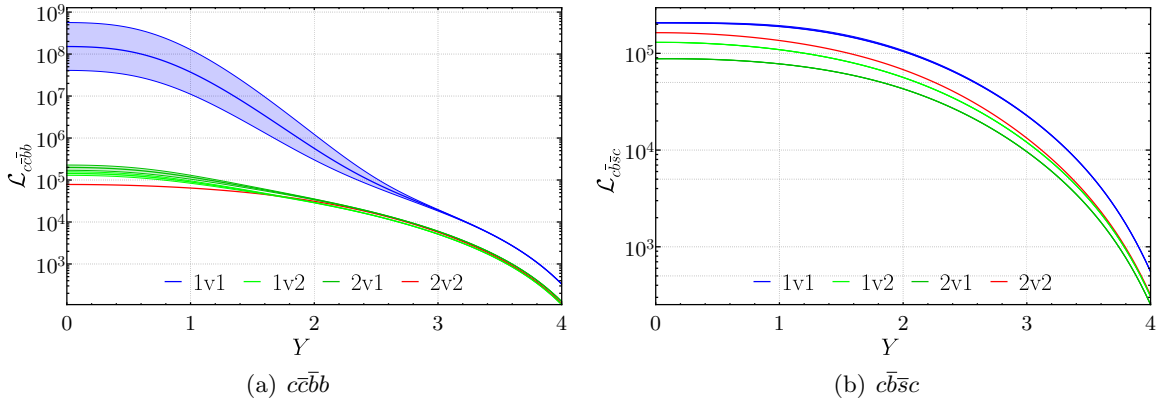


Figure 26: Double parton luminosities at $\mu = m_W$ for the W production setting, computed in the massive scheme of section 3.3 with $\alpha = 1/4$ and $\beta = 2$. Central values correspond to a cutoff parameter $\nu = \mu$, and bands to the variation of ν between $\mu/2$ and 2μ .

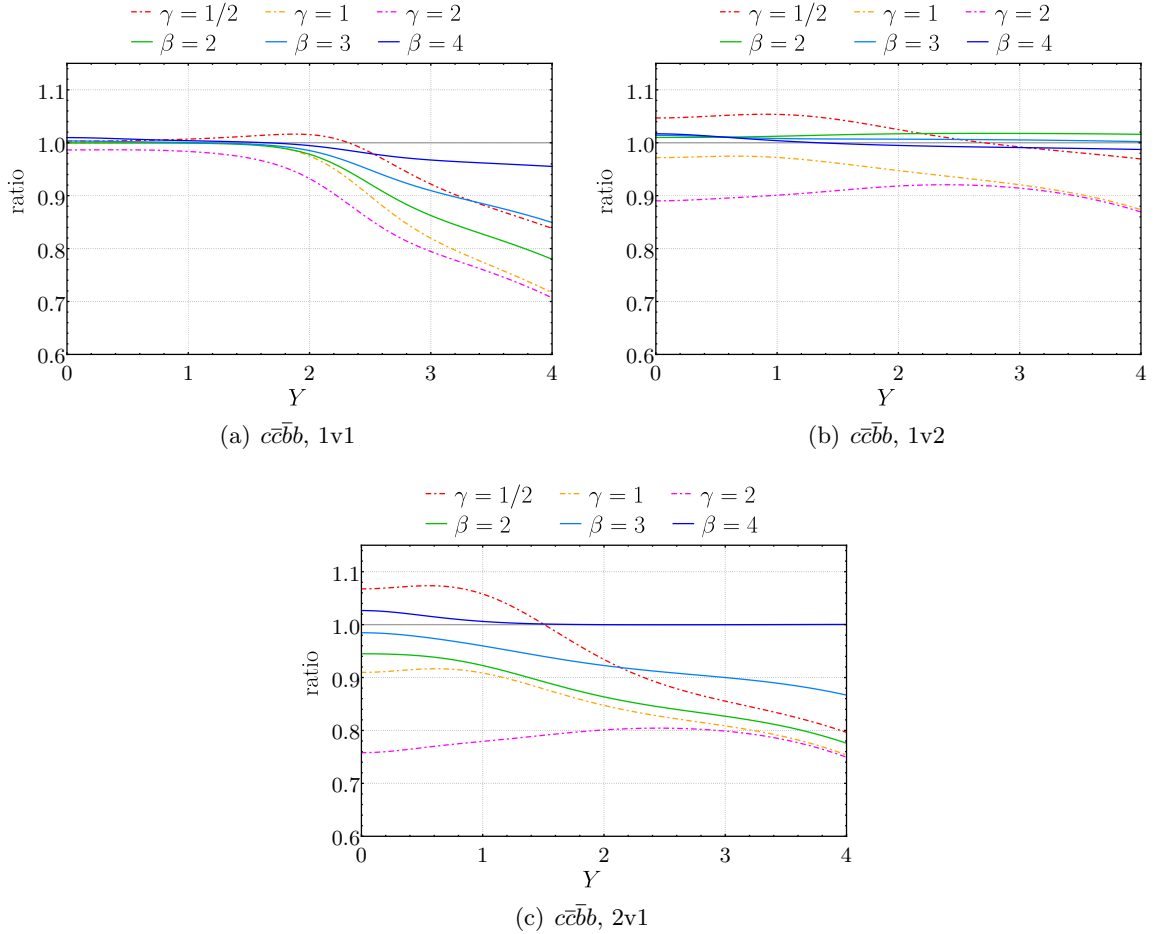


Figure 27: Double parton luminosity ratios (4.12) for $c\bar{c}b\bar{b}$ in the W production setting with $\nu = \mu = 25$ GeV. Solid (dashed) lines correspond to the numerator computed in the (massless) scheme. The corresponding plot for $c\bar{c}b\bar{b}$ in the dijet production setting is shown in figure 13.

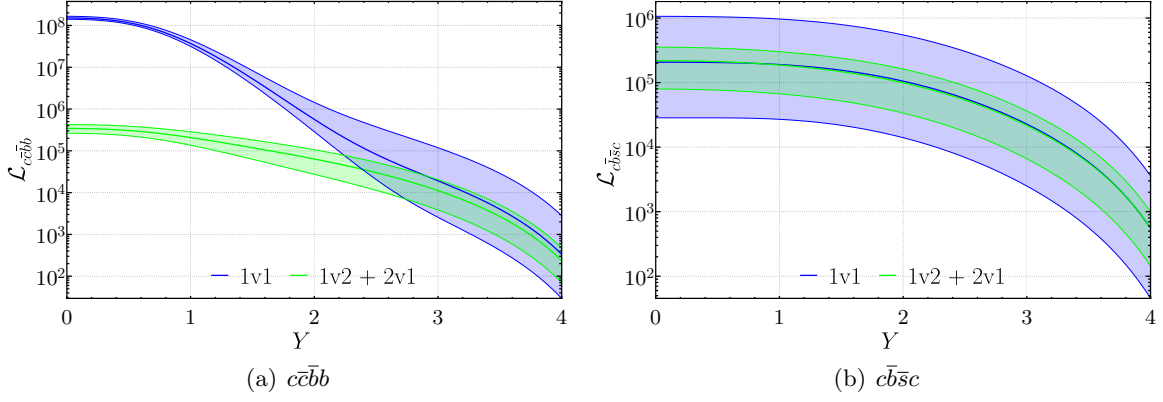


Figure 28: Splitting scale variation of the double parton luminosities shown in figure 26 for the W production setting. Central curves are for $\mu_{\text{split}} = \mu_{y^*}$, and bands correspond to the variation specified in (4.13).

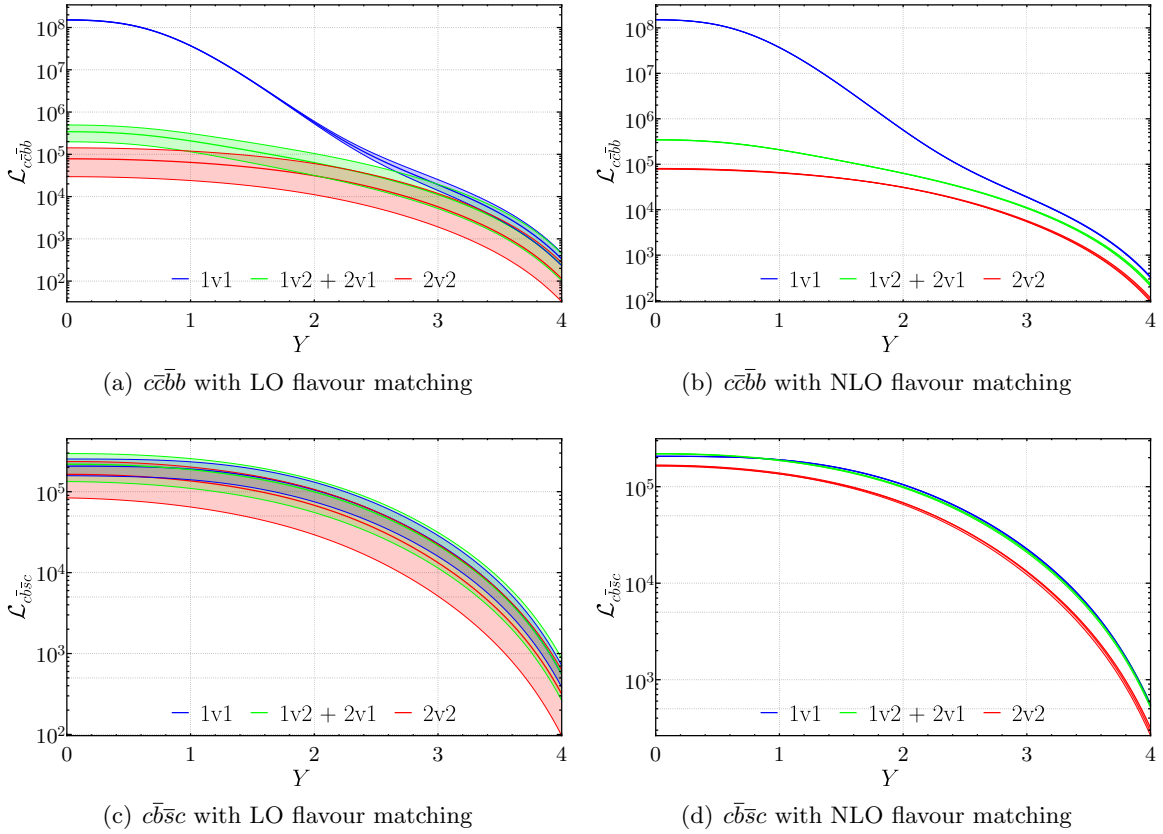


Figure 29: Dependence on the flavour matching scale of the double parton luminosities shown in figure 26 for the W production setting. Central curves are for $\mu_Q = m_Q$, and bands correspond to the variation specified in (4.14).

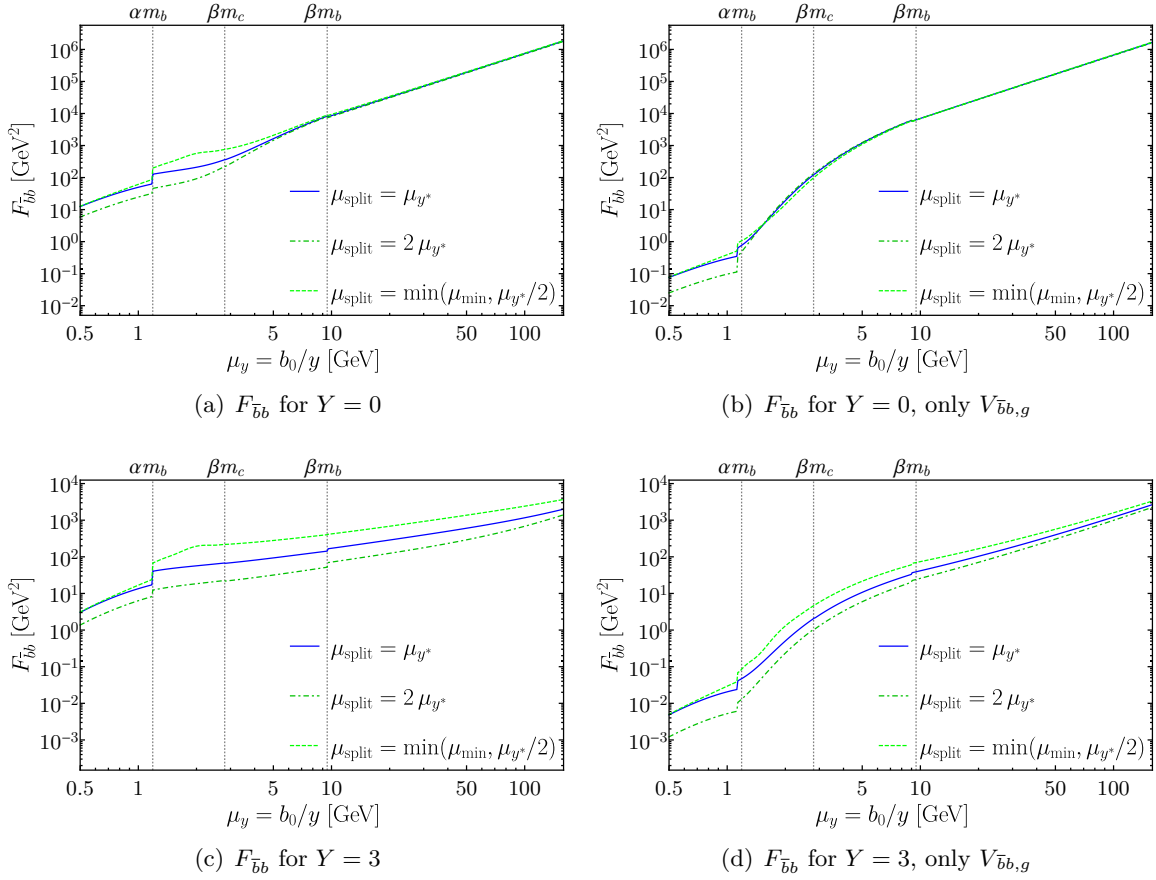


Figure 30: Dependence on μ_{split} of the $\bar{b}b$ splitting DPD in the W production setting, computed with $\alpha = 1/4$ and $\beta = 2$ in the massive scheme. The parton momentum fractions correspond to the $c\bar{c}\bar{b}b$ luminosity at $Y = 0$ (top row) or at $Y = 3$ (bottom row). According to (4.9) this means $x_1 = x_2 \approx 5.7 \times 10^{-3}$ for $Y = 0$ and $x_1 \approx 2.9 \times 10^{-4}$, $x_2 \approx 0.12$ for $Y = 3$. In the left column the complete result is shown, whereas in the right column only the contribution from $g \rightarrow \bar{b}b$ is taken into account in the DPD splitting formula.

matching is performed at LO, even though the matching scales for charm and bottom are much smaller than the scale $\mu = m_W$ at which the DPDs are evaluated. As in the kinematic settings for dijet or $t\bar{t}$ production, the scale variation becomes small when the NLO matching coefficients are included in the calculation.

Let us finally investigate the reason for the peculiar splitting scale dependence in channels with a heavy $Q\bar{Q}$ pair in both DPDs, seen in figures 16(a), 17(a), and 28(a). In the left panels of figure 30, we show the $\bar{b}b$ splitting DPD with momentum fractions that correspond to the $c\bar{c}\bar{b}b$ luminosity at $Y = 0$ or $Y = 3$ in the W production setting. For $Y = 0$ there is some dependence on the splitting scale at low μ_y , but in this region the DPD is very small and has little influence on $\mathcal{L}_{c\bar{c}\bar{b}b}$. For $Y = 3$, there is a strong splitting scale dependence over the full range of μ_y , which results in a strong scale dependence of $\mathcal{L}_{c\bar{c}\bar{b}b}$.

To elucidate the origin of this behaviour, we show in the right panels of figure 30 what happens if we set all DPD splitting kernels other than $V_{\bar{b}b,g}$ to zero. For $Y = 0$ this has almost no impact on the DPD if μ_y is above 10 GeV, whereas for $Y = 3$ it significantly decreases the DPD unless μ_y is close to the final scale μ . This means that for $x_1 = x_2$ (corresponding to $Y = 0$) the $\bar{b}b$ distribution at large μ_y arises almost entirely from direct $g \rightarrow \bar{b}b$ splitting. For

$x_1 \ll x_2$ (corresponding to $Y = 3$), a significant part of $F_{\bar{b}b}^r$ originates from other splitting channels such as F_{gb} and F_{gg} by DGLAP evolution. This is not surprising because the $1 \rightarrow 2$ splitting kernels for these channels are enhanced for asymmetric momentum fractions with a soft emitted gluon. This kinematic enhancement partially compensates the factor of a_s that comes with each DGLAP evolution step.

With DGLAP evolution after the $1 \rightarrow 2$ splitting process playing an important role for large Y , changing μ_{split} has a big impact because it significantly changes the interval $[\mu_{\text{split}}, \mu]$ in which the DPD can evolve. For $Y = 0$, DPD evolution after the $1 \rightarrow 2$ splitting plays a minor role at high μ_y , and the plot in figure 30(a) shows that the resulting splitting scale dependence is very weak.

The preceding analysis is corroborated by the y dependence of the DPD at large μ_y . One can read off in figure 30 that for $Y = 0$ it is very close to the $1/y^2$ behaviour of the massless DPD splitting formula, whereas it is much flatter (close to $1/y$) for $Y = 3$. The significant flattening of the y dependence of splitting DPDs by DGLAP evolution was already observed in [13].

B Basis functions for the model in section 8

In this appendix, we specify the basis functions that appear in the decompositions (8.10) to (8.12) and (8.22) to (8.25). Given their large number, we discuss their general structure and common building blocks here. An explicit list of all basis functions can be found in the ancillary files associated with this paper on the [arXiv](#).

Note that the kernels for NLO channels are functions, whereas the kernels for the LO channels $g \rightarrow Q\bar{Q}$ and $g \rightarrow gg$ include plus- or δ -distributions. This reflects the structure of the corresponding massless kernels.

Basis functions for $v_{Q\bar{Q},q}^I$

The overall structure of the 72 basis functions for this kernel is rather simple. One finds rational functions of the form

$$\frac{(z_1^2 + z_2^2)^n}{(z_1 + z_2)^m} \quad (\text{B.1})$$

with $n = 0, 1$ and $m = 0, \dots, 4$, which are multiplied by logarithms and products of logarithms. The arguments of these logarithms are

$$z_1, \quad z_2, \quad z_1 + z_2, \quad 1 - z_1 - z_2. \quad (\text{B.2})$$

Since the overall $q \rightarrow Q\bar{Q}$ kernel is symmetric under $z_1 \leftrightarrow z_2$, each basis function is symmetrised if necessary.

Basis functions for $v_{Qq,q}^I$

The structure of the 197 basis functions is again rather simple. They involve rational prefactors

$$\frac{z_1^n}{(1 - z_2)^m} \quad (\text{B.3})$$

with $n = 0, 2$ and $m = 0, \dots, 4$, which are multiplied by logarithms, products of logarithms, or dilogarithms. The logarithms encountered in this channel have the arguments

$$z_1, \quad z_2, \quad 1 - z_2, \quad z_1 + z_2, \quad 1 - z_1 - z_2, \quad (\text{B.4})$$

whilst the arguments of the dilogarithms read

$$z_2, \quad -\frac{z_1}{z_2}, \quad \frac{z_1}{1-z_2}, \quad z_1+z_2. \quad (\text{B.5})$$

Basis functions for $v_{Q\bar{Q},g}^I$

For this kernel, one has two sets of basis functions for the colour factors C_A and C_F . Each set includes members with plus- and δ -distributions.

Colour factor C_A . The regular basis functions can be decomposed into rational prefactors

$$\frac{z_1^m}{(z_1+z_2)^n}, \quad \frac{z_2^m}{(z_1+z_2)^n} \quad (\text{B.6})$$

with $m = 0, 1, 2$ and $n = 0, \dots, 4$, multiplied by logarithms, products of logarithms, or dilogarithms. The arguments of the logarithms read

$$z_1, \quad z_2, \quad 1-z_1, \quad 1-z_2, \quad z_1+z_2, \quad 1-z_1-z_2, \quad (\text{B.7})$$

and those of the dilogarithms are given by

$$z_1, \quad z_2, \quad -\frac{z_1}{z_2}, \quad -\frac{z_2}{z_1}, \quad \frac{z_1}{1-z_2}, \quad \frac{z_2}{1-z_1}, \quad z_1+z_2. \quad (\text{B.8})$$

In addition, one finds terms with a denominator $(1-z_1-z_2)$. These terms have combinations of logarithms and dilogarithms as numerators, which vanish sufficiently fast for $z_1+z_2 \rightarrow 1$ such that the singularity of the denominator is cancelled or becomes integrable.

The basis functions that contain a δ -distribution can be written as a prefactor

$$\delta(1-z_1-z_2) [z_1(1-z_1)]^n \quad (\text{B.9})$$

with $n = 0, 1$, multiplied by products of up to three logarithms, dilogarithms, products of dilogarithms and logarithms, and trilogarithms. The arguments of the logarithms, dilogarithms, and trilogarithms read

$$z_1, \quad 1-z_1. \quad (\text{B.10})$$

Here it has been used that one can replace z_2 by $1-z_1$ due to the factor $\delta(1-z_1-z_2)$.

Finally one finds plus-distribution terms with the simple structure

$$\frac{z_1^n + z_2^n}{[1-z_1-z_2]_+} \quad (\text{B.11})$$

with $n = 0, 1, 2$.

Since the basis functions should be symmetric under $z_1 \leftrightarrow z_2$ (or under $z_1 \leftrightarrow 1-z_1$ for the δ -distribution terms), it is understood that an appropriate symmetrisation is performed where necessary.

Colour factor C_F . In this colour channel, the regular basis functions can again be decomposed into a rational prefactor

$$\frac{z_1^m}{(1-z_2)^n}, \quad \frac{z_2^m}{(1-z_1)^n} \quad (\text{B.12})$$

with $m = 0, 1$ and $n = 0, 1, 2$, multiplied by logarithms, products of logarithms, and dilogarithms with the same arguments as given in (B.7) and (B.8) for the colour factor C_A . In addition to these terms, one finds again terms with a denominator $1 - z_1 - z_2$ and combinations of logarithms and dilogarithms in the numerator that lead to a finite value or an integrable singularity of the function in the $z_1 + z_2 \rightarrow 1$ limit.

The structure of the δ - and plus-distribution terms is identical to the ones for the colour factor C_A . Again, an appropriate symmetrisation of the basis functions is understood.

Basis functions for $v_{Qg,g}^I$

Also for this kernel, one has two sets of basis functions for the colour factors C_A and C_F .

Colour factor C_A . The basis functions multiplying C_A have the same structure encountered as the channels discussed so far, with rational prefactors multiplied by logarithms, products of logarithms, and dilogarithms. The rational prefactors are

$$\frac{z_1^m}{(1 - z_2)^n}, \quad \frac{z_1^m}{z_2}, \quad z_2 \quad (\text{B.13})$$

with $m = 0, 1, 2$ and $n = 0, 1, \dots, 4$. The arguments of the logarithms read

$$z_1, \quad z_2, \quad 1 - z_1, \quad 1 - z_2, \quad z_1 + z_2, \quad 1 - z_1 - z_2, \quad (\text{B.14})$$

whilst the arguments of the dilogarithms are given by

$$z_1, \quad z_2, \quad -\frac{z_2}{z_1}, \quad \frac{z_1}{1 - z_2}, \quad \frac{z_2}{1 - z_1}, \quad z_1 + z_2. \quad (\text{B.15})$$

Colour factor C_F . The basis functions multiplying C_F can again be written as discussed above, with rational prefactors

$$z_1, \quad z_2, \quad \frac{z_2^m}{(1 - z_1)^n}, \quad \frac{z_1^m}{(z_1 + z_2)^n}, \quad (\text{B.16})$$

where $m = 0, 1, 2$ and $n = 1, 2$. These prefactors are multiplied by logarithms and products of logarithms with arguments

$$z_1, \quad z_2, \quad 1 - z_1, \quad z_1 + z_2, \quad 1 - z_1 - z_2, \quad (\text{B.17})$$

and by dilogarithms with arguments

$$z_1, \quad -\frac{z_1}{z_2}, \quad \frac{z_2}{1 - z_1}, \quad z_1 + z_2. \quad (\text{B.18})$$

Basis functions for $v_{gg,g}^I$

Due to the kinematic constraint in (5.39), the set of basis functions is very small in this case:

$$\begin{aligned} h_1(z_1, z_2) &= \delta(1 - z_1 - z_2), \\ h_2(z_1, z_2) &= \delta(1 - z_1 - z_2) \left(\frac{1}{1 - z_1} + \frac{1}{z_1} \right), \\ h_3(z_1, z_2) &= \delta(1 - z_1 - z_2) [z_1 \log(1 - z_1) + (1 - z_1) \log z_1]. \end{aligned} \quad (\text{B.19})$$

Acknowledgements

This work is in part supported by the Deutsche Forschungsgemeinschaft (DFG, German Research Foundation) – grant number 409651613 (Research Unit FOR 2926) and grant number 491245950. The work of RN is supported by the ERC Starting Grant REINVENT-714788. The Feynman graphs in this manuscript were produced with JaxoDraw [69,70]. The numerical studies have been performed using the CHLIPDF library [55], which is under development. We gratefully acknowledge the contributions of our collaborators Florian Fabry, Oskar Grocholski, Mees van Kampen, and Frank Tackmann to this project.

References

- [1] J. R. Gaunt and W. J. Stirling, *Double Parton Distributions Incorporating Perturbative QCD Evolution and Momentum and Quark Number Sum Rules*, *JHEP* **03** (2010) 005 [[0910.4347](#)].
- [2] B. Blok, Y. Dokshitzer, L. Frankfurt and M. Strikman, *The Four jet production at LHC and Tevatron in QCD*, *Phys. Rev. D* **83** (2011) 071501 [[1009.2714](#)].
- [3] J. R. Gaunt and W. Stirling, *Double Parton Scattering Singularity in One-Loop Integrals*, *JHEP* **06** (2011) 048 [[1103.1888](#)].
- [4] M. G. Ryskin and A. M. Snigirev, *A Fresh look at double parton scattering*, *Phys. Rev. D* **83** (2011) 114047 [[1103.3495](#)].
- [5] B. Blok, Yu. Dokshitzer, L. Frankfurt and M. Strikman, *pQCD physics of multiparton interactions*, *Eur. Phys. J. C* **72** (2012) 1963 [[1106.5533](#)].
- [6] M. Diehl, D. Ostermeier and A. Schäfer, *Elements of a theory for multiparton interactions in QCD*, *JHEP* **03** (2012) 089 [[1111.0910](#)].
- [7] A. V. Manohar and W. J. Waalewijn, *A QCD Analysis of Double Parton Scattering: Color Correlations, Interference Effects and Evolution*, *Phys. Rev. D* **85** (2012) 114009 [[1202.3794](#)].
- [8] A. V. Manohar and W. J. Waalewijn, *What is Double Parton Scattering?*, *Phys. Lett. B* **713** (2012) 196 [[1202.5034](#)].
- [9] M. G. Ryskin and A. M. Snigirev, *Double parton scattering in double logarithm approximation of perturbative QCD*, *Phys. Rev. D* **86** (2012) 014018 [[1203.2330](#)].
- [10] J. R. Gaunt, *Single Perturbative Splitting Diagrams in Double Parton Scattering*, *JHEP* **01** (2013) 042 [[1207.0480](#)].
- [11] B. Blok, Y. Dokshitzer, L. Frankfurt and M. Strikman, *Perturbative QCD correlations in multi-parton collisions*, *Eur. Phys. J. C* **74** (2014) 2926 [[1306.3763](#)].
- [12] M. Diehl, J. R. Gaunt, D. Ostermeier, P. Plößl and A. Schäfer, *Cancellation of Glauber gluon exchange in the double Drell-Yan process*, *JHEP* **01** (2016) 076 [[1510.08696](#)].
- [13] M. Diehl, J. R. Gaunt and K. Schönwald, *Double hard scattering without double counting*, *JHEP* **06** (2017) 083 [[1702.06486](#)].
- [14] M. Diehl and R. Nagar, *Factorisation of soft gluons in multiparton scattering*, *JHEP* **04** (2019) 124 [[1812.09509](#)].

- [15] B. Cabouat, J. R. Gaunt and K. Ostrolenk, *A Monte-Carlo Simulation of Double Parton Scattering*, *JHEP* **11** (2019) 061 [[1906.04669](#)].
- [16] B. Cabouat and J. R. Gaunt, *Combining single and double parton scatterings in a parton shower*, *JHEP* **10** (2020) 012 [[2008.01442](#)].
- [17] CDF collaboration, F. Abe et al., *Double parton scattering in $\bar{p}p$ collisions at $\sqrt{s} = 1.8\text{ TeV}$* , *Phys. Rev. D* **56** (1997) 3811.
- [18] D0 collaboration, V. M. Abazov et al., *Study of double parton interactions in diphoton + dijet events in $p\bar{p}$ collisions at $\sqrt{s} = 1.96\text{ TeV}$* , *Phys. Rev. D* **93** (2016) 052008 [[1512.05291](#)].
- [19] LHCb collaboration, R. Aaij et al., *Measurement of the J/ψ pair production cross-section in pp collisions at $\sqrt{s} = 13\text{ TeV}$* , *JHEP* **06** (2017) 047 [[1612.07451](#)].
- [20] ATLAS collaboration, M. Aaboud et al., *Study of the hard double-parton scattering contribution to inclusive four-lepton production in pp collisions at $\sqrt{s} = 8\text{ TeV}$ with the ATLAS detector*, *Phys. Lett.* **B790** (2019) 595 [[1811.11094](#)].
- [21] CMS collaboration, *Observation of same-sign WW production from double parton scattering in proton-proton collisions at $\sqrt{s} = 13\text{ TeV}$* , [2206.02681](#).
- [22] O. Fedkevych and A. Kulesza, *Double parton scattering in four-jet production in proton-proton collisions at the LHC*, *Phys. Rev. D* **104** (2021) 054021 [[2008.08347](#)].
- [23] P. Bartalini and J. R. Gaunt, eds., *Multiple Parton Interactions at the LHC*, vol. 29. WSP, 2019, [10.1142/10646](#).
- [24] H.-M. Chang, A. V. Manohar and W. J. Waalewijn, *Double Parton Correlations in the Bag Model*, *Phys. Rev. D* **87** (2013) 034009 [[1211.3132](#)].
- [25] M. Rinaldi, S. Scopetta and V. Vento, *Double parton correlations in constituent quark models*, *Phys. Rev. D* **87** (2013) 114021 [[1302.6462](#)].
- [26] W. Broniowski and E. Ruiz Arriola, *Valence double parton distributions of the nucleon in a simple model*, *Few Body Syst.* **55** (2014) 381 [[1310.8419](#)].
- [27] M. Rinaldi, S. Scopetta, M. Traini and V. Vento, *Double parton correlations and constituent quark models: a Light Front approach to the valence sector*, *JHEP* **12** (2014) 028 [[1409.1500](#)].
- [28] W. Broniowski, E. Ruiz Arriola and K. Golec-Biernat, *Generalized Valon Model for Double Parton Distributions*, *Few Body Syst.* **57** (2016) 405 [[1602.00254](#)].
- [29] T. Kasemets and A. Mukherjee, *Quark-gluon double parton distributions in the light-front dressed quark model*, *Phys. Rev. D* **94** (2016) 074029 [[1606.05686](#)].
- [30] M. Rinaldi, S. Scopetta, M. C. Traini and V. Vento, *Correlations in Double Parton Distributions: Perturbative and Non-Perturbative effects*, *JHEP* **10** (2016) 063 [[1608.02521](#)].
- [31] M. Rinaldi and F. A. Ceccopieri, *Relativistic effects in model calculations of double parton distribution function*, *Phys. Rev. D* **95** (2017) 034040 [[1611.04793](#)].
- [32] M. Rinaldi, S. Scopetta, M. Traini and V. Vento, *A model calculation of double parton distribution functions of the pion*, *Eur. Phys. J. C* **78** (2018) 781 [[1806.10112](#)].

- [33] A. Courtoy, S. Noguera and S. Scopetta, *Double parton distributions in the pion in the Nambu–Jona-Lasinio model*, *JHEP* **12** (2019) 045 [[1909.09530](#)].
- [34] W. Broniowski and E. Ruiz Arriola, *Double parton distribution of valence quarks in the pion in chiral quark models*, *Phys. Rev. D* **101** (2020) 014019 [[1910.03707](#)].
- [35] G. S. Bali, L. Castagnini, M. Diehl, J. R. Gaunt, B. Gläßle, A. Schäfer et al., *Double parton distributions in the pion from lattice QCD*, *JHEP* **02** (2021) 067 [[2006.14826](#)].
- [36] G. S. Bali, M. Diehl, B. Gläßle, A. Schäfer and C. Zimmermann, *Double parton distributions in the nucleon from lattice QCD*, *JHEP* **09** (2021) 106 [[2106.03451](#)].
- [37] K. Golec-Biernat and E. Lewandowska, *How to impose initial conditions for QCD evolution of double parton distributions?*, *Phys. Rev. D* **90** (2014) 014032 [[1402.4079](#)].
- [38] K. Golec-Biernat, E. Lewandowska, M. Serino, Z. Snyder and A. M. Stasto, *Constraining the double gluon distribution by the single gluon distribution*, *Phys. Lett. B* **750** (2015) 559 [[1507.08583](#)].
- [39] M. Diehl, J. Gaunt, D. Lang, P. Plöbl and A. Schäfer, *Sum rule improved double parton distributions in position space*, *Eur. Phys. J. C* **80** (2020) 468 [[2001.10428](#)].
- [40] K. Golec-Biernat and A. M. Stasto, *The momentum sum rule and factorization of double parton distributions*, [2212.02289](#).
- [41] A. Snigirev, N. Snigireva and G. Zinovjev, *Perturbative and nonperturbative correlations in double parton distributions*, *Phys. Rev. D* **90** (2014) 014015 [[1403.6947](#)].
- [42] B. Blok and P. Gunnellini, *Dynamical approach to MPI four-jet production in Pythia*, *Eur. Phys. J. C* **75** (2015) 282 [[1503.08246](#)].
- [43] B. Blok and P. Gunnellini, *Dynamical approach to MPI in W+dijet and Z+dijet production within the PYTHIA event generator*, *Eur. Phys. J. C* **76** (2016) 202 [[1510.07436](#)].
- [44] K. Golec-Biernat and E. Lewandowska, *Electroweak boson production in double parton scattering*, *Phys. Rev. D* **90** (2014) 094032 [[1407.4038](#)].
- [45] J. R. Gaunt, R. Maciula and A. Szczurek, *Conventional versus single-ladder-splitting contributions to double parton scattering production of two quarkonia, two Higgs bosons and $c\bar{c}c\bar{c}$* , *Phys. Rev. D* **90** (2014) 054017 [[1407.5821](#)].
- [46] P. Pietrulewicz, D. Samitz, A. Spiering and F. J. Tackmann, *Factorization and Resummation for Massive Quark Effects in Exclusive Drell-Yan*, *JHEP* **08** (2017) 114 [[1703.09702](#)].
- [47] K. G. Chetyrkin, B. A. Kniehl and M. Steinhauser, *Strong coupling constant with flavor thresholds at four loops in the \overline{MS} scheme*, *Phys. Rev. Lett.* **79** (1997) 2184 [[hep-ph/9706430](#)].
- [48] M. Buza, Y. Matiounine, J. Smith and W. L. van Neerven, *Charm electroproduction viewed in the variable flavor number scheme versus fixed order perturbation theory*, *Eur. Phys. J. C* **1** (1998) 301 [[hep-ph/9612398](#)].
- [49] J. Ablinger, J. Blümlein, A. De Freitas, A. Hasselhuhn, A. von Manteuffel, M. Round et al., *The Transition Matrix Element $A_{gq}(N)$ of the Variable Flavor Number Scheme at $O(\alpha_s^3)$* , *Nucl. Phys. B* **882** (2014) 263 [[1402.0359](#)].

- [50] A. Behring, I. Bierenbaum, J. Blümlein, A. De Freitas, S. Klein and F. Wißbrock, *The logarithmic contributions to the $O(\alpha_s^3)$ asymptotic massive Wilson coefficients and operator matrix elements in deeply inelastic scattering*, *Eur. Phys. J. C* **74** (2014) 3033 [[1403.6356](#)].
- [51] J. Ablinger, A. Behring, J. Blümlein, A. De Freitas, A. Hasselhuhn, A. von Manteuffel et al., *The 3-Loop Non-Singlet Heavy Flavor Contributions and Anomalous Dimensions for the Structure Function $F_2(x, Q^2)$ and Transversity*, *Nucl. Phys. B* **886** (2014) 733 [[1406.4654](#)].
- [52] M. Diehl, J. R. Gaunt, P. Plößl and A. Schäfer, *Two-loop splitting in double parton distributions*, *SciPost Phys.* **7** (2019) 017 [[1902.08019](#)].
- [53] M. Diehl, J. R. Gaunt and P. Plößl, *Two-loop splitting in double parton distributions: the colour non-singlet case*, *JHEP* **08** (2021) 040 [[2105.08425](#)].
- [54] A. Bacchetta, M. G. Echevarria, P. J. G. Mulders, M. Radici and A. Signori, *Effects of TMD evolution and partonic flavor on e^+e^- annihilation into hadrons*, *JHEP* **11** (2015) 076 [[1508.00402](#)].
- [55] M. Diehl, R. Nagar and F. J. Tackmann, *ChiliPDF: Chebyshev interpolation for parton distributions*, *Eur. Phys. J. C* **82** (2022) 257 [[2112.09703](#)].
- [56] A. Kulesza and W. Stirling, *Like sign W boson production at the LHC as a probe of double parton scattering*, *Phys. Lett. B* **475** (2000) 168 [[hep-ph/9912232](#)].
- [57] J. R. Gaunt, C.-H. Kom, A. Kulesza and W. Stirling, *Same-sign W pair production as a probe of double parton scattering at the LHC*, *Eur. Phys. J. C* **69** (2010) 53 [[1003.3953](#)].
- [58] F. A. Ceccopieri, M. Rinaldi and S. Scopetta, *Parton correlations in same-sign W pair production via double parton scattering at the LHC*, *Phys. Rev. D* **95** (2017) 114030 [[1702.05363](#)].
- [59] S. Cotogno, T. Kasemets and M. Myska, *Spin on same-sign W -boson pair production*, *Phys. Rev. D* **100** (2019) 011503 [[1809.09024](#)].
- [60] S. Cotogno, T. Kasemets and M. Myska, *Confronting same-sign W -boson production with parton correlations*, *JHEP* **10** (2020) 214 [[2003.03347](#)].
- [61] CMS collaboration, A. M. Sirunyan et al., *Evidence for WW production from double-parton interactions in proton–proton collisions at $\sqrt{s} = 13$ TeV*, *Eur. Phys. J. C* **80** (2020) 41 [[1909.06265](#)].
- [62] S. Bailey, T. Cridge, L. A. Harland-Lang, A. D. Martin and R. S. Thorne, *Parton distributions from LHC, HERA, Tevatron and fixed target data: MSHT20 PDFs*, *Eur. Phys. J. C* **81** (2021) 341 [[2012.04684](#)].
- [63] H1, ZEUS collaboration, H. Abramowicz et al., *Combination of measurements of inclusive deep inelastic $e^\pm p$ scattering cross sections and QCD analysis of HERA data*, *Eur. Phys. J. C* **75** (2015) 580 [[1506.06042](#)].
- [64] NNPDF collaboration, R. D. Ball et al., *The path to proton structure at 1% accuracy*, *Eur. Phys. J. C* **82** (2022) 428 [[2109.02653](#)].

- [65] A. Buckley, J. Ferrando, S. Lloyd, K. Nordström, B. Page, M. Rüfenacht et al., *LHAPDF6: parton density access in the LHC precision era*, *Eur. Phys. J. C* **75** (2015) 132 [[1412.7420](#)].
- [66] M. Diehl, P. Plößl and A. Schäfer, *Proof of sum rules for double parton distributions in QCD*, *Eur. Phys. J. C* **79** (2019) 253 [[1811.00289](#)].
- [67] J. Ablinger, J. Blümlein, A. De Freitas, C. Schneider and K. Schönwald, *The two-mass contribution to the three-loop pure singlet operator matrix element*, *Nucl. Phys. B* **927** (2018) 339 [[1711.06717](#)].
- [68] J. Blümlein, A. De Freitas, C. Schneider and K. Schönwald, *The Variable Flavor Number Scheme at Next-to-Leading Order*, *Phys. Lett. B* **782** (2018) 362 [[1804.03129](#)].
- [69] D. Binosi and L. Theussl, *JaxoDraw: A Graphical user interface for drawing Feynman diagrams*, *Comput. Phys. Commun.* **161** (2004) 76 [[hep-ph/0309015](#)].
- [70] D. Binosi, J. Collins, C. Kaufhold and L. Theussl, *JaxoDraw: A Graphical user interface for drawing Feynman diagrams. Version 2.0 release notes*, *Comput. Phys. Commun.* **180** (2009) 1709 [[0811.4113](#)].